UNIV OF MICHIGA
FEB 1 2 1952
ENGINEERING LIBRARY

JOURNAL OF THE AERONAUTICAL SCIENCES

VOLUME 19 FEBRUARY, 1952 NUMBER 2

CONTENTS

Measurement of Instantaneous Vector Air Velocity by Hot-Wire Methods.....CARL E. PEARSON 73

Air Drag on Cubes at Mach Numbers 0.5 to 3.5.....GEORGE E. HANSCHE AND JOHN S. RINEHART 83

On Unsteady Nonlinearized Conical Flow.....S. F. BORG 85

A Study of an Analogous Model Giving the Nonlinear Characteristics in the Buckling Theory of Sandwich Cylinders.....CHI-TEH WANG AND G. V. R. RAO 93

Theoretical Investigation of Several Types of Single Degree of Freedom Flutter.....HARRY L. RUNYAN, HERBERT J. CUNNINGHAM, AND CHARLES E. WATKINS 101

Supersonic Flow Around Cones at Large Yaw.....G. B. W. YOUNG AND C. P. SISKA 111

Heat Transfer by Laminar Flow from a Rotating Plate...KNOX MILLSAPS AND KARL POHLHAUSEN 120

An Experimental Investigation of the Isothermal Laminar Boundary Layer on a Porous Flat Plate.....PAUL A. LIBBY, LAWRENCE KAUFMAN, AND R. PAUL HARRINGTON 127

Readers' Forum: "Effect of Wind-Tunnel Nozzle on Steady-Flow Nonuniformities," by Stanley Corrsin; "On Nonplanar Surfaces of Very Low Aspect Ratio," by H. M. Voss; "Note About Secondary Flow in Cascades," by Hans P. Eichenberger; "On Chang's Function for Nonstationary Flow," by John W. Miles; "On the Stability of the Boundary Layer with Respect to Disturbances of Large Wave Velocity," by C. C. Lin; "A Method of Solving the Linear Potential Equation for Axially Symmetric Flow," by R. Probstein and J. V. Charyk; "On Slender Wing-Body Theory," by John W. Miles; "A Note on the Design of Supersonic Wind-Tunnel Nozzles," by R. E. Meyer; "Parameters Predicting Failure of Partial Diagonal Tension Beams," by Bertram Klein.....135–142

Published by the

INSTITUTE OF THE AERONAUTICAL SCIENCES, INC.

JOURNAL OF THE AERONAUTICAL SCIENCES

Editor: HUGH L. DRYDEN, *Director, N.A.C.A.*

Associate Editor: ROBERT R. DEXTER *Managing Editor:* BERNEICE H. JARCK

Editorial Committee

Aerodynamics

Francis Clauser
Howard Emmons
Alexander Flax
R. Paul Harrington
R. T. Jones
Carl Kaplan
H. W. Liepmann
C. C. Lin
H. F. Ludloff
Harold Luskin
John R. Markham
Clark B. Millikan
Shatswell Ober
W. Bailey Oswald
Allen E. Puckett
Elliott G. Reid
H. J. F. Reid
Russell Robinson
G. B. Schubauer
W. R. Sears
John Stack
Theodore von Kármán
Richard von Mises

Flight Testing

W. K. Ebel
R. R. Gilruth
Melvin N. Gough
E. G. Stout

Meteorology

C. F. Brooks
D. M. Little
E. J. Minser
F. W. Reichelderfer
H. C. Willett

Structures and Materials

W. B. Bleakney
E. W. Conlon
L. H. Donnell
E. C. Hartmann
N. J. Hoff
Samuel Levy
E. E. Lundquist
J. S. Newell
Alfred S. Niles
W. Ramberg
E. Reissner
F. R. Shanley
H. W. Sibert
C. R. Strang
S. Timoshenko
H. S. Tsien
Chi-Teh Wang

Rotating Wing Aircraft

F. B. Gustafson
K. H. Hohenemser
Bartram Kelley
R. B. Maloy
Ralph McClarren
R. H. Miller
R. H. Prewitt
Igor I. Sikorsky

Physiologic Problems

H. G. Armstrong
Louis H. Bauer
Eugene Du Bois
W. Randolph Lovelace, II
Ross A. MacFarland
A. D. Tuttle

Flight Propulsion

George W. Brady
Frank W. Caldwell
L. S. Hobbs
E. E. Johnson
Joseph Keenan
R. P. Kroon
Hans Reissner
Abe Silverstein
C. Fayette Taylor
E. S. Taylor
P. Taylor
E. S. Thompson
H. S. Tsien

Aircraft Design

W. E. Beall
W. K. Ebel
Hall L. Hibbard
Richard Hutton
C. L. Johnson
A. A. Kartveli
C. J. McCarthy
Fred E. Weick
Robert J. Woods

Air Transport

Charles Froesch
J. A. Herlihy
R. D. Kelly
Otto E. Kirchner
Jerome Lederer
John C. Leslie
R. Dixon Speas

Instruments

Allan G. Binnie
J. R. Bradburn
Charles H. Colvin
C. S. Draper
S. G. Eskin
O. E. Esval
H. W. Holzapfel
W. L. Howland
George H. Purcell
C. F. Savage
O. Hugo Schuck
C. L. Seward, Jr.
L. D. Statham
R. C. Sylvander
D. K. Warner

Vibration and Flutter

Lee Arnold
M. A. Biot
R. L. Bisplinghoff
William Bollay
Chieh-Chien Chang
I. E. Garrick
Martin Goland
J. P. Den Hartog

Fuels and Oils

D. P. Barnard
J. H. Doolittle
Graham Edgar
R. T. Goodwin
S. D. Heron
A. M. Rothrock

SUBSCRIPTION RATES

JOURNAL OF THE AERONAUTICAL SCIENCES, Published Monthly.—United States and Possessions: 1 Year, $12.00; Single Copies, $1.50. Foreign Countries Including Canada (American Currency Rates): 1 Year, $13.00; Single Copies, $1.50.

AERONAUTICAL ENGINEERING REVIEW, Published Monthly.—United States and Possessions: 1 Year, $3.00; Single Copies, $0.50. Foreign Countries Including Canada (American Currency Rates): 1 Year, $3.50; Single Copies, $0.50.

Notices of change of address should be sent to the Institute at least 30 days prior to actual change of address.

Manuscripts for publication, proofs, and all correspondence should be addressed to the Editorial Office of the JOURNAL.

Correspondence regarding subscriptions may be addressed to Publication Office, 20th and Northampton Sts., Easton, Pa., or to the Editorial Office of the JOURNAL OF THE AERONAUTICAL SCIENCES, 2 East 64th Street, New York 21, New York.

Copyright, 1952, by the Institute of the Aeronautical Sciences, Inc.

Entered as Second Class Matter at the Post Office, Easton, Pa., May 1, 1937. Acceptance for mailing at a special rate of Postage provided for in the Act of August 24, 1912. Authorized April 29, 1937.

JOURNAL OF THE AERONAUTICAL SCIENCES

VOLUME 19 FEBRUARY, 1952 NUMBER 2

Measurement of Instantaneous Vector Air Velocity by Hot-Wire Methods*

CARL E. PEARSON†

Harvard University

GENERAL SUMMARY

One of the major problems encountered in improving the design of jet-engine compressors has been to examine experimentally the airflow present in any given compressor stage. Because of the rapid and large fluctuations in velocity, the usual types of instrumentation will give a (doubtful) measure of the average velocity alone. However, a hot-wire probe has been developed which permits measurement of instantaneous, as well as average, direction and magnitude under the above conditions of airflow.

Details of the construction, theory, and use of this hot-wire instrument are presented. Each wire used need be calibrated only once; although the characteristics of a given wire change rapidly and somewhat erratically, a correction method has been devised which automatically compensates for such changes. This correction method, based on the hypothesis that the changes in characteristics are due to a combination of oxidation and plastic flow of the hot-wire material, has been firmly validated by extensive experimental work.

In the measurement of instantaneous air velocity, it might appear that, because of the predominant effect of the heat capacity of the wire, the instantaneous velocity should be proportional to the rate of change of voltage across the hot-wire. This is indeed the case, but to prove this rigorously (for large velocity changes), as well as to determine the constant of proportionality, requires considerable algebraical manipulation.

There are many ways in which the present theory may be checked experimentally; in general, the agreement is excellent. A typical example is given in which the instantaneous air velocity behind an axial compressor is measured in three different directions.

The instrument has so far been examined only for Mach Numbers less than 0.7. For $M < 0.3$, an accuracy of better than 2 per cent in average and 10 per cent in instantaneous velocities is claimed; at $M = 0.7$, the error in instantaneous velocity measurement may be 25 per cent.

It appears that hot-wire instruments of the present type will extend considerably the range of experimental work possible in compressors and other mechanisms. The instrument as here discussed has now been used satisfactorily over a period of about 1 year in the analysis of the airflow in the axial and centrifugal compressors, both in and out of pulsation.

Received May 25, 1951. Revised and received October 6, 1951.

* This work represents a portion of an axial-compressor research program recently carried out at Harvard University; the work was supported by the Pratt & Whitney Division, United Aircraft Corporation, to whom the author is indebted for permission to publish this material. The author also wishes to express his gratitude to Prof. Howard W. Emmons, who initiated and encouraged the project; to H. P. Grant, who assisted the author in experimental work; and to E. J. Boudreau, W. Batteau, and Mrs. P. Mitchell, who helped with the experimental, electronic, and photographic work.

† Research Associate, Pratt & Whitney Project, Gordon McKay Laboratory.

(I) INTRODUCTION

IF A THIN WIRE IS HEATED by an electric current and inserted in an air stream, its rate of heat loss will depend on the velocity of the air and on the temperature difference between wire and air. Since about 1910, this fact has been used to a small extent in the measurement of mean velocities of steady airflows and to a considerable extent in turbulence research.

The usual turbulence circuit is as shown in Fig. 1. The battery B supplies the hot-wire H with heating current through a series resistance R sufficiently large that the current is almost independent of hot-wire resistance. The voltage across the wire is measured

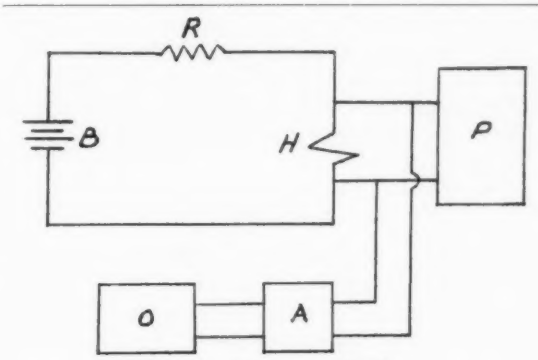

FIG. 1. Turbulence circuit.

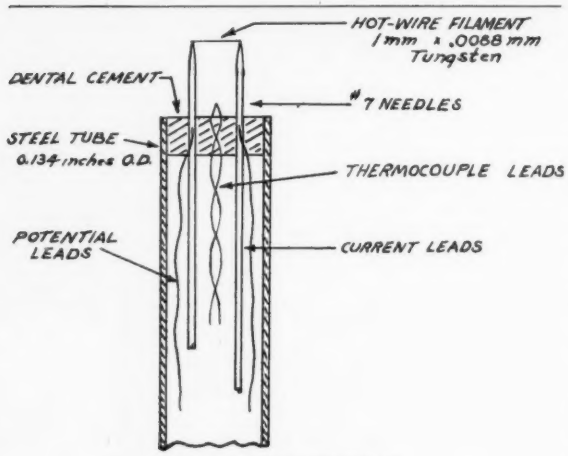

FIG. 2. Probe construction.

by the potentiometer P; the mean air velocity is then a function of this potentiometer voltage, the air temperature, and the characteristics of the wire.

Since the air stream is, in general, not perfectly uniform, the voltage across the wire will possess an a.c. component that is amplified by A and presented on an oscilloscope O. The magnitude of this voltage affords a measure of air-stream turbulence; to simplify calculations, it is customary to add a special circuit to the amplifier which will automatically compensate for the way in which the hot-wire response is modified by its own heat capacity. This compensating network is valid only for small velocity fluctuations and can therefore not be used in the present investigation.

The object of the hot-wire work at Harvard has been to develop an instrument that will give an accurate reading of the average and instantaneous vector velocity of airflow behind the impeller of a compressor. For this purpose, it was necessary to modify the circuit of Fig. 1 in several ways. In addition, it became necessary to find a correction method applicable to the irregular changes in operating level to which all hot-wire materials are subject.

Various minor troubles, such as dirt collection on the upstream surface of the hot-wire, existence of variable contact potentials, hunting in electronic power supplies, etc., were overcome by filtering, careful soldering of contacts, use of battery power supplies alone, etc.

Both theory and instrumentation went through several changes as the various difficulties arose; the final forms of each will now be discussed in detail.

(II) Probe Construction and Measuring Apparatus

To avoid the temperature dependent voltage drop in the leads between probe and measuring apparatus, separate current and potential leads are used (since the potential leads do not carry current, the voltage drop across them is always zero). To measure accurately the average air temperature at the probe, a small copper-iron thermocouple is built into the probe just below the hot-wire.

The arrangement is as in Fig. 2. A total of six wires is required, each of which must be insulated from the others and from the metal tubing containing them. The most satisfactory hot-wire material is tungsten; it is copper plated at its ends and soldered onto the supports. During soldering (carried out under a microscope), the supports are pressed slightly together so as to hold the wire straight after release. It is important that the wire be well soldered at each end, without bends.

The apparatus is shown schematically in Fig. 3. The amplifier is direct-coupled so as to avoid phase shift in coupling condensers. D is a differentiating circuit. The resistors R' and R'' are noninductive standard dial boxes. The switching arrangement shown allows the potentiometer P to measure the voltage across either R'' or the wire itself; in practice, R' is adjusted so as to keep constant the voltage across R'' (and therefore also the hot-wire current).

In the sequel it will be shown that the resistance of the hot-wire must be measured frequently; to do this a low-voltage dry cell is substituted for the battery B so that the resulting current will be too small to raise the wire temperature appreciably above air temperature. The oscilloscope used is a Du Mont 304H (possessing an internal d.c. amplifier); it is synchronized to the compressor by means of a tiny rotating magnet-coil system.

(III) Properties of a Hot-Wire in Steady Flow

In an inviscid incompressible steady flow of fluid, the equation governing the conduction of heat from a hot-

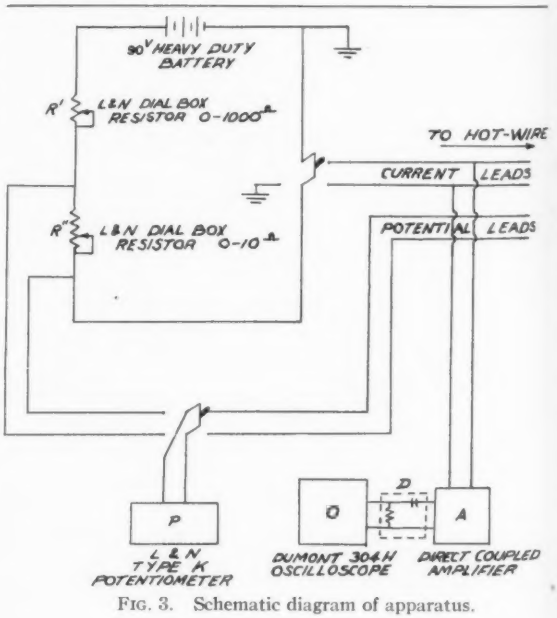

FIG. 3. Schematic diagram of apparatus.

wire is

$$c\,(dT/dt) = K_0\,\nabla^2 T \tag{1}$$

where

c = fluid heat capacity per unit volume
K_0 = thermal conductivity (assumed constant)
T = temperature of fluid
dT/dt = material derivative of $T = (\partial T/\partial x)u_x + (\partial T/\partial y)u_y + (\partial T/\partial z)u_z$ in steady flow where u_x, etc., are the components of velocity at the point in question

The boundary conditions are that $T = T_A$ at infinity and $T = T_w$ at the wire (it is assumed that the wire has constant temperature throughout its mass). It is difficult to find an analytic solution of this boundary value problem, but one property of the solution is easily obtained—viz., that the rate of heat flow H from the wire has the form

$$H = (T_w - T_A)f(V) \tag{2}$$

where $f(V)$ is a quantity depending only on the velocity V at infinity. Suppose that a solution of Eq. (1) were known for a certain value of $T_w - T_A$; then, since Eq. (1) is linear, it is clear that, if $T_w - T_A$ were doubled, the new temperature gradient would be found by merely doubling the value of the gradient of the previous solution at every point, and therefore the total rate of heat loss (proportional to the gradient at the surface of the wire) would also be doubled. A generalization of this reasoning leads to Eq. (2). It may be noted that, since air is neither incompressible nor inviscid, this result is indicative only.

The accuracy of the empirical formulas for $f(V)$ arrived at experimentally by various authors is not sufficient for our purposes, and it is necessary to find $f(V)$ for each wire used by calibration in a wind tunnel.

The hot-wire material used is unplated tungsten wire with a measured diameter of 0.00885 mm. and a mass of 0.234 mg. per 200-mm. length. The resistivity at room temperature is of the order of 8.2×10^{-6} ohm-cm., the deviation from the handbook value of 5.5×10^{-6} ohm-cm. being due to the drawing process. The temperature coefficient of resistance is 0.0045 per °C., as found experimentally by use of a constant-temperature distilled water bath. At the normal operating current of 100 ma., the current density is 163,000 amp. per sq.cm.; because of this high density, it was necessary to check the validity of Ohm's law, and this was done at various temperatures by means of the water bath. No significant deviation was observed.

(IV) Effect of Temperature Variation Throughout Mass of Wire

Consider first the temperature variation in a direction normal to the axis of the wire. The rate of heat loss from the wire surface is about 0.02 watt; using a surface area of 0.0003 sq.cm. and a coefficient of heat conductivity for tungsten of 0.4 cal. per sec. cm. °C., this heat-loss rate requires a temperature gradient of the order of 40°C. per cm. Since the wire diameter is only 8.85×10^{-4} cm., it is reasonable to assume that the wire temperature is substantially constant in a direction perpendicular to the axis. This assumption is lent further strength by the fact that if any portion of the wire were at a lower temperature, the resistivity of this portion would be correspondingly lower and the current distribution would automatically readjust itself, the result being to increase the temperature of this portion.

Consider now the effect of temperature variation along the length of the wire. It will be assumed that the two ends of the tungsten wire are at air temperature T_A; this assumption has been verified experimentally by measurement of thermal e.m.f.'s.

Assume the heat loss per unit length to be given by

$$H = K_0(T_w - T_A)\phi(M) \tag{3}$$

where K_0 is the thermal conductivity of air; $T_w - T_A$, as before, is the difference between wire and air temperature; M is the rate of mass flow of air; and ϕ is an empirical function of M. Let the wire have length L, area A, and resistivity ρ_A at air temperature T_A. The resistance at T_A is then $R_A = \rho_A(L/A)$. Under operating conditions, the wire temperature T_w will vary along the wire; the resistivity at a particular value of T_w will be given by

$$\rho = \rho_A[1 + \alpha(T_w - T_A)]$$

where α is the temperature coefficient of resistance. The wire resistance will then be given by

$$R = R_A + \frac{\rho_A \alpha}{A}\int_0^L (T_w - T_A)\,dx \tag{4}$$

Since the wire is in equilibrium, the rate at which energy enters an elemental wire portion of length dx must equal the rate at which it leaves; if I is the current and K is the thermal conductivity of tungsten, the resultant equation reads

$$\frac{I^2\rho_A}{A}[1 + \alpha(T_w - T_A)] + AK\frac{d^2T_w}{dx^2} = (T_w - T_A)K_0\phi \tag{5}$$

which may be solved subject to the end conditions $T_w = T_A$ at $x = 0$ and $x = L$ to give

$$T_w - T_A = \frac{I^2\rho_A}{\phi K_0 A - \alpha I^2\rho_A} \times \left(1 + \frac{\sinh r(x - L) - \sinh rx}{\sinh rL}\right) \tag{6}$$

where

$$r^2 = (\phi K_0/AK) - (\alpha I^2\rho_A/A^2K) \tag{7}$$

Numerical values show that $rL \cong 8$ at 150 ft. per sec.; since the e^{-rL} portions of cosh rL and sinh rL are then negligible in comparison with the e^{rL} portions, Eqs. (4) and (6) give

$$R - R_A = \frac{I^2\rho_A\,\alpha\,R_A}{A^2Kr^2}\left(1 - \frac{2}{rL}\right) \tag{8}$$

which is a cubic in r. To find ϕ, the value of r as obtained from Eq. (8) is merely substituted in Eq. (7).

The energy lost through the ends of the wire may be found by

$$2KA\left.\frac{dT_w}{dx}\right]_{x=0} \cong I^2\rho_A\frac{2}{rL} \tag{9}$$

For a typical wire at 150 ft. per sec., the value of ϕK_0 is 4.36×10^{-3} watts per cm. °C., and $r = 61.6$ per cm. Then Eq. (11) gives the rate of heat loss through both ends as about 23 per cent of a total energy delivery of 0.01919 watt.

(V) Corrections for Change in Conditions

Even after elimination of contact resistance, provision of better air filtering to reduce the effect of dirt collection, implementation of the various circuit changes previously discussed, and consideration of local air temperature, the wire potential was still subject to erratic and sometimes frequent changes in potential, usually in the direction of an increase. Discriminatory experiments showed that the cause of this effect—other than the easily corrected for dirt collection—was a combination of oxidation and plastic flow; it therefore became desirable to develop a rapid correction technique to account for these processes.

Essentially, the method of correction for oxidation and plastic flow is to designate a certain set of conditions as standard and to then calculate what a given reading would be under these conditions.

In the following, standard conditions, to which all observations must be reduced, will be denoted by the subscript "1." Thus, at standard conditions, the air temperature will be denoted by T_{A1}, the wire resistance at T_{A1} will be R_{A1}, and the wire will have length L_1 and diameter D_1. Then Eq. (8) will read

$$R_1 - R_{A1} = \frac{I_1^2\rho_{A1}\alpha R_{A1}}{\phi K_{01}A_1 - \alpha I_1^2\rho_{A1}}\left(1 - \frac{2}{r_1L_1}\right) \tag{10}$$

For the same mass flow rate M, but under a new nonstandard condition that will be indicated by subscript "2" (e.g., due to plastic flow, wire length is now L_2, etc.), Eq. (8) will read

$$R_2 - R_{A2} = \frac{I_2^2\rho_{A2}\alpha R_{A2}}{p\phi K_{02}A_2 - \alpha I_2^2\rho_{A2}}\left(1 - \frac{2}{r_2L_2}\right) \tag{11}$$

where the heat loss rate ϕ has been replaced by $p\phi$ because of the modifying influence of the change in diameter from D_1 to D_2 (due to oxidation and plastic flow) on the heat-loss rate. The factor p is close to unity, for otherwise the wire resistance would change much more drastically than measurements indicate.

If the wire was subject to plastic flow without oxidation, there would be no change in volume; because of possible oxidation,

$$L_1D_1^2 = qL_2D_2^2 \tag{12}$$

where q is also close to unity. The air-temperature resistances are connected by

$$R_{A2} = R_{A1}\frac{L_2}{L_1}\frac{D_1^2}{D_2^2}\left[1 + \alpha(T_{A2} - T_{A1})\right] \tag{13}$$

Using Eq. (12), Eq. (13) may be written

$$\frac{L_2}{L_1} = \left\{\left(\frac{R_{A2}}{R_{A1}}\right)\left(\frac{1}{q[1 + \alpha(T_{A2} - T_{A1})]}\right)\right\}^{1/2} \tag{14}$$

Combining Eqs. (10) and (11) so as to eliminate $\phi(M)$ and using Eq. (14) to put L_2/L_1 in terms of R_{A2}/R_{A1}, some algebraic manipulation yields

$$R_1 = \left(R_2\frac{R_{A1}}{R_{A2}}\right)\frac{\left[1 - S\left(\frac{I_1}{I_2}\right)^2\frac{2}{r_1L_1}\right] + \frac{R_{A2}}{R_2}\left[S\left(\frac{I_1}{I_2}\right)^2\frac{2}{r_1L_1} - \frac{2}{r_2L_2}\right]}{\left[S\left(\frac{I_1}{I_2}\right)^2 - \frac{2}{r_2L_2}\right] + \frac{R_2}{R_{A2}}\left[1 - \left(\frac{I_1}{I_2}\right)^2 S\right]} \tag{15}$$

where

$$S = \frac{K_{02}p}{K_{01}\,q^{1/2}}\left[1 + \alpha(T_{A2} - T_{A1})\right]^{-1/2}\left(\frac{R_{A2}}{R_{A1}}\right)^{1/2} \tag{16}$$

For generality, I_1 and I_2 have until now been assumed different. Almost always, however, $I_1 = I_2$; using the fact that $S \cong 1$ and $1/r_1L_1 \cong 1/r_2L_2$, Eq. (15) then reduces to (approximately)

$$R_1 = R_2\,(R_{A1}/R_{A2}) \tag{17}$$

If the conditions "subscript 2" and "standard" are considerably different, Eq. (15) may be used directly (q alone is unknown; may be set = 1). However, Eq. (17) is almost always sufficiently accurate. Since e.m.f.'s rather than resistance are measured, define $E_1 = R_1I_1$, etc.; then Eq. (17) becomes

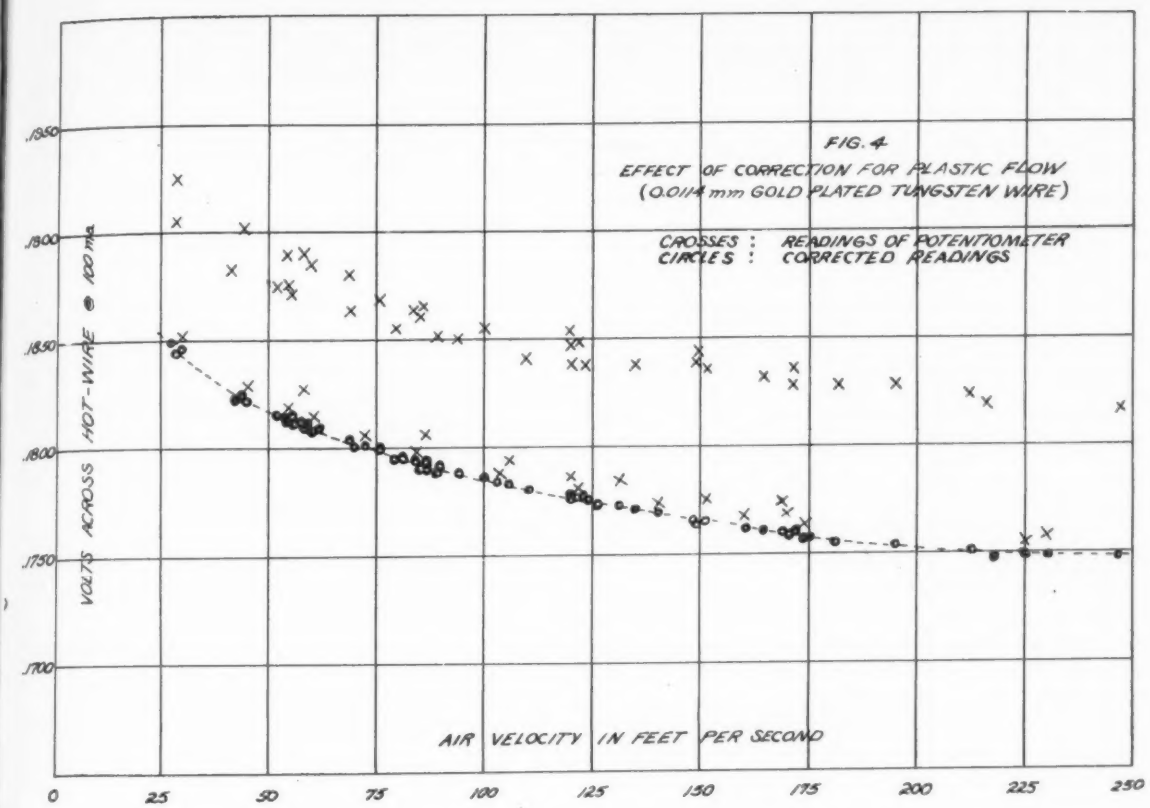

FIG. 4
EFFECT OF CORRECTION FOR PLASTIC FLOW
(0.0114 mm GOLD PLATED TUNGSTEN WIRE)

CROSSES : READINGS OF POTENTIOMETER
CIRCLES : CORRECTED READINGS

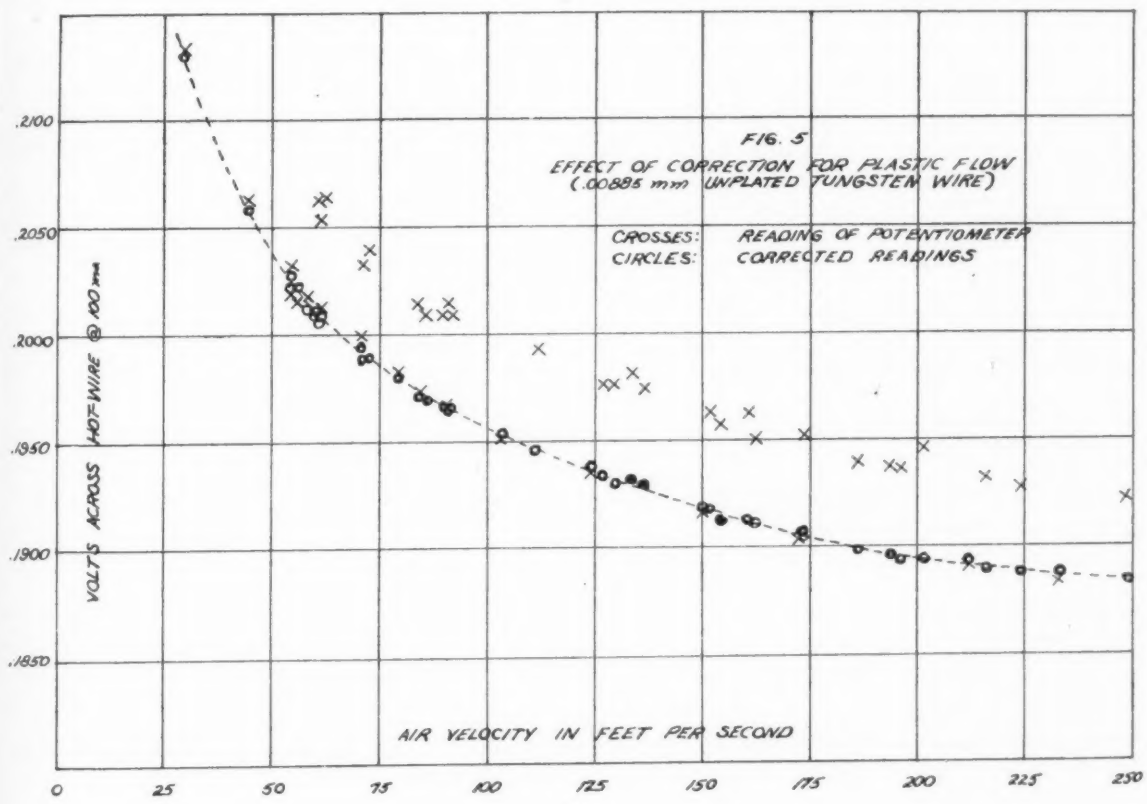

FIG. 5
EFFECT OF CORRECTION FOR PLASTIC FLOW
(.00885 mm UNPLATED TUNGSTEN WIRE)

CROSSES: READING OF POTENTIOMETER
CIRCLES: CORRECTED READINGS

$$E_1 = E_2(E_{A1}/E_{A2}) \tag{18}$$

(Of course, E_1, etc., are less than the measured e.m.f.'s by the voltage drop across the previously mentioned 2 cm. of needle supports. However, for rapidity of calculation, the e.m.f.'s of Eq. (18) may be replaced by the actually measured e.m.f.'s without appreciable error.)

An example may clarify the method. Suppose that a potential reading of 0.1972 volt is obtained at 150 ft. per sec. at an air temperature of 21.7°C. The resistance at this air temperature is 1.673 ohms. Standard conditions for this wire are chosen as $T_{A1} = 20°C.$, $R_{A1} = 1.650$ ohms. $I_1 = I_2 = 0.1$ amp.; then E_1 is given by Eq. (18)

$$E_1 = 0.1972\ (0.1650/0.1673) = 0.1945$$

In order to check the correction theory described above, a large number of tests were carried out under widely varying conditions. Two typical curves are shown in Figs. 4 and 5. Both curves include measurements taken over a 3-day period, the wire being occasionally cleaned and washed. It will be noticed that most of the experimental results lie above the corrected values; this is because the initial resistance of the wire was used as a basis for the corrected curve and the resistance gradually increased with time. In general, the resistance varies sufficiently slowly that it need be measured only every 10 min. or so; its value at intermediate times may be obtained by linear interpolation (taking into account air temperature, of course).

(VI) Variable Airflow

As before, subscripts "1" and "2" will refer to standard and test conditions, respectively. Let c be the specific heat of tungsten (joules per Gm. per °C.) and σ its density. Then, for an elemental portion of the hot-wire, of length dx, the rate of accumulation of energy is

$$(A_2\,dx)\sigma c(\partial T_{w2}/\partial t)$$

where $\partial T_{w2}/\partial t$ is the time rate of change of temperature of this portion. Equating this rate of accumulation to the difference between rates of input and loss of energy gives

$$A_2\sigma c\,\frac{\partial T_{w2}}{\partial t} = I_2^2\frac{\rho_2}{A_2} + KA_2\,\frac{\partial^2 T_{w2}}{\partial x^2} - K_{02}p\phi\,[M(t)]\,(T_{w2} - T_{A2}) \tag{19}$$

where the notation $\phi[M(t)]$ means that ϕ depends on the mass flow rate M, which in turn depends only on the time t—i.e., the scale of the fluctuation is large in comparison with the wire size.

Integration of Eq. (19) with respect to x yields

$$A_2\sigma c\,\frac{\partial}{\partial t}\int_0^{L_2} T_{w2}\,dx = I_2^2\,R_2 + KA_2\,\frac{\partial T_{w2}}{\partial x}\Bigg]_0^{L_2} - K_{02}p\phi\int_0^{L_2}(T_{w2} - T_{A2})\,dx \tag{20}$$

Using $T_{w2} - T_{A2} = (\rho_2 - \rho_{A2})/\rho_{A2}\alpha$, Eq. (20) becomes

$$\frac{A_2\sigma c}{\rho_{A2}}\,\frac{\partial R_2}{\partial t} = I_2^2R_2 + KA_2\,\frac{\partial T_{w2}}{\partial x}\Bigg]_0^{L_2} - \frac{K_{02}p\phi A_2}{A\rho_2\alpha}\,(R_2 - R_{A2}) \tag{21}$$

The term

$$KA_2\,\frac{\partial T_{w2}}{\partial x}\Bigg]_0^{L_2}$$

represents the instantaneous heat-loss rate through the ends of the wire. Now, the quantities R_2, T_{w2}, and ϕ may each be written as the sum of a steady component (denoted by subscript "0") and a fluctuating component (denoted by a prime)

$$\left.\begin{aligned} R_2 &= R_{20} + R_2' \\ T_{w2} &= T_{w20} + T_{w2}' \\ \phi &= \phi_0 + \phi' \end{aligned}\right\} \tag{22}$$

Substituting Eqs. (22) into Eq. (21) gives

$$\frac{A_2^2\sigma c}{\rho_{A2}\alpha}\,\frac{\partial R_2'}{\partial t} = I_2^2\,(R_{20} + R_2') - 2KA_2\,\frac{\partial}{\partial x}\,(T_{w20} + T_{w2}')]_{x=0} - \frac{K_{02}p(\phi_0 + \phi')A_2}{\rho_{A2}\alpha}\,(R_{20} + R_2' - R_{A2}) \tag{23}$$

Taking mean values by integrating Eq. (23) in time from 0 to τ and dividing by τ gives, after using

$$\int_0^\tau \frac{\partial R_2'}{\partial t}\,dt = R_2'(\tau) - R_2'(0)$$

and allowing τ to approach

$$0 \quad {}_2^2R_{20} - 2KA_2\,\frac{\partial}{\partial x}\,(T_{w20})]_{x=0} - \frac{K_{02}p\phi_0A_2}{\rho_{A2}\alpha}\,(R_{20} - R_{A2}) \tag{24}$$

where the averaging process carried out for the last term on the right-hand side is permissible only if R_2' is extremely small in comparison with $R_{20} - R_{A2}$; for the present, this is assumed.

Substitution of Eq. (24) into Eq. (23) gives

$$\phi' = \frac{-2KA_2\frac{\partial}{\partial x}(T_{w2}')]_{x=0} - \frac{A_2{}^2\sigma c}{\rho_{A2}\alpha}\frac{\partial R_2'}{\partial t} - \frac{K_{02}p\phi_0 A_2}{\rho_{A2}\alpha}R_2' + I_2{}^2R_2'}{(K_{02}pA_2/\rho_{A2}\alpha)\,(R_{20} + R_2' - R_{A2})} \tag{25}$$

With no greater error than about 2 per cent, the denominator may be simplified by neglecting R_2' with respect to $R_{20} - R_{A2}$; then, using Eq. (24) again gives

$$\frac{K_{02}\phi'}{K_{02}\phi_0} = \frac{-2KA_2\frac{\partial T_{w2}'}{\partial x}\Big]_{x=0} - \frac{A_2 2\sigma c}{\rho_{A2}\alpha}\frac{\partial R_2'}{\partial t} - \frac{K_{02}p\phi_0 A_2}{\rho_{A2}\alpha}R_2' + I_2{}^2R_2'}{I_2{}^2R_{20} - I_2{}^2R_{A2}\,(2/r_{20}L_2)} \tag{26}$$

It is now necessary to examine the numerical magnitudes of the various quantities involved. From experiment, the denominator has a magnitude of the order of 0.015 watt, $p \cong 1$, $R_2' \cong 4 \times 10^{-3}$ ohms, $K_{02}\phi_0 \cong 4 \times 10^{-3}$ watts per cm. °C., $A_2/\rho_{A2} = 0.07$ cm. per ohm, and $\alpha = 0.0045$ per °C. Then,

$$(K_{02}p\phi_0 A_2/\rho_{A2}\alpha)R_2' \cong 0.0003 \text{ watt}$$

which is sufficiently small in comparison with the denominator that it may be omitted from Eq. (26), for the variations in $K_{02}\phi'/K_{02}\phi$ of interest in this report are of the order of 0.2. Writing

$$\frac{\partial}{\partial x}(T_{w2}')]_{x=0} = \frac{1}{\alpha\rho_{A2}}\frac{\partial}{\partial x}\rho_2'$$

where, as before, $\rho_2 = \rho_{20} + \rho_2'$, it may be reasonably expected that the order of magnitude of

$$\frac{1}{\alpha\rho_{A2}}\frac{\partial}{\partial x}\rho_2'\Big]_{x=0} \cong \frac{1}{\alpha\rho_{A2}\,(L/2)}\rho_2'\left(\frac{L}{2}\right) \cong \frac{2R_2'}{\alpha R_{A2}} \cong 1$$

therefore the first term in the numerator has a magnitude of about 10^{-6} and may consequently be neglected. The result is

$$\frac{K_{02}\phi'}{K_{02}\phi} = -\frac{(A_2{}^2\sigma c/\rho_{A2}\alpha)\,(dR_2'/dt)}{I_2{}^2R_{20} - I_2{}^2R_{A2}\,(2/r_{20}L_2)} \tag{27}$$

$K_{02}\phi'$ and $K_{02}\phi_0$ may now be put in terms of the standard resistance R_1. From Eq. (8),

$$\frac{\phi_0 + \phi'}{\phi_0} = \frac{[R_{A1}/(R_1 - R_{A1})]\,[1 - (2/r_1L_1)] + 1}{[R_{A1}/(R_{10} - R_{A1})]\,[1 - (2/r_{10}L_1)] + 1}$$

which may be solved for R_1 to give

$$R_1 = R_{A1} + \frac{R_{A1}\,[1 - (2/r_1L_1)]}{\frac{R_{A1}}{R_{10} - R_{A1}}\left(1 - \frac{2}{r_{10}L_1}\right) + \frac{\phi'}{\phi_0}\left[1 + \frac{R_{A1}}{R_{10} - R_{A1}}\left(1 - \frac{2}{r_{10}L_1}\right)\right]} \tag{28}$$

Substituting for ϕ'/ϕ_0 from Eq. (27), Eq. (28) may be written

$$R_1 = R_{A1} + (R_{10} - R_{A1})\left(\frac{1 - \frac{2}{r_1L_1}}{1 - \frac{2}{r_{10}L_1}}\right)\frac{1}{\left\{1 - \frac{\frac{A_2{}^2\sigma c}{\alpha\rho_{A2}}\frac{dR_2'}{dt}\left[\frac{R_{10} - R_{A1}(2/r_{10}L_1)}{R_{A1} - R_{A1}(2/r_{10}L_1)}\right]}{I_2{}^2R_{20} - I_2{}^2R_{A2}\,(2/r_{20}L_2)}\right\}} \tag{29}$$

Because of the magnitudes of the various terms involved, the use of only the first term on the Taylor expansion of Eq. (29) will not result in substantial error.

Further, since r depends on the square root of ϕ, the difference between $2/r_1L_1$ and $2/r_{10}L_1$ is small for the velocity changes under consideration and may be neglected

$$R_1 \cong R_{10} + \left[\frac{R_{10} - R_{A1}}{I_2{}^2R_{20} - I_2{}^2R_{A2}\,(2/r_{20}L_2)}\right]\left(\frac{A_2{}^2\sigma c}{\rho_{A2}\alpha}\right)\left[\frac{R_{10} - R_{A1}\,(2/r_{10}L_1)}{R_{A1} - R_{A1}\,(2/r_{10}L_1)}\right]\frac{dR_2'}{dt} \tag{30}$$

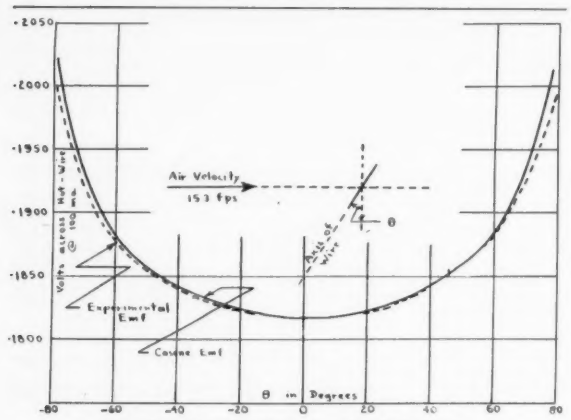

FIG. 6. Examination of cosine behavior.

If C is the total specific heat of the wire in joules per °C., then

$$c = A_2^2 \sigma c R_{A2}/\rho_{A2} \tag{31}$$

The reason for the differentiating circuit is now clear. Because of the differentiation, the oscilloscope deflection is proportional to de_2'/dt and from a knowledge of the constant of proportionality and by use of Eq. (30), the instantaneous value of the standard resistance may be calculated and, therefore, also the corresponding instantaneous mass flow rate. Since the curve of Fig. 5 is fairly flat, the oscilloscope deflection is approximately proportional to the velocity fluctuation, and this fact may be used whenever it is necessary to calculate approximately a large number of velocity patterns.

In the previous analysis, it was tacitly assumed that the rate of heat loss H of steady flow may be used in cases of variable airflow. This is true only if the heat gradient field is set up around the wire rapidly in comparison with the velocity fluctuation rates; an order-of-magnitude analysis shows this to be probably true for the flow behind the axial compressor. However, there exists a method of experimentally checking the above assumption; such a check will be described shortly.

It may also be noted that the current is not quite steady because of the variation in hot-wire resistance; however, an easy calculation shows the effect to be negligible.

Because of the relatively minor change in slope of the potential-velocity curve as the wire flows plastically [see Eq. (12)], a wire may be used indefinitely for the measurement of velocity fluctuation without recalibration.

Further refinements in the theory are possible; for example, the fact that the thermocouple reads only the mean temperature of a steady flow could be considered. If it is assumed that the air is adiabatically compressible, the temperature fluctuation corresponding to any velocity fluctuation could be calculated and incorporated into the analysis is straightforward and will not be included here, since it is of little importance for the subsonic flows of present interest.

It should be emphasized that, in distinction to the case of turbulence analysis, the preceding analysis holds for large velocity fluctuations (of the order of the main-stream velocity).

(VII) Angular Variation

In the preceding analysis, the axis of the hot-wire has been assumed perpendicular to the direction of the air stream. In practice, of course, this is not the case; if the angle between the normal to the wire axis and the air-stream direction is denoted by θ, then it seems reasonable that the velocity component parallel to the wire have little cooling effect, so that the wire resistance corresponds to a velocity of $V \cos \theta$. Various experimenters have checked this and found good agreement for θ less than about 70°.

In the measurement of mean velocities, this approximation is not sufficiently accurate, and it is necessary to calibrate each wire. A typical test is shown in Fig. 6; the dotted line represents the e.m.f. that the wire would indicate on the basis of the cosine hypothesis, and the solid line passes through the experimental results. It will be noted that, as expected, the wire is cooled slightly more than by the amount predicted on the cosine hypothesis.

Since the hot-wire responds (approximately) only to that velocity component perpendicular to its axis, the magnitude and direction of a given air stream may be determined by merely orienting the hot-wire axis along each of three noncoplanar directions. The trigonometry is straightforward—e.g., if the directions are mutually perpendicular, it is easy to show that the square of the magnitude of the velocity is given by one-half the sum of the squares of the three velocity components perpendicular to the axis. In accurate work, a two-step procedure is necessary, as to the approximate angles of incidence must first be calculated on the assumption that the correction due to the deviation from the cosine law is zero; given these angles, the exact correction may be obtained from the calibration curve (as in Fig. 6).

If the flow is two-dimensional—as it is approximately, behind the rotor of an axial compressor—then the hot-wire e.m.f.'s obtained by placing the wire axis in each of two mutually perpendicular directions, each in the plane of the flow, will give the two-velocity component directly. (The two-dimensionality of the flow may be checked by comparing predicted and observed e.m.f.'s at other orientations.)

The above remarks hold for both the average and the instantaneous components of air velocity. If the fluctuations repeat themselves—as again happens in an axial compressor—then the two components of velocity fluctuation may be photographed in sequence; other-

wise, two simultaneous photographs are necessary, and these may be obtained by the use of two perpendicular hot-wires.

(VIII) Measurement of Average Velocity

Even after compensation for plastic flow and air-temperature changes, several difficulties remain in the measurement of average velocities. The most annoying of these are the collection of heat-insulating dirt on the wire and changes in the thermal conductivity of air (due, for example, to the presence of oil vapor). If an absolute measurement of the average velocity at any point is required, special precautions must be taken (for example, the wire may be inserted with its axis parallel to the air stream so as to collect no dirt; when a velocity reading is required, the wire is then rotated into the correct orientation and held there a few seconds). A typical measurement (carried out with only average care) is shown in Table 1. Here the velocities (feet per second) in the right-hand columns are calculated from the hot-wire readings at $\theta = 0°$ and $90°$ (as before, θ is the angle between the air stream direction and the normal to the hot-wire axis). These readings were taken about $^1/_4$ in. behind the rotor of a single-stage axial compressor. The corresponding pressure probe reading for $\theta = 0°$ was 169 ft. per sec.

In some applications, the presence of airflow fluctuations will affect the average velocity reading. This is because of the fact that, in averaging Eq. (23), the last term is given correctly by Eq. (24) only if R_2' is extremely small, for, in general, the average of a product is not the product of the averages. This difficulty may again be removed by the use of a two-step averaging process, in which the average velocities are calculated in the ordinary way, the fluctuation velocities then being calculated as to be described. Knowing these fluctuation velocities, the corrections to average velocity may be obtained from Eq. (23). To date, this procedure has not been found necessary in compressor studies.

The most common use of the hot-wire instrument to the present has been the carrying out of traverses of axial and tangential velocities across compressor passages. A convenient method for doing this is to choose one point in the passage as a reference point and continually to refer e.m.f.'s to the e.m.f. experienced at this point. Even though the level of the e.m.f. at this point will change because of dirt collection, etc., the slope of the e.m.f.-velocity curve changes only slowly, and relative velocities may therefore be measured accurately without any special precautions. This "slope method" results in a velocity profile across the passage; the height of the profile is then obtained by continuity (the total flow being assumed known).

Table 1

θ	Measured Velocity	Calculated Velocity
0	171	...
30	188	191
45	182	184
60	158	162
90	88	...

(IX) Measurement of Velocity Fluctuations

As indicated previously, a knowledge of the average velocities will permit calculation of the instantaneous velocity value from a photograph of the (amplified) differentiated voltage across the hot-wire. Before Eq. (30) can be used, the value of the specific heat C must be determined and the amplifications and phase shifts of the amplifier and oscilloscope amplifier must be known.

The value of C may be found either by calculation from the physical dimensions of the wire or by carrying out an experiment in which the wire is placed in a steady air stream and an alternating current superposed on the heating current. Both methods have been used with fair agreement; in general, the calculation method is probably the more accurate. For the wire used in finding the velocity patterns to be discussed, the value of $c/\alpha R_{A2}$ was 2.71×10^{-5} joules per ohm.

In order to eliminate phase shift in the external amplifier and in the oscilloscope amplifier, direct-coupling is necessary (i.e., no coupling condensers can be used). The differentiation is obtained by use of the well-known

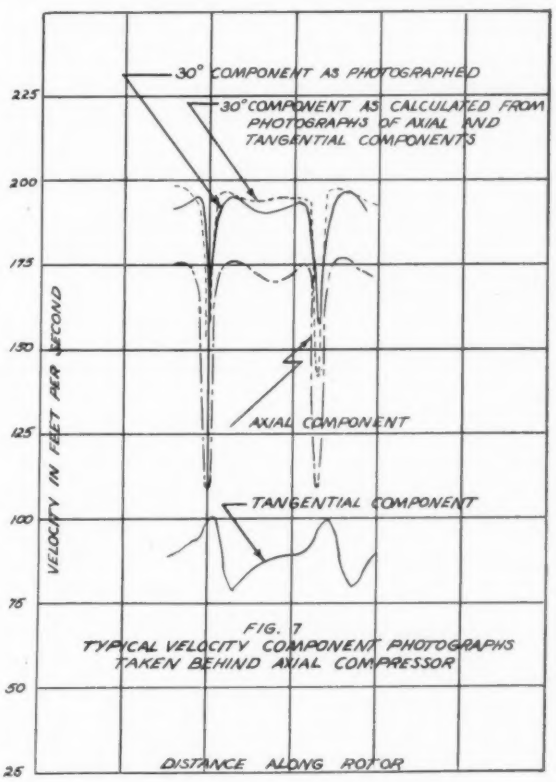

FIG. 7
TYPICAL VELOCITY COMPONENT PHOTOGRAPHS TAKEN BEHIND AXIAL COMPRESSOR

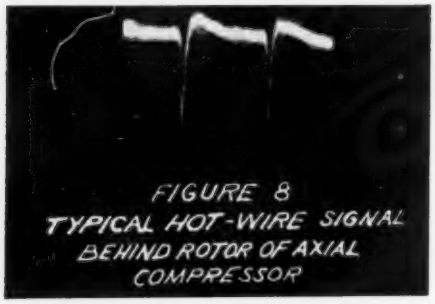

FIGURE 8
TYPICAL HOT-WIRE SIGNAL
BEHIND ROTOR OF AXIAL
COMPRESSOR

capacity-resistance circuit; other circuits may, of course, be substituted. The attenuation due to the differentiating circuit must be included in the calculation of the overall amplification.

The results of a typical experiment are shown in Fig. 7; the photographs (tracings being reproduced) were taken with the hot-wire behind the rotor of an axial compressor. Each minimum in the axial velocity component corresponds to the passage of a blade. Knowing the axial and tangential components, the velocity pattern for $\theta = 30°$ may be calculated; the result is compared with the experimental pattern for $\theta = 30°$. The reasonable agreement lends support to the fundamental assumptions of the analysis.

As only the alternating component of hot-wire voltage is presented on the oscilloscope screen, hot-wire probes without separate potential leads are quite satisfactory for use in obtaining velocity fluctuations.

There are some cases (e.g., passage of a rotor blade wake) in which the instantaneous value of θ falls outside the 70° range; in such cases the cosine law fails to apply and an obvious two-step calculation technique must again be applied.

As an example of the degree of resolution obtained in practice, a typical photograph of axial velocity variation is reproduced in Fig. 8.

(X) General Remarks

Although considerable experimental technique and experience are necessary for efficient operation of the hot-wire, the results obtained from it are quite satisfactory. Even without the preceding quantitative theory, the knowledge of the effect of the differentiating circuit allows rapid and fruitful qualitative surveys of airflows to be made; such surveys are particularly useful in the understanding of such phenomena as compressor surging (pulsation).

For brevity, many of the experimental checks carried out on the theory are not recorded here. For example, the effect of a change in hot-wire heating current is almost exactly as predicted. The compensation method has so far not been found in error even over periods of a year.

The use of hot-wires in high-speed flows (up to 700 ft. per sec.) requires no new theory, except for obvious effects of compressibility; the details are therefore omitted.

Some further hot-wire possibilities may be suggested. If a high-frequency square wave of heating current were used and the two portions of the response were separated by a gate circuit, enough evidence would be present for the calculation of both temperature and velocity; if a more oxidation-resistant material than tungsten could be found, such an instrument might be useful in combustion studies. Alternatively, it is possible to construct a hot-wire that will give an accurate (but not continuous) measurement of the instantaneous velocity without the use of our assumption concerning rate of heat loss. Suppose a wire to be initially unheated and at a certain instant apply to it a fixed heating current. Then the rate at which energy accumulates in the wire depends only on the instantaneous air velocity (provided the air temperature is known); therefore the initial rate of rise of wire resistance is a measure of the instantaneous air velocity. The necessary data for use of this instrument would, of course, be obtained by calibration in steady flow.

Air Drag on Cubes at Mach Numbers 0.5 to 3.5*

GEORGE E. HANSCHE† AND JOHN S. RINEHART‡

New Mexico School of Mines

ABSTRACT

The air drag on two sizes of steel cubes, 1/4 and 3/8 in., has been carefully determined in the approximate range from Mach 0.5 to 3.5. In general, the results are consistent and in substantial agreement with similar data obtained by Charters and Thomas on spheres. The present data do not yield an explicit value of the drag coefficient C_D but rather an average value of the quantity C_DA for a rotating cube where A is proportional to the area of the cube. An "average" value for A of $1.50d^2$, where d is the length of one edge of the cube, is assumed and C_D is calculated. The two sizes of cubes give essentially equal values for C_D at corresponding Mach Numbers.

INTRODUCTION

KNOWLEDGE OF THE AERODYNAMIC BEHAVIOR of a missile having a cubical shape is of considerable practical importance in connection with certain ordnance problems. The present study was made in order to obtain an experimental value for the drag coefficient of a cube in flight as a function of Mach Number. The air drag on two sizes of steel cubes, 1/4 and 3/8 in., has been carefully determined in the approximate range from Mach 0.5 to 3.5.

EXPERIMENTAL

The general experimental procedure used to determine the drag coefficients was somewhat similar to that used by Charters and Thomas[1] for spheres with the exception that spark photographs of the cubes were not taken.

The 1/4- and 3/8-in. cubes were fired one at a time from smooth-bore 30- and 50-cal. guns, respectively. No sabots were used in launching them, except at the highest velocities when a small rag wad was placed just behind them. The 3/8-in. cubes were fired at several velocities ranging from about 600 to about 4,000 ft. per sec.; the 1/4-in. cubes were fired over the range from 400 to 3,500 ft. per sec. The highest velocity in each case was the maximum obtainable by this method of firing. The data from 19 3/8- and 26 1/4-in. cubes were used in the drag calculations.

A six-spark Aberdeen chronograph, which had six grid stations spaced at 25-ft. intervals, was used to obtain a distance-time trace for each cube. The grids were 30 in. square and consisted of two sheets of 0.001-in. aluminum foil spaced slightly less than 1/4 in. apart and separated by a sheet of crepe paper. This type of grid proved the most satisfactory of a number of types tried. The amount that the grids retarded the cubes was measured by suspending a grid on a ballistic pendulum and firing a cube through it.

The velocity lost by a 1/4-in. steel cube in passing through the grid was found to be about 3 ft. per sec. In calculating the present results, this error was neglected since it is considerably less than other probable errors.

The masses of all cubes were kept within 1 per cent of one another. One dimension of the 1/4-in. cubes differed by about 0.003 in. from the other two dimensions. The uncertainty in area for the steel cubes was less than 2 per cent. Recovery of several cubes after firing showed that the loss in mass due to travel through the gun barrel was negligible, although the corners of the cubes in most cases were rolled over slightly.

RESULTS

The calculation of drag, from chronograph readings, is subject to certain inaccuracies and approximations that have been adequately discussed by Charters and Thomas.[1] The manner in which the present data were reduced is described below.

The differential equation of the forward motion of a body through air may be written in the form

$$m(dv/dt) = -C_D\rho Av^2/2 \qquad (1)$$

where m is the mass of the body, ρ is the density of the air, v is the velocity of the body in motion, A is its presentation area, and C_D is the drag coefficient. A solution of the above equation is

$$v = v_0e^{-C_D(\rho/2)(A/m)(x-x_0)} \qquad (2)$$

where v is the velocity at the point x and v_0 is the velocity at x_0.

It is obvious that the values both of C_D and of A will depend upon the orientation of the cube. The presentation area of a cube may vary by a factor of 1.73. The shape of this presented area may be flat, wedgelike, or

Received February 27, 1951.

* The authors wish to acknowledge the continual interest shown by Dr. E. J. Workman and the numerous helpful suggestions made by him throughout the course of the investigation, as well as the financial support from the Bureau of Ordnance, Navy Department, which made this work possible.

† Formerly, Senior Physicist, Research and Development Division. Now at Sandia Corporation, Albuquerque, N.M.

‡ Formerly, Head Physicist, Research and Development Division. Now, Head, Mechanics Branch, Naval Ordnance Test Station, China Lake, Calif.

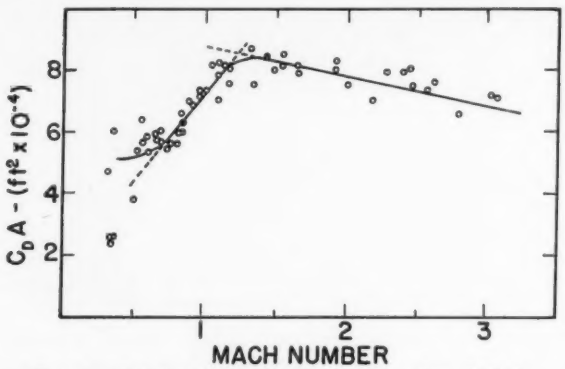

FIG. 1. C_DA for $^1/_4$-in. steel cube as a function of Mach Number.

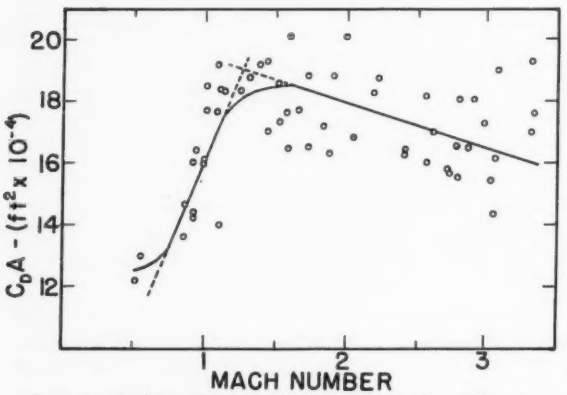

FIG. 2. C_DA for $^3/_8$-in. steel cube as a function of Mach Number.

nearly conical. No precautions were taken to prevent rotation of the cubes, and examination of the holes made by them in the chronograph grids showed that they rotated. Hence, the present data were not expected to yield explicit values for C_D and A but rather an average value of the quantity, C_DA, for a rotating cube. If it is assumed that A is a sort of average value of area which is proportional to the square of one side of the cube, then an average value of C_D may be calculated by arbitrarily choosing a value for the proportionality constant.

In calculating values of C_DA, the difference, $(x - x_0)$, was taken to be 25 ft. Information from three consecutive grids was used. The average velocities of the cube during its travel from the first to the second grid and during its travel from the second to the third grid were calculated from the chronograph time-distance trace. These values were substituted for v_0 and v, respectively, in Eq. (2), and C_DA was calculated. Thus, each six-point trace yielded four values of C_DA.

The values of C_DA so obtained for $^1/_4$- and $^3/_8$-in. cubes are plotted in Figs. 1 and 2, respectively, against the midpoint of the average velocities used in obtaining them.

If it is assumed that the scatter of the points is due to the area and shape variations mentioned above, the average values of C_D for the two sizes of cubes should be equal. Values of C_D, calculated using one and one-half times the area of one face of the cube as the "average" presentation area, are plotted against Mach Number in Fig. 3. Agreement between the two sets of values is seen to be good. Use of the data to predict the behavior of cubes of sizes other than $^1/_4$ and $^3/_8$ in. seems justified.

The general form of the C_D curve follows closely that of the curve for spheres obtained by Charters and Thomas.[1] The transition from subsonic to supersonic takes place over a relatively wide range of velocities as is the case with spheres. There is no abrupt change as the cube reaches the velocity of sound. The curve begins to rise at about Mach 0.6 and begins to start down at about Mach 1.4. The Charters and Thomas curve for a sphere behaves similarly at substantially the same points.

In passing through the transonic region C_D increases from about 0.84 to 1.26 or, percentagewise, about 50 per cent. This increase is considerably less than that for spheres, where C_D increases by about 100 per cent. The scarcity of points in the subsonic region makes the 0.84 value somewhat uncertain. Moreover, little weight has been given the lowest $^1/_4$-in. cube points since their accuracy is somewhat in doubt. It may be that the subsonic end of the true curve lies lower than the curve drawn in Fig. 3.

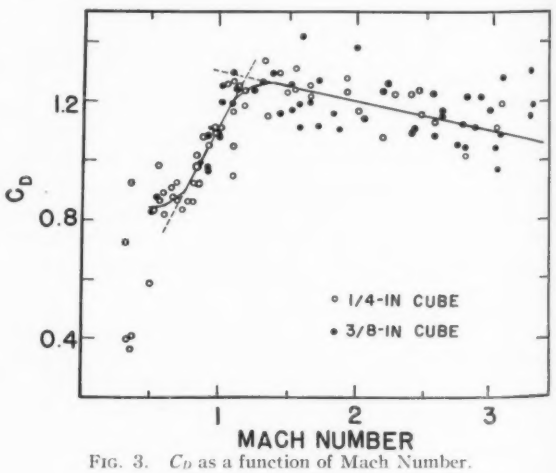

FIG. 3. C_D as a function of Mach Number.

REFERENCE

[1] Charters, A. C., and Thomas, R. N., *The Aerodynamic Performance of Small Spheres from Subsonic to High Supersonic Velocities*, Journal of the Aeronautical Sciences, Vol. 12, No. 4, p. 468, October, 1945.

On Unsteady Nonlinearized Conical Flow*

S. F. BORG†

U.S. Naval Postgraduate School

SUMMARY

It is shown that the equations of unsteady, nonlinear, nonviscous, nonheat-conducting flow may be put in a conical form. The problem of a shock striking an infinite wedge is considered. An invariance relation is established, and certain properties of the reflected shock are examined. These include a discussion of a possible form of reciprocal flows; a calculation indicating the impossibility of a certain reflected shock shape for air; and, based upon an analysis of the characteristics of the flow, a nonexistence proof for certain combinations of shock strengths and wedge angles.

SYMBOLS

0	= subscript designating ahead of incident shock
1	= subscript designating behind incident shock
2	= subscript designating behind reflected shock
a	= velocity of sound
p	= pressure
x, y, t	= physical plane and time coordinates
u, v	= flow velocity components in the physical plane
I	= letter designating incident shock
M	= Mach Number
$\mathfrak{M}$	= letter designating Mach reflection shock
Q	= reduced velocity $(u - \xi, v - \eta)$
R	= letter designating reflected shock
S	= entropy
ss.	= slipstream
$\bar{X}, \bar{Y}, \bar{U}, \bar{V}$	= physical coordinates and velocities referred to a moving origin
α, ω, ω'	= various angular quantities relating to the shock reflection pattern
ρ	= density
θ	= wedge angle
θ_w	= angle between attached wedge shock and horizontal line
ξ	= x/t } conical coordinates
η	= y/t } conical coordinates
$\bar{\xi}$	= p_0/p_1, strength of incident shock

INTRODUCTION

IT WILL BE SHOWN THAT, subject to appropriate conditions, the nonviscous nonheat-conducting time-dependent equations can be given in terms of new variables

$$\xi = x/t, \qquad \eta = y/t$$

The flow equations in this form do not contain the length dimension alone, and in the ξ, η field the flow is represented by a single map that represents the flow at all times. This implies that such time-dependent flow fields grow uniformly with time. If, in addition, the boundary does not specifically contain a length parameter, then in the sense of Lagerstrom's discussion[1] the flow field is conical. The more descriptive phrase for this case—"unsteady conical flow"—is applied to the fields under discussion.

In order to satisfy the conical conditions for the boundary, we will consider the case of a straight shock traveling in an infinite field and striking an infinite wedge (Fig. 1).

The shock reflection phenomena was first considered by Mach.[2] Since 1943, Von Neumann and his coworkers at Princeton have issued various reports[3–11] describing their work on this problem, both theoretical and experimental.

Additional related experimental work has been done by Liepmann[12, 13] and at the University of Michigan.[14]

Von Neumann[3] considered local conditions only, in the neighborhood of the shock intersection. By applying the Rankine-Hugoniot relations across the shocks, with reference to origins at the shock intersections, it was possible to obtain various angular

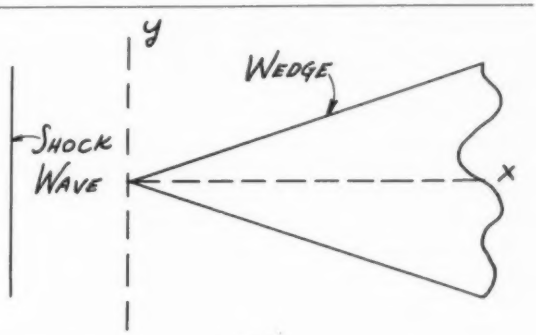

FIG. 1.

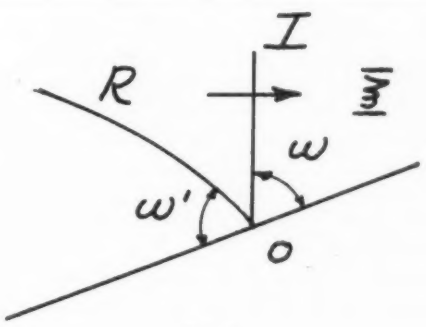

FIG. 2.

Received June 4, 1951.

* The writer wishes to acknowledge many helpful discussions with Dr. Francis Clauser, of The Johns Hopkins University.

† Associate Professor of Aeronautical Engineering. Now, Structures Engineer, Grumman Aircraft Engineering Corporation.

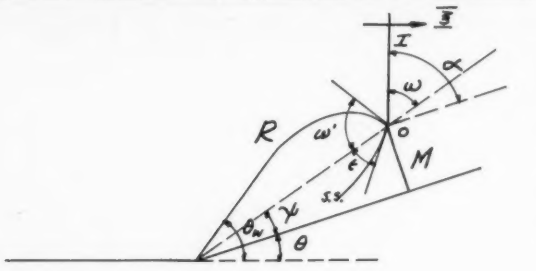

FIG. 3.

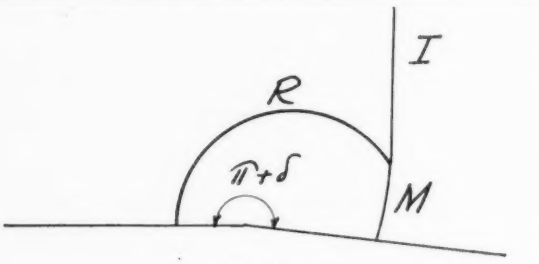

FIG. 4.

relations that must hold. Thus he considered the regular two-shock configuration (Fig. 2) and the Mach reflection, three-shock condition (Fig. 3).

For the case shown in Fig. 2, with respect to the point 0, and for a given shock strength $\bar{\xi}$, the angles ω and ω' can be computed.

For the case shown in Fig. 3, again with respect to point 0, and for a given shock strength $\bar{\xi}$, it is possible to obtain solutions corresponding to the following conditions:[15]

(1) The pressure across the slipstream (ss.) must be continuous.

(2) The velocity of the fluid must be tangential to ss. for flow through the lower (M) shock and also for flow through the upper two (I, R) shocks.

(3) The kinematic, dynamic, and thermodynamic relations across the shocks must be satisfied.

Shock-tube experiments performed by Smith[6] and the photographs he obtained permit an experimental check on the results obtained by Von Neumann and his coworkers. It was found that the two-shock solution angles check fairly well throughout the range of incident shock strengths. However, the three-shock solutions for glancing incidence do not check the experimental data. Bargmann[4] considered the problem of the infinitesimal shock hitting an infinitesimal concave corner, and by showing that, to the approximation considered, the flow is irrotational, he solved the resulting Laplace equation subject to the given boundary conditions.

Lighthill[16, 17] considered the problem from the theoretical point of view and obtained linearized solutions to the following:

(1) A shock of any strength striking a convex corner of angle $\pi + \delta$ with δ small, Fig. 4.

(2) A shock of any strength striking head-on a very nearly plane corner of angle $\pi + \delta$ with δ small, Fig. 5.

In both cases Lighthill shows that, by use of the Busemann conical flow transformation, the pressure field satisfies the Laplace equation. A solution by means of complex variable is then obtained.

More recently, Ting and Ludloff—in a short note in the February, 1951, issue of the JOURNAL OF THE AERONAUTICAL SCIENCES—show a solution for a finite shock hitting a concave wedge of very small angle. The wedge face need not necessarily be a straight line in this linearized analysis. Their solution does not utilize the ξ, η coordinates and is based on a Possio integral.

The present investigation considers the problem from a different point of view than has heretofore been done. The complete nonlinearized form of the equations is considered (although viscosity and heat conduction effects are neglected).

A brief outline of the present investigation follows:

(1) The mathematical equations are obtained in conical form and an invariance relation is established.

(2) It will be shown that a two-shock, attached shock pattern cannot exist for air.

(3) The possibility of obtaining reciprocal flows is discussed.

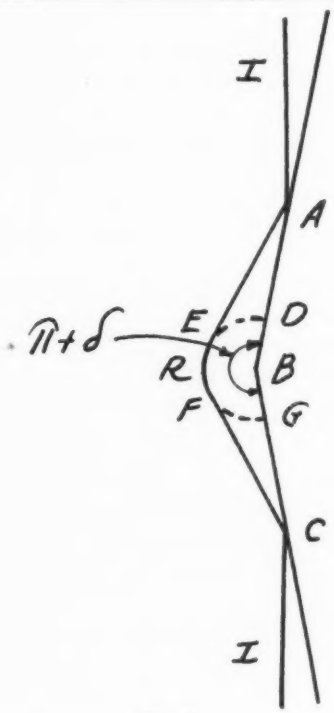

FIG. 5.

(4) The existence of patching curves will be shown which leads to (a) a form of discontinuity in the solutions and (b) a nonexistence for certain flows.

Development of the Equations

We consider the two-dimensional, unsteady nonviscous, nonheat-conducting flow, with

$$u = u(x, y, t), \qquad v = v(x, y, t)$$

Physically, the problem under consideration is a shock striking a (for the present) symmetrical wedge, whose point is at the origin in the x, y plane and which extends to infinity in the positive x, y directions, Fig. 1. If we assume that u and v can be given in terms of the new variables, ξ, η, defined by

$$\begin{aligned} u &= u(x/t, y/t) = u(\xi, \eta) \\ v &= v(\xi, \eta) \end{aligned}$$

then it will be found that our equations are independent of x and y, and because our boundary is also independent of any length parameter, it follows that the flow pattern can be represented in the ξ, η plane. That is, the unsteady pattern will be represented by a single map in the ξ, η plane. The above fact was initially deduced by Von Neumann and has been amply verified experimentally.

The equations governing the flow are conservation of mass

$$\left.\begin{aligned} \rho_t + u\rho_x + v\rho_y + \rho u_x + \rho v_y &= 0 \\ \rho_t + (\rho u)_x + (\rho v)_y &= 0 \end{aligned}\right\} \tag{1}$$

also conservation of momentum

$$(\rho u)_t + (\rho u^2)_x + (\rho vu)_y + p_x = 0 \tag{2}$$

$$(\rho u)_t + (\rho uv)_x + (\rho v^2)_y + p_y = 0 \tag{3}$$

In addition, an equation of state

$$p = p(\rho, S) \tag{4}$$

and if we assume that changes of state are adiabatic (i.e., do not consider a shock or other dissipation inside the field under consideration), then

$$S_t + uS_x + vS_y = 0 \tag{5}$$

so that, corresponding to the five unknowns, u, v, ρ, p, S, we have five equations.

Now, from Eqs. (4) and (5), it follows that

$$\frac{d\rho}{dt} = \left(\frac{\partial \rho}{\partial p}\right)_S \frac{dp}{dt} + \left(\frac{\partial \rho}{\partial S}\right)_p \frac{dS}{dt} \tag{6}$$

and

$$\frac{d\rho}{dt} = \frac{\partial \rho}{\partial t} + u\frac{\partial \rho}{\partial x} + v\frac{\partial \rho}{\partial y} = \left(\frac{\partial \rho}{\partial p}\right)_S \frac{dp}{dt}$$

or

$$\frac{\partial \rho}{\partial t} + u\frac{\partial \rho}{\partial x} + v\frac{\partial \rho}{\partial y} = \frac{1}{a^2}\left(\frac{\partial p}{\partial t} + u\frac{\partial p}{\partial x} + v\frac{\partial p}{\partial y}\right) \tag{7}$$

Therefore, Eq. (1) becomes

$$\frac{1}{a^2}\left[\frac{\partial p}{\partial t} + u\frac{\partial p}{\partial x} + v\frac{\partial p}{\partial y}\right] + \rho\left[\frac{\partial u}{\partial x} + \frac{\partial v}{\partial y}\right] = 0 \tag{8}$$

Now, if we assume $f = f(\xi, \eta)$ only, then

$$\begin{aligned} \frac{\partial}{\partial t} &= \frac{\partial}{\partial \xi}\frac{\partial \xi}{\partial t} + \frac{\partial}{\partial \eta}\frac{\partial \eta}{\partial t} \\ \frac{\partial}{\partial x} &= \frac{\partial}{\partial \xi}\frac{\partial \xi}{\partial x} + \frac{\partial}{\partial \eta}\frac{\partial \eta}{\partial x} \\ \frac{\partial}{\partial y} &= \frac{\partial}{\partial \xi}\frac{\partial \xi}{\partial y} + \frac{\partial}{\partial \eta}\frac{\partial \eta}{\partial y} \end{aligned}$$

and, for $\xi = x/t$, $\eta = y/t$, these become

$$\begin{aligned} \frac{\partial}{\partial t} &= -\frac{\xi}{t}\frac{\partial}{\partial \xi} - \frac{\eta}{t}\frac{\partial}{\partial \eta} \\ \frac{\partial}{\partial x} &= \frac{1}{t}\frac{\partial}{\partial \xi}, \qquad \frac{\partial}{\partial y} = \frac{1}{t}\frac{\partial}{\partial \eta} \end{aligned}$$

so that Eq. (8) becomes

$$\frac{1}{a^2}\left[-\xi\frac{\partial p}{\partial \xi} - \eta\frac{\partial p}{\partial \eta} + u\frac{\partial p}{\partial \xi} + v\frac{\partial p}{\partial \eta}\right] + \rho\left[\frac{\partial u}{\partial \xi} + \frac{\partial v}{\partial \eta}\right] = 0 \tag{8a}$$

and Eqs. (2) and (3) become

$$-\xi\frac{\partial u}{\partial \xi} - \eta\frac{\partial u}{\partial \eta} + u\frac{\partial u}{\partial \xi} + v\frac{\partial u}{\partial \eta} + \frac{1}{\rho}\frac{\partial p}{\partial \xi} = 0 \tag{2a}$$

$$-\xi\frac{\partial v}{\partial \xi} - \eta\frac{\partial v}{\partial \eta} + u\frac{\partial v}{\partial \xi} + v\frac{\partial v}{\partial \eta} + \frac{1}{\rho}\frac{\partial p}{\partial \eta} = 0 \tag{3a}$$

and we see that these equations are independent of x, y, and t as assumed.

We may rewrite Eqs. (8a), (2a), and (3a) in the following form:

$$\frac{u - \xi}{a^2}\frac{\partial p}{\partial \xi} + \frac{v - \eta}{a^2}\frac{\partial p}{\partial \eta} + \rho\left(\frac{\partial u}{\partial \xi} + \frac{\partial v}{\partial \eta}\right) = 0 \tag{8b}$$

$$(u - \xi)\frac{\partial u}{\partial \xi} + (v - \eta)\frac{\partial u}{\partial \eta} + \frac{1}{\rho}\frac{\partial p}{\partial \xi} = 0 \tag{2b}$$

$$(u - \xi)\frac{\partial v}{\partial \xi} + (v - \eta)\frac{\partial v}{\partial \eta} + \frac{1}{\rho}\frac{\partial p}{\partial \eta} = 0 \tag{3b}$$

Substituting $\partial p/\partial \xi$ from Eq. (2b) and $\partial p/\partial \eta$ from Eq. (3b) into Eq. (8b) we obtain, after collecting terms,

$$\frac{\partial u}{\partial \xi}[a^2 - (u - \xi)^2] + \frac{\partial v}{\partial \eta}[a^2 - (v - \eta)^2] - (u - \xi)(v - \eta)\left[\frac{\partial u}{\partial \eta} + \frac{\partial v}{\partial \xi}\right] = 0 \tag{9}$$

Note, the two-dimensional steady-state irrotational equation is

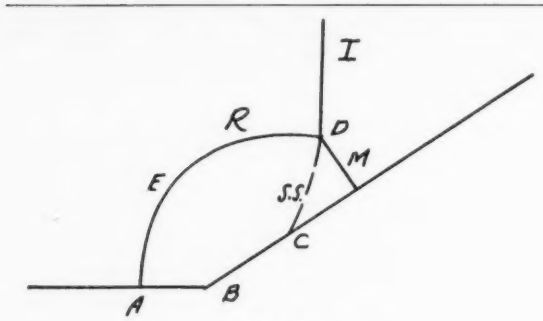

FIG. 6.

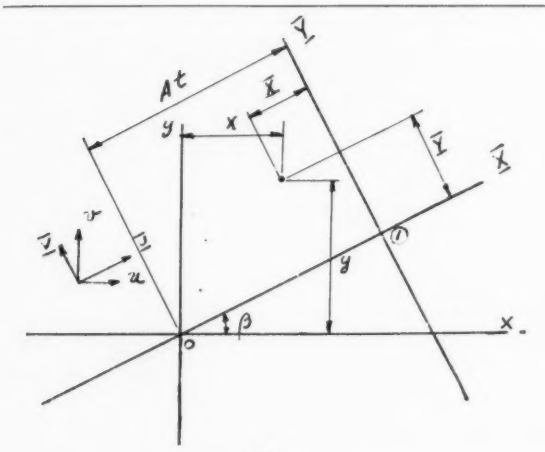

FIG. 7.

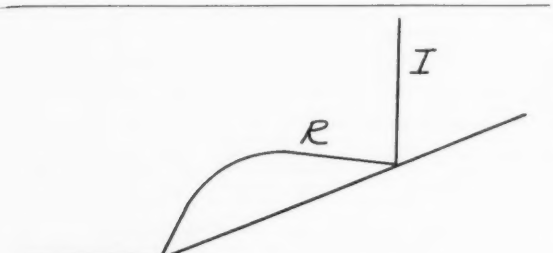

FIG. 8.

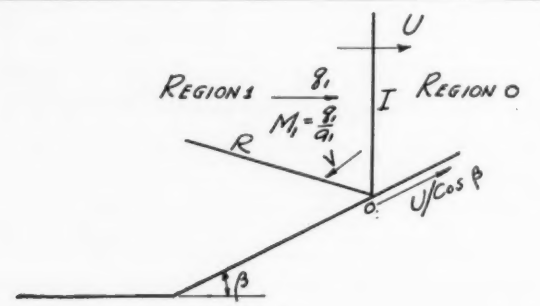

FIG. 9.

$$\frac{\partial u}{\partial x}\left[a^2 - u^2\right] + \frac{\partial v}{\partial y}\left[a^2 - v^2\right] - uv\left(\frac{\partial u}{\partial y} + \frac{\partial v}{\partial x}\right) = 0$$

Eq. (9) holds everywhere in the flow in the field ABCDE of Fig. 6 and will be used later in connection with a study of the characteristics of the field.

As a first problem, we consider the form the equations take in a moving $\bar{X}$, $\bar{Y}$ system of coordinates, where the origin of the $\bar{X}$, $\bar{Y}$ system is moving along a straight line making an angle β with the x axis at a constant velocity A, Fig. 7. Let u, v be the velocity components in x, y, and let $\bar{U}$, $\bar{V}$ be the components in $\bar{X}$, $\bar{Y}$.

Then it may be shown that our equations of flow are invariant with respect to the new $\bar{X}$, $\bar{Y}$ system. This can be proved in several ways. The simplest proof is that which utilizes a well-known invariance property of a vector equation—namely, the equation is invariant with respect to a translated origin. We can show easily that in the ξ, η plane our equation of continuity becomes

$$\bar{\xi}\cdot\nabla\rho = \nabla\cdot(\rho\bar{u})$$

and conservation of momentum becomes

$$(\bar{u} - \bar{\xi})\cdot\nabla\bar{u} + (1/\rho)\nabla p = 0$$

where the bars represent the corresponding vector quantities.

This invariance property of the flow equations will be considered shortly in connection with the possibility of having reciprocal flow fields. For the present, we may note that the invariance property is the essential requirement behind the two-shock and three-shock angle solutions obtained by the Princeton group. That is, if we take as an origin the triple shock point, for example, then the equation in the $\bar{X}$, $\bar{Y}$ plane of this point indicates the existence of conical flow with respect to this point. This in turn permits the assumption that the field is growing uniformly about this point as an origin, which is the assumption made in computing the three-shock angular relations.

The following theorem will now be proved:

First Theorem.—Given a two-shock pattern, with air, Fig. 8, then the reflected shock cannot be attached to the wedge point.

Proof: We prove this theorem by assuming an attached reflected shock and then proving that a two-shock pattern is impossible under this condition. The various regions and quantities referred to are indicated on Fig. 9, in which we use the notation of Lighthill I. In addition, some of the formulas that follow concerning relations between velocities in regions ① and ⓪ are from Lighthill I.

With respect to point 0, we have

$$V^2 = q_1^2 + \frac{U^2}{\cos^2\beta} - 2q_1\frac{U}{\cos\beta}\cos\beta$$

or

$$V = \sqrt{q_1^2 + (U^2/\cos^2\beta) - 2q_1U}$$

also

$$\mathfrak{M}_1 = \frac{V}{a_1} = \sqrt{M_1^2 + \frac{U^2}{a_1^2 \cos^2 \beta} - 2M_1 \frac{U}{a_1}}$$

and we will show that $\mathfrak{M}_1 < 1$, which indicates that a shock R is not possible as shown on Fig. 8. That is, we will show that

$$M_1^2 + \frac{U^2}{a_1^2 \cos^2 \beta} - 2M_1 \frac{U}{a_1} < 1$$

Now we may easily show that

$$\frac{q_1}{a_1} = \frac{5}{6} \frac{U}{a_1} \left(1 - \frac{a_0^2}{U^2}\right)$$

or

$$\frac{U}{a_1} = \frac{(6/5)(q_1/a_1)}{1 - (a_0^2/U^2)} = \frac{6}{5} \frac{M_1}{1 - (1/M^2)}$$

therefore, we must show that

$$M_1^2 \left\{1 + \frac{36}{25 \cos^2 \beta [1 - (1/M^2)]} - \frac{12}{5[1 - (1/M^2)]}\right\} < 1$$

M_1, M, and $\cos \beta$ are interdependent, and the simplest method for proving the above inequality is to plot the maximum values of the left-hand side for various assumed values of, say, M. This has been done in Table 1, from which it is apparent that $\mathfrak{M}_1 < 1$; therefore, the attached two-shock pattern is not possible.

TABLE 1

M	M_1	Min. Val. $\cos^2 \beta$	$\mathfrak{M}_1$
2.1	1.0	1.0	0.35
5	1.66	0.92	0.55
10	1.83	0.89	0.77
∞	1.89	0.87	0.86

The extension of this theorem to gases other than air will be considered in another paper.

Should it be found that the two-shock attached pattern exists, then reciprocal flows of the type discussed in the next section may be possible.

Reciprocal Flows

Because of the previously derived invariance property of the flow field, we are led to examine the possibility of the existance of reciprocal fields. To explain this, consider Fig. 10.

Because the equations of flow are identical for both D and D′ as origins, it follows that, (1) if shock angle and flow deflection at C and A equal shock angle and flow deflection at C′ and A′, (2) if angle CDA equals angle C′D′A′, and (3) if conditions along AD are the same as along A′D′, then the two flow fields are identical.

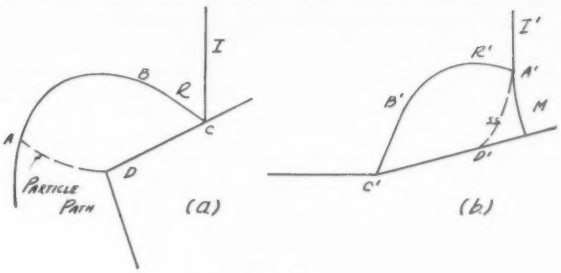

FIG. 10.

While the reciprocal property seems possible from both the physical and mathematical points of view, the difficulty in obtaining reciprocal pairs is magnified by our ignorance concerning the slipstream shape and position. The only known solutions available at this time (Lighthill, Ludloff, and Bargmann) can be shown to be without reciprocals. Whether this is due to the linearized form of the equations used or to some other reason is unknown.

The reciprocal relations, if they exist, would seem to be an important property of the shock reflection phenomena. It is therefore suggested that this matter might bear further investigation, particularly from the experimental point of view—especially in the direction of checking photographs for possible evidence of this phenomena.

The Characteristics and Their Application to the Given Problem

In this section the flow field will be considered for the special case in which the shock is attached to the wedge point (or equivalently for the regular two-shock patterns). Under these conditions, a necessary condition for the existence of characteristic curves will be determined. This necessary condition, when used in conjunction with an inequality to be derived in this section, will then be examined further, and it will be found that a type of transonic singularity or discontinuity occurs. In addition, it will be shown that for certain shocks an attached straight shock solution is not possible.

The Characteristics

When the Mach Number behind the incident shock is greater than unity, for small enough wedge angles, straight shocks attached to the wedge point can exist, since with respect to this point as an origin the steady-state solution is possible (see Fig. 11). The statements that follow can also be applied to the case of Fig. 12, with the two-shock point considered as the origin.

Referring to Fig. 11 and confining the discussion to the region ABFDA, we see that there is a region behind the straight shock which is in uniform irrotational motion.

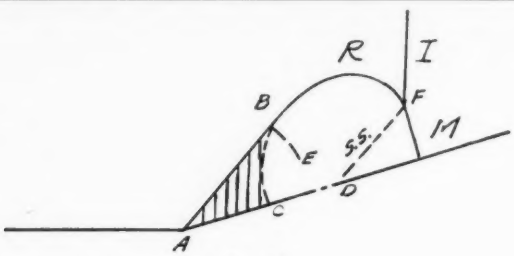

FIG. 11.

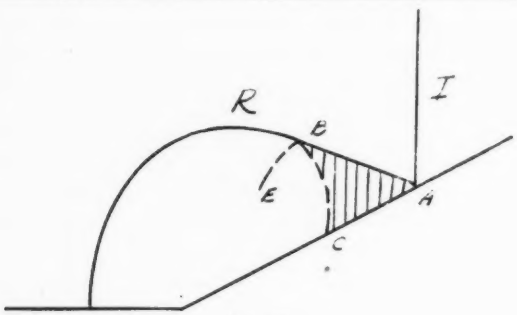

FIG. 12.

Because there are particles in the disturbed flow field which have come through the curved shock, it follows that there is also a region of rotational flow behind the shock.[19]

Thus, in general, we have two separate pairs of regions distinguished by discontinuities, both originating at the point B, Fig. 11:

(1) A region of uniform flow separated from a region of nonuniform flow; the nonuniform flow region is not necessarily rotational.

(2) A region of irrotational flow separated from a region of rotational flow.

In mathematical terms, the first pair is characterized by the requirement that there be a curve in the (ξ, η) plane along which u and v are continuous, but $\partial u/\partial \xi$, $\partial u/\partial \eta$, $\partial v/\partial \xi$, $\partial v/\partial \eta$ are not necessarily continuous. That is, there is a patching curve along which the derivatives in the velocities may be discontinuous.

Similarly, the second pair is characterized by the requirement that the vorticity is continuous along the corresponding patching curve, but the rate of change of vorticity is discontinuous. Physically, this patching curve must be a particle path (BE, Fig. 11) through the intersection of the straight and curved parts of the reflected shock. This will satisfy the known physical fact that particles passing through a curved shock become rotational and, in addition, satisfies the known fact that a particle path may be a characteristic or curve of permissible discontinuity of a flow function.[20]

It is the first patching curve, however, which is of interest at this time. In the mathematical treatment of this curve we use essentially the same method used by Murnaghan[21] in his analysis of steady-state compressible flows.

We have our fundamental equation

$$\frac{\partial u}{\partial \xi}\left[a^2 - (u-\xi)^2\right] + \frac{\partial v}{\partial \eta}\left[a^2 - (v-\eta)^2\right] - (u-\xi)(v-\eta)\left[\frac{\partial a}{\partial \eta} + \frac{\partial v}{\partial \xi}\right] = 0$$

and along the patching curve

$$(\partial v/\partial \xi) - (\partial u/\partial \eta) = 0$$

Now, we consider an arbitrary curve C in the (ξ, η) plane given by $\xi = \xi(\alpha)$, $\eta = \eta(\alpha)$, α being any convenient parameter or independent variable, and we suppose that the value of u, v and vorticity are prescribed along this curve. Then, since

$$\frac{du}{d\alpha} = \frac{\partial u}{\partial \xi}\frac{d\xi}{d\alpha} + \frac{\partial u}{\partial \eta}\frac{d\eta}{d\alpha} \tag{3}$$

$$\frac{dv}{d\alpha} = \frac{\partial v}{\partial \xi}\frac{d\xi}{d\alpha} + \frac{\partial v}{\partial \eta}\frac{d\eta}{d\alpha} \tag{4}$$

A necessary condition for the existence of the velocity characteristic is that

$$\begin{vmatrix} a^2-(u-\xi)^2 & -(u-\xi)(v-\eta) & -(u-\xi)(v-\eta) & a^2-(v-\eta)^2 \\ \dfrac{d\xi}{d\alpha} & \dfrac{d\eta}{d\alpha} & 0 & 0 \\ 0 & 0 & \dfrac{d\xi}{d\alpha} & \dfrac{d\eta}{d\alpha} \\ 0 & 1 & -1 & 0 \end{vmatrix} = 0$$

and this will have a solution if

$$(u-\xi)^2 + (v-\eta)^2 \gtrless a^2 \tag{5}$$

In this equation, a is the velocity of sound in the uniform flow irrotational region just behind the straight portion of the reflected shock.

We may note, too, that the Eq. (5) corresponds to the usual steady-state characteristic theory requirement that

$$q^2 = u^2 + v^2 \geq a^2$$

or that the flow be supersonic.

If the determinant of the coefficients of Eqs. (1)–(4) is zero, then the further condition that must be imposed on u and v in order that the four equations connecting the derivatives may have a solution is

$$\begin{vmatrix} \frac{d\xi}{d\alpha} & \frac{du}{d\alpha} & 0 & 0 \\ 0 & \frac{dv}{d\alpha} & \frac{d\xi}{d\alpha} & \frac{d\eta}{d\alpha} \\ 0 & 0 & 1 & 0 \\ a^2 - (u-\xi)^2 & 0 & -(u-\xi)(v-\eta) & a^2 - (v-\eta)^2 \end{vmatrix} = 0$$

from which a sufficient condition for the existence of solutions of the four equations for the four derivatives of u and v along C (when the determinant of these four equations is zero) is

$$[a^2 - (v-\eta)^2]\frac{d\xi}{d\alpha}\frac{dv}{d\alpha} + [a^2 - (u-\xi)^2]\frac{d\eta}{d\alpha}\frac{du}{d\alpha} = 0 \tag{6}$$

From Eq. (6) we can determine the slope $d\eta/d\xi$ of the patching curve; for, dividing through by $(d\xi)^2$ and solving the resulting quadratic equation, we have

$$\frac{d\eta}{d\xi} = \frac{-2(u-\xi)(v-\eta) \pm \sqrt{4(u-\xi)^2(v-\eta)^2 - 4[a^2 - (v-\eta)^2][a^2 - (u-\xi)^2]}}{2[a^2 - (u-\xi)^2]}$$

or, if we call Q, the reduced velocity, having components $(u-\xi, v-\eta)$, then

$$\frac{d\eta}{d\xi} = -\frac{(u-\xi)(v-\eta) \pm a\sqrt{Q^2 - a^2}}{a^2 - (u-\xi)^2} \tag{8}$$

For use in later applications of the patching curve relations, the following Theorem II is proved, Fig. 13:

> "The attached shock at the wedge point will always intersect the circle of radius a (velocity of sound behind the shock) which is centered at (u, v), these being the uniform velocity components behind the shock."

Note that the point (u, v) is on the wedge angle line. To prove the above theorem, we must show (see Fig. 13) that $\mu + \theta \geq \epsilon$, and, since $\epsilon = \beta + \theta$, we must show that $\mu \geq \beta$. This is equivalent to showing that

$$\sin \mu \geq \sin \beta$$

But $\sin \mu = 1/M_2$, where M_2 is the Mach Number of the flow behind the shock. We must therefore show that

$$1 \geq M_2 \sin \beta$$

This is done by noting (see Eq. 125, page 45, reference 18) that

$$\frac{\tan t}{\tan \beta} = \frac{2}{\gamma + 1}\left(\frac{1}{M_2^2 \sin^2 \beta} + \frac{\gamma - 1}{2}\right)$$

which obviously ≥ 1 for any finite wedge angle θ. The equality holds for $\theta = 0$.

From the above,

$$\frac{2}{\gamma + 1}\left[\frac{2 + (\gamma - 1)\alpha}{2\alpha}\right] \geq 1$$

where $\alpha = M_2^2 \sin^2 \beta$ or

$$(\alpha\gamma + 2 - \alpha)/(\alpha\gamma + \alpha) \geq 1$$

and we see that for $\alpha = 1$ (that is, $\theta = 0$) the equality holds, but only for $\alpha < 1$ will the inequality be true This proves Theorem II.

Along the patching curve we have

$$(u-\xi)^2 + (v-\eta)^2 \geq a^2$$

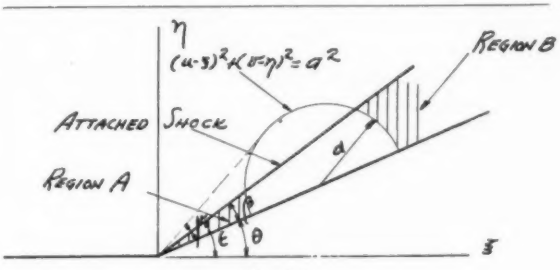

FIG. 13.

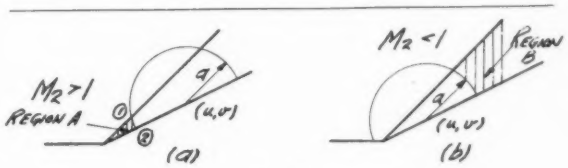

FIG. 14.

that is, if a circle of radius a is drawn centered at (u, v), the patching curve must be on or outside this circle. Also, Theorem II states that the straight attached shock intersects this circle. It follows, therefore, that the patching curve must lie in either Region A or Region B of Fig. 13.

One other fact may be noted: For $M_2 > 1$, the circle is disposed as shown in Fig. 14a; for $M_2 < 1$, it is as shown in Fig. 14b.

For an infinitesimal shock, the patching curve corresponds to the arc of circle ① ② of Fig. 14a. As the wedge angle increases, the patching curve lies in Region A of Fig. 13, except as noted later.

But, it is a well-known fact (see, for example, reference 18) that, for stationary attached shocks, as the wedge angle increases, the Mach Number M_2 behind the shock decreases from supersonic values to subsonic values. The subsonic values occur only for a small range of wedge angles just before separation of the shock from the wedge point. The subsonic values do, however, occur, and, in addition, they occur for all strengths of incident shocks.

This phenomena leads to the following curious behavior of the straight shock in the present problem:

We consider a shock of given strength (strong enough to form attached shocks for a given range of wedge angles), and we examine the sequence of events as the wedge angle θ is increased.

For the smaller angles θ, the patching curve lies in the Region A, Fig. 13. As θ increases, Region A becomes smaller and smaller, but the patching curve still lies in this region; hence, the straight attached shock becomes smaller and smaller. Finally, a wedge angle $\theta_{cr.}$ is reached such that $M_2 = 1$. For this value, Region A becomes a point, and the patching curve also degenerates to a point. For $\theta > \theta_{cr.}$, if the shock is still straight and still attached, then because $M_2 < 1$, the patching curve must lie in the Region B.

Now, we see from Fig. 14b that the velocity of the curve AB is greater than q, the velocity of the fluid behind the straight shock. Therefore, AB must sweep over fluid particles that passed through the curved portion of the shock AC. This means that AB sweeps over a nonisentropic fluid, and, if AB is a patching curve, this fluid must then be of uniform velocity and isentropic. But the energy equation

$$DS/Dt = 0$$

states that in the disturbed field the entropy does not change. We are thus led to a contradiction of requirements and must conclude that the straight attached shock solution for $M_2 < 1$ shown in Fig. 14b cannot exist.

However, an attached curved shock solution as shown in Fig. 15 can exist for those cases in which $M_2 < 1$; the shock slope at the wedge point is the slope of the steady-state straight shock for the wedge angle θ and Mach Number M_1, but there is no region of uniform flow behind the shock, and the flow is rotational throughout the entire field.

This effect may be thought of as representing a discontinuity in the solution as follows: For $M_2 > 1$, we have the attached straight shock, with a uniform region corresponding to the steady-state solution. However, for $M_2 < 1$, this quasi-steady state attached straight shock solution cannot exist; hence, at $M = 1$, we have a discontinuity in this type of solution.

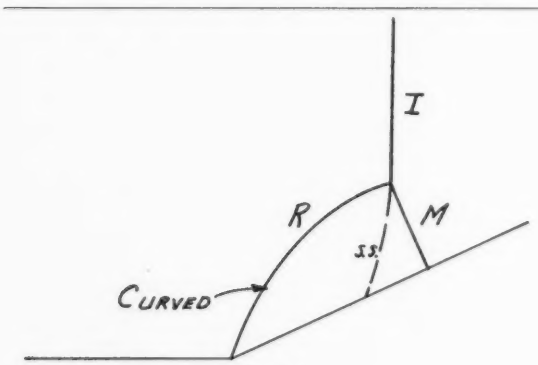

FIG. 15.

CONCLUSION

The following has been done in this paper: (1) The mathematical nonlinearized equations (neglecting viscosity and heat conduction) have been obtained in conical form; (2) an invariance relation for these nonlinear equations has been proved; (3) it was shown that an attached shock, two-shock pattern is not possible for air; (4) the possibility of the existence of reciprocal flows has been discussed; (5) the patching curve relations were obtained, and with the aid of these, (6) the existence of a form of transonic singularity in the straight attached wedge shock was obtained; (7) it was shown that a certain type of attached shock flow cannot exist.

REFERENCES

[1] Lagerstrom, P. A., *Linearized Supersonic Theory of Conical Wings*, N.A.C.A. T.N. No. 1685, January, 1950.

[2] Mach, E., Akad. Wiss. Wien, Vol. 77, p. 819, 1878.

[3] Von Neumann, John, *Oblique Reflection of Shocks*, Explosives Research Report No. 12, October, 1943.

[4] Bargmann, Valentine, *On Nearly Glancing Reflection of Shocks*, AMP Rep. 108.2R, March, 1945.

[5] Bargmann, V., and Montgomery, D., *Prandtl Meyer Zones in Mach Reflection*, OSHD-50116, April, 1945.

[6] Smith, Lincoln G., *Photographic Investigation of the Reflection of Plane Shocks in Air*, NDRC Rep. No. A-350, 1945.

[7] Polacheck, H., and Seeger, R. J., *Regular Reflection of Shocks in Ideal Gases*, Explosives Research Report No. 13, Bu. Ord., 1944.

[8] Polacheck, H., and Seeger, R. J., *On Shock Wave Phenomena; Interaction of Shock Waves in Gases*, Proc. in Symposia on Applied Math., Vol. 1, Amer. Math. Soc. Publ., 1949.

(*Continued on page 100*)

A Study of an Analogous Model Giving the Nonlinear Characteristics in the Buckling Theory of Sandwich Cylinders*

CHI-TEH WANG† AND G. V. R. RAO‡
New York University

SUMMARY

In previous papers,[1,2] the problem of buckling of sandwich cylinders under axial compression has been investigated both theoretically and experimentally. For sandwich cylinders with weak core, it was found that the buckling load given by the small deflection theory checks well with the experimental one. Whereas for homogeneous cylinders, it is well known that this is not the case, and the buckling phenomenon must be explained by the nonlinear large deflection theory. The limiting case of a sandwich cylinder with a strong core is an homogeneous cylinder. Thus the weakness of the shear rigidity of the sandwich cylinder must have compensated the importance of the nonlinear terms in the large deflection theory. To show this effect, nonlinear theory must be applied to sandwich cylinders with various degrees of weakness in the shear rigidity of the core. This, however, is a difficult problem. With a view to getting a qualitative picture in this respect, a model originally proposed by von Kármán, Dunn, and Tsien[3] which will reproduce the nonliner behavior in the buckling phenomena is studied, and a satisfactory explanation is obtained.

INTRODUCTION

IN PREVIOUS PAPERS,[1, 2] it was found that for sandwich cylinders with weak core the theoretical buckling loads based on the small-deflection theory agreed well with the experimental values. The limiting case of a sandwich cylinder with strong core is a homogeneous thin cylinder, but in that case it is well known that the classical linear theory fails to predict the buckling stress. Many investigators have attempted to explain the discrepancies between theoretical and experimental results in this latter case. Although the question of just how to define the "buckling load" is still a subject of controversy,[3–6] it is clear, however, that the reason for this discrepancy is due to the fact that the nonlinear terms in the governing differential equations which have been left out in the classical theory become important here. By introducing second-order terms in the shell theory, von Kármán and Tsien found that there exists a buckling phenomenon entirely different from that given by the linear theory. Based on these results, Tsien[4, 6, 7] proposed new definitions of the buckling loads which depend on whether the load was applied by a rigid testing machine or dead-weight loading. On the other hand, Donnell and Wan[5] have suggested that the buckling load should be the maximum load that a cylinder with initial imperfections can sustain.

The investigation of the buckling of sandwich cylinders introduces another factor into this already complicated phenomenon—namely, the influence of shear. A study of the effect of shear on the buckling load is not only important in the buckling theory of the sandwich cylinder itself but may also throw some light on the buckling behavior of curved structure in general. A rigorous treatment of the buckling of a sandwich cylinder by the second-order approximate theory should be based on the large deflection equations. These equa-

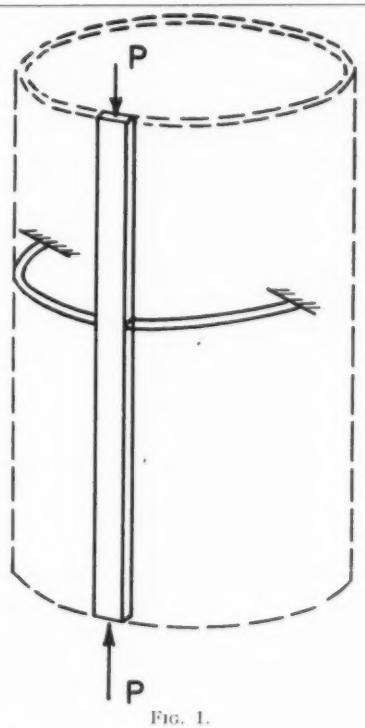

FIG. 1.

Received August 22, 1950. Revised and received June 8, 1951.

* The work reported in this paper was carried out under Contract No. N6-onr-279, Task Order V, sponsored by the Office of Naval Research.

† Professor of Aeronautical Engineering, Daniel Guggenheim School of Aeronautics.

‡ Now, Assistant Professor, Department of Aeronautical Engineering, Indian Institute of Science, Bangalore, India.

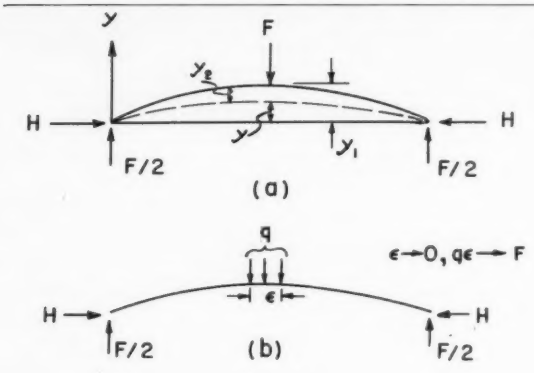

FIG. 2.

tions have been formulated in reference 2, but in that case five nonlinear differential equations must be solved simultaneously. It is evident that the actual solution of these equations will be exceedingly difficult and involved.

However, the essential characteristics of buckling phenomenon retaining these nonlinear terms in the buckling equations can be studied by an analogous simple model that does not involve any mathematical difficulty in its treatment. In the paper by von Kármán, Dunn, and Tsien,[3] it was shown that the typical features of the buckling of curved shells can be reproduced by the buckling of a column with nonlinear lateral supports. This follows from the fact that a longitudinal strip of a cylindrical shell may be considered as a column supported on rings (Fig. 1). With finite deflections, these rings behave as nonlinear springs. Following the same considerations, it appears that the nonlinear behavior of the buckling of sandwich cylinders may also be seen from a study of sandwich columns supported on sandwich rings. Based on this analogy, a study is carried out in this paper to show the effect of shear rigidity of the core on the nonlinear characteristics of the buckling phenomenon.

The Characteristics of the Nonlinear Support

In the original paper by von Kármán, Dunn, and Tsien,[3] the nonlinear support was considered to be derived from a semicircular ring clamped at both ends. A theoretical treatment of this problem has been carried out by Biezeno and Koch.[8] In the actual buckling of thin circular cylinders, tests have shown that there exist somewhere from 16 to 20 buckles in the circumferential directions. In the case of sandwich cylinders, a similar number of buckles has also been observed. Therefore, it appears to be a better approximation to consider the nonlinear support to be derived from a segment of circular arc with simply supported ends rather than the semicircular ring with clamped ends. At the same time, the treatment of a circular arc with simply supported ends is a much simpler problem.

The load-deflection relation of an arch with small curvature and with hinged ends has been studied in detail by Timoshenko.[9] A small segment of circular arc can be treated with good approximation as a flat arch, the initial centerline of which is given by the equation

$$y_1 = a \sin (\pi x/l) \tag{1}$$

where a is the rise of the arch and l is the projected length (Fig. 2a). Under loading, deflections y_2 will be produced so that the final ordinates of the deflection curve are $y = y_1 - y_2$. Assume that y_2 can be represented by the sine series

$$y_2 = \sum_{n=1}^{\infty} a_n \sin (n\pi x/l) \tag{2}$$

where the undetermined parameters a_n can be determined by the variational method, which is more usually referred to as the energy method.

Denote the shear at any section of the arch by Q. The change of curvature produced by the bending moment and the shear force is

$$\frac{d^2y_1}{dx^2} - \frac{d^2y}{dx^2} = \frac{d^2y_2}{dx^2} = \frac{1}{EI}\left(M + \frac{\alpha EI}{AG}\frac{dQ}{dx}\right) \tag{3}$$

where E is the Young's modulus, I is the moment of inertia, G is the modulus in shear, A is cross-sectional area, and α is a factor with which the average shearing stress must be multiplied in order to obtain the shearing stress at the centroid of the cross sections. For homogeneous beams with rectangular cross sections, $\alpha = 1.5$. For sandwich sections with thin faces and weak cores, α is approximately equal to 1. In the following calculations, for simplicity α will be taken as 1. From Eq. (3),

$$M = EI[(d^2y_2/dx^2) - (1/AG)(dQ/dx)] \tag{4}$$

In order to include the effect of shearing force on the deflection of arch, the concentrated load F should be considered as the limiting case of a uniformly distributed load q over an extremely short portion ϵ of the beam (Fig. 2b). The shear at any section x is, therefore,

$$\left.\begin{aligned} Q &= (F/2) - H(dy/dx) \\ &\text{when } 0 \leqslant x \leqslant (1/2)(l - \epsilon) \\ Q &= \frac{F}{2} - H\frac{dy}{dx} - q\left(x - \frac{l}{2} + \frac{\epsilon}{2}\right) \\ &\text{when } (1/2)(l - \epsilon) \leqslant x \leqslant (1/2)(l + \epsilon) \\ Q &= -[(F/2) + H(dy/dx)], \\ &\text{when } (1/2)(l + \epsilon) \leqslant x \leqslant l. \end{aligned}\right\} \tag{5}$$

The bending strain energy is

$$V_b = \frac{1}{2}\int_0^l \frac{M^2}{EI}\,dx = \frac{EI}{2}\int_0^l \left(\frac{d^2y_2}{dx^2} - \frac{1}{AG}\frac{dQ}{dx}\right)^2 dx \tag{6}$$

The shearing strain energy is

$$V_s = \frac{1}{2}\int_0^l \frac{Q^2}{AG}\,dx \tag{7}$$

The work done by the axial forces H due to end shortening is

$$W_H = \frac{1}{2}H\int_0^l \left[\left(\frac{dy}{dx}\right)^2 - \left(\frac{dy_1}{dx}\right)^2\right] dx \tag{8}$$

and the work done by the lateral load F is

$$W_F = F(y_2)_{x=l/2} \tag{9}$$

The principle of minimum potential energy requires that the potential energy U

$$U = V_b + V_s - W_H - W_F \tag{10}$$

to be a minimum. The coefficients a_n may be determined by setting the first variation of U with respect to a_n to zero. Carrying out the calculation, we obtain

$$\left.\begin{aligned} a_1 &= \left[\frac{Hl^2}{\pi^2 EI}\left(1 + \frac{\pi^2 EI}{l^2 AG}\right)a - \left(\frac{2Fl^3}{\pi^4 EI} + \frac{2Fl}{\pi^2 AG}\right)\right] \Big/ \left[1 - \frac{Hl^2}{\pi^2 EI}\left(1 + \frac{\pi^2 EI}{l^2 AG}\right)\right] \\ a_n &= -\left(\frac{2Fl^3}{\pi^4 EI} + \frac{2Fln^2}{\pi^2 AG}\right)\sin\frac{n\pi}{2} \Big/ n^2\left[n^2\left(1 - \frac{H}{AG}\right) - \frac{Hl^2}{\pi^2 EI}\right] \end{aligned}\right\} \tag{11}$$

In obtaining the above relationship, we have used the condition that as ϵ approaches zero, $q\epsilon \to F$. Taking only one term in the series, the rise of the arch under load becomes

$$a - a_1 = \left[a - \left(\frac{Fl^3}{48.7EI} + \frac{Fl}{4.93AG}\right)\right] \Big/ \left[1 - \frac{Hl^2}{\pi^2 EI}\left(1 + \frac{\pi^2 EI}{l^2 AG}\right)\right] \tag{12a}$$

In the subsequent calculation, we shall only retain one term in the series; in such a case, a better approximation may be obtained by replacing $(a - a_1)$ in Eq. (12a) by the exact value of maximum rise, which is

$$(a - a_1)_{\text{exact}} = \left[a - \left(\frac{Fl^3}{48EI} + \frac{Fl}{4AG}\right)\right] \Big/ \left[1 - \frac{Hl^2}{\pi^2 EI}\left(1 + \frac{\pi^2 EI}{l^2 AG}\right)\right] \tag{12b}$$

The centerline of the arch after loading then becomes

$$y = \left[1 - \frac{Fl^3}{48aEI}\left(1 + \frac{12EI}{l^2 AG}\right)\right]\left(a\sin\frac{\pi}{l}x\right) \Big/ \left[1 - \frac{Hl^2}{\pi^2 EI}\left(1 + \frac{\pi^2 EI}{l^2 AG}\right)\right] \tag{13}$$

The deflection curve, Eq. (13), of the arch, however, is still undetermined unless H is known. The equation for calculating the axial load H is obtained by putting the change in length of the span due to deflection equal to the compression of the arch due to axial load. Assuming for flat curves that the compressive force along the length of arch is constant and equal to H, we obtain

$$\frac{Hl}{AE} = \frac{1}{2}\int_0^l (dy_1/dx)^2\,dx - \frac{1}{2}\int_0^l (dy/dx)^2\,dx \tag{14}$$

Substituting Eqs. (1) and (13) into Eq. (14) and integrating, we obtain

$$\frac{Hl}{AE} = \frac{\pi^2 a^2}{4l}\left\{1 - \left[1 - \frac{Fl^3}{48aEI}\left(1 + \frac{12EI}{l^2 AG}\right)\right]^2 \Big/ \left[1 - \frac{Hl^2}{\pi^2 EI}\left(1 + \frac{\pi^2 EI}{l^2 AG}\right)\right]^2\right\} \tag{15}$$

A sandwich-type structure consists of two external layers of thin high strength material and a thick internal layer of lightweight weak material. The former are usually called the "face layer" and the latter "the core." For such type of structure, AG in the above formulas may be replaced by A_cG_c, where the subscript c refers to the properties of the core. We shall not neglect the normal stress carrying ability of the core as usually assumed, in order that our final equations will reduce to those of homogeneous structure. From the analysis of composite beams, it can be easily shown that the flexural formula $1/\rho = M/EI$ for homogeneous beam becomes $1/\rho = M/(E_fI_f + E_cI_c)$, where ρ is the radius of curvature and the subscript f refers to properties of the face layers. The axial compressive strain Hl/AE should be written as $Hl/(A_fE_f + A_cE_c)$. E_c may be expressed in terms of G_c by using the relation $E_c = 2(1 + \nu_c)G_c$, where ν_c is the Poisson's ratio for the core material.

Writing $E_fI_f + E_cI_c = EI$, we obtain, for sandwich beams,

$$\frac{Hl}{A_fE_f + 2(1 + \nu_c)A_cG_c} = \frac{\pi^2 a^2}{4l}\left\{1 - \left[1 - \frac{Fl^3}{48aEI}\left(1 + \frac{12EI}{l^2 A_cG_c}\right)\right]^2 \Big/ \left[1 - \frac{Hl^2}{\pi^2 EI}\left(1 + \frac{\pi^2 EI}{l^2 A_cG_c}\right)\right]^2\right\} \tag{15a}$$

Eq. (15a) reduces to the equation for the homogeneous beam with finite shear rigidity if we let $E_c = E_f$, $\nu_c = \nu_f$, $I_f + I_c = I$, and $A = A_f + A_c \cong A_c$. Let t be the thickness of the face layer, $2h$ be the thickness of the core, and b be the width of the beam. Let $t \ll h$. Thus,

$$A_f = 2bt, \qquad A_c = 2bh$$
$$I_f \cong 2bth^2, \qquad I_c = 2bh^3/3$$

To simplify the writing, let us introduce the following symbols:

$$u = Fl^3/48aEI, \qquad \beta = Hl^2/\pi^2EI$$
$$K_1 = E_f/G_c, \qquad K_2 = A_f/A_c = t/h$$
$$K_3 = a^2/l^2, \qquad K_4 = h^2/a^2$$

$$m = 4EI/E_fA_ca^2 = 4(E_fI_f + E_cI_c)/E_fA_ca^2 = 4K_4[K_2 + 2(1 + \nu_c)/3K_1]$$

In terms of these parameters, Eq. (15a) becomes

$$\frac{m\beta}{K_2 + 2(1 + \nu_c)/K_1} = 1 - [1 - u(1 + 3mK_1K_3)]^2/[1 - \beta(1 + 0.25\pi^2mK_1K_3)]^2 \tag{16}$$

For given values of K_1, K_2, K_3, K_4, and ν_c, β can be solved in terms of u from Eq. (16). With β known, the deflection δ of the arch measured from the unloaded position may be found from Eq. (13) to be

$$\delta/a = 1 - [1 - u(1 + 3mK_1K_3)]/[1 - \beta(1 + 0.25\pi^2mK_1K_3)] \tag{17}$$

For numerical calculation, the circumference of the cylinder is assumed to buckle into 20 buckles, which gives $a/l = \sqrt{K_3} = 0.04$. For $K_1 = 2.6$, we take $\nu_c = \nu_f = 0.3$. For $K_1 = 500$, 1,000, and 5,000, we take $\nu_c = 0$. Taking $K_2 = 0.1$ and $K_4 = 0.2$, the nondimensional load deflection curves of the arch are computed from Eqs. (16) and (17) for these values of K_1. The curves showing u vs. δ/a are plotted in Fig. 3.

Buckling of a Sandwich Column with Nonlinear Lateral Supports

Having determined the characteristics of the nonlinear support, we shall now proceed to treat the problem of buckling of sandwich columns with such lateral supports. Let the column be initially straight and its centerline be taken as the x-axis (Fig. 4). Assume that the column is supported laterally by g nonlinear springs at $x_1, x_2, \ldots, x_g$. Let $\delta_1, \delta_2, \ldots, \delta_g$ be the deflections at these points. Depending upon the load-deflection characteristics of the springs, the spring forces at these points are $F_1(\delta_1), F_2(\delta_2), \ldots, F_g(\delta_g)$. The elastic energy V_{sp} stored in these springs at the deflections $\delta_1, \delta_2, \ldots, \delta_g$ can be easily calculated as

$$V_{sp} = \sum_{m=1}^{g} \int_0^{\delta_m} F_m(\xi)d\xi \tag{18}$$

Assuming the column as simply supported at the two ends, the deflection of the column may be represented by the following Fourier series:

$$y = \sum_{n=1}^{\infty} a_n \sin(n\pi x/L) \tag{19}$$

where a_n are again undetermined parameters that may be ascertained by the variational method. The deflection of spring m at $x = x_m$ is, therefore,

$$\delta_m = y(x_m) = \sum_{n=1}^{\infty} a_n \sin(n\pi x_m/L) \tag{20}$$

Similar to Eq. (4), the bending moment at any section of the column may be written in terms of the curvature as

$$M = EI_b\left(\frac{d^2y}{dx^2} - \frac{1}{A_cG_c}\frac{dQ}{dx}\right) \tag{21}$$

where I_b is the moment of inertia of the cross section of the column. Again in the computation of the deflection we shall consider the concentrated load F_m as the limit-

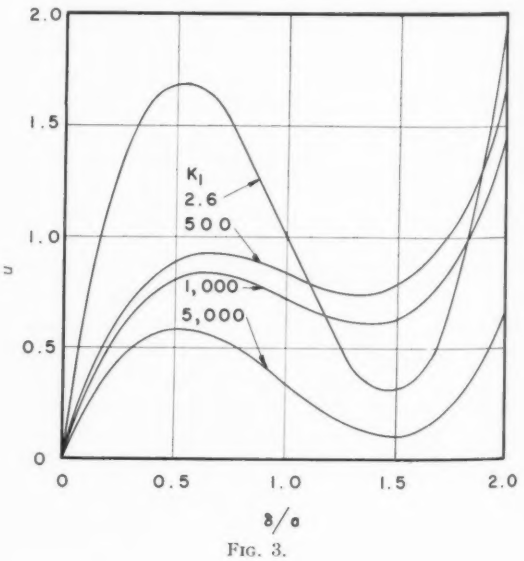

Fig. 3.

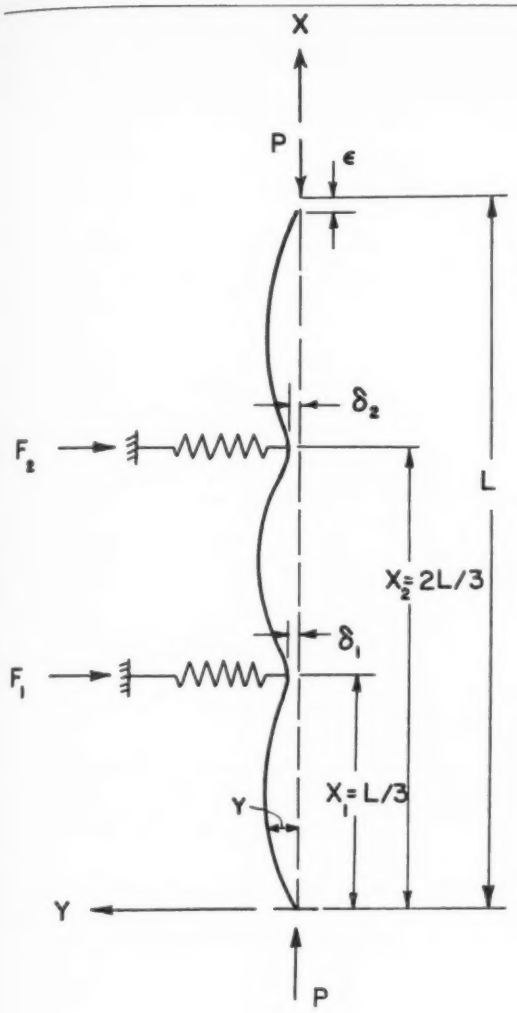

FIG. 4.

ing case of a uniformly distributed load q_m over a short portion ϵ_m of the column, and

$$\lim_{\epsilon m \to 0} q_m \epsilon_m = F_m.$$

The shear at any section x is, therefore,

$$Q = \frac{1}{2}\sum_{m=1}^{g} F_m - P\frac{dy}{dx}$$

when $0 \leqslant x \leqslant [x_1 - (\epsilon_1/2)]$

$$Q = \frac{1}{2}\sum_{m=1}^{g} F_m - P\frac{dy}{dx} - q_1\left(x - x_1 + \frac{\epsilon_1}{2}\right) \qquad (22)$$

when $[x_1 - (\epsilon_1/2)] \leqslant x \leqslant [x_1 + (\epsilon_1/2)]$

$$Q = \frac{1}{2}\sum_{m=1}^{g} F_m - P\frac{dy}{dx} - F_1$$

when $[x_1 + (\epsilon_1/2)] \leqslant x \leqslant [x_2 - (\epsilon_2/2)]$, . . ., etc.

The bending strain energy is

$$V_b = \frac{EI_b}{2}\int_0^L \left(\frac{d^2y}{dx^2} - \frac{1}{A_cG_c}\frac{dQ}{dx}\right)^2 dx \qquad (23)$$

and the shearing strain energy is

$$V_s = \frac{1}{2A_cG_c}\int_0^L Q^2\,dx \qquad (24)$$

The work done by the axial compression P applied at the ends of the column due to the lateral deflection is

$$W_a = \frac{P}{2}\int_0^L \left(\frac{dy}{dx}\right)^2 dx \qquad (25)$$

The potential energy U in this case is, then,

$$U = V_b + V_s + V_{sp} - W_a \qquad (26)$$

and the coefficients a_n may again be calculated by setting the first variation of U with respect to a_n to zero

Now, consider the case of sandwich column supported on two equally spaced springs with the same characteristics. Carrying out the calculation and noting that $F_1 = F_2 = F$, we see that the condition $\partial U/\partial a_n = 0$ leads to

$$\frac{EI_bL}{2}\left(1 - \frac{P}{A_cG_c}\right)^2\left(\frac{n\pi}{L}\right)^4 a_n - \frac{PL}{2}\left(1 - \frac{P}{A_cG_c}\right)\left(\frac{n\pi}{L}\right)^2 a_n + F\left(1 - \frac{P}{A_cG_c}\right)\left(\sin\frac{n\pi}{3} + \sin\frac{2n\pi}{3}\right) + EI_b\left(1 - \frac{P}{A_cG_c}\right)\times$$

$$\frac{F}{A_cG_c}\left(\frac{n\pi}{L}\right)^2\left(\sin\frac{n\pi}{3} + \sin\frac{2n\pi}{3}\right) + \frac{FL}{3A_cG_c}\left(\frac{\partial F_1}{\partial\delta_1}\sin\frac{n\pi}{3} + \frac{\partial F_2}{\partial\delta_2}\sin\frac{2n\pi}{3}\right) - \frac{P}{A_cG_c}\left(\frac{\partial F_1}{\partial\delta_1}\delta_1\sin\frac{n\pi}{3} + \frac{\partial F_2}{\partial\delta_2}\delta_2\sin\frac{2n\pi}{3}\right) = 0$$

where the relation $\partial\delta_m/\partial a_n = \sin(n\pi x_m/L)$ has been used. The coefficient a_n can therefore be written as

$$\frac{a_n}{L} = \frac{2}{\pi^2}\frac{\sum_{m=1}^{2}\frac{F_m}{P_e}\sin\left(\frac{n\pi x_m}{L}\right)\left\{(1+n^2R) + \frac{R}{3}\frac{\partial(F_m/P_e)}{\partial(\delta_m/L)} - R\frac{P}{P_e}\left[1 + n^2R + \frac{\delta_m/L}{F_m/P_e}\frac{\partial(F_m/P_e)}{\partial(\delta_m/L)}\right]\right\}}{\left(1 - \frac{RP}{P_e}\right)^2 n^2\left[\frac{P/P_e}{1-(RP/P_e)} - n^2\right]} \qquad (27)$$

where, for simplicity of writing, the notations $P_e = \pi^2 EI_b/L^2$ and $R = P_e/A_cG_c$ have been introduced. Eq. (27) gives the coefficients a_n if the F_m, $\partial(F_m/P_e)/\partial(\delta_m/L)$, and $(\delta_m/L)/(F_m/P_e)$ are known. The quantities, however, again depend on a_n. To determine a_n uniquely, we may proceed as follows: Recalling Eq. (20),

$$\delta_s/L = \sum_{n=1}^{\infty} (a_n/L) \sin (n\pi x_s/L) \tag{28}$$

Substitution of Eq. (27) into Eq. (28) gives

$$\frac{\delta_s}{L} = \sum_{m=1}^{2} \frac{F_m}{P_e}\left\{1 + \frac{R}{3}\frac{\partial(F_m/P_e)}{\partial(\delta_m/L)} - R\frac{P}{P_e}\left[1 + \frac{\delta_m/L}{F_m/P_e}\frac{\partial(F_m/P_e)}{\partial(\delta_m/L)}\right]\right\} \times$$

$$\left\{\frac{2}{\pi^2[1-(RP/P_e)]^2}\sum_{n=1}^{\infty}\frac{\sin(n\pi x_m/L)\sin(n\pi x_s/L)}{n^2\left[\dfrac{P/P_e}{1-(RP/P_e)} - n^2\right]}\right\} + \sum_{m=1}^{2} R\frac{F_m}{P_e}\frac{2}{\pi^2[1-(RP/P_e)]} \times$$

$$\sum_{n=1}^{\infty}\frac{\sin(n\pi x_m/L)\sin(n\pi x_s/L)}{\left[\dfrac{P/P_e}{1-(RP/P_e)} - n^2\right]} \tag{29}$$

If we define

$$\left.\begin{aligned} K_{sm} &= \frac{2}{\pi^2[1-(RP/P_e)]^2}\sum_{n=1}^{\infty}\frac{\sin(n\pi x_m/L)\sin(n\pi x_s/L)}{n^2[(P/P_e)/1-(RP/P_e)] - n^4} \\ k_{sm}' &= \frac{2}{\pi^2[1-(RP/P_e)]}\sum_{n=1}^{\infty}\frac{\sin(n\pi x_m/L)\sin(n\pi x_s/L)}{[(P/P_e)/1-(RP/P_e)] - n^2} \end{aligned}\right\} \tag{30}$$

Eq. (29) can then be written as

$$\frac{\delta_s}{L} = \sum_{m=1}^{2} K_{sm}\frac{F_m}{P_e}\left\{1 + \frac{R}{3}\frac{\partial(F_m/P_e)}{\partial(\delta_m/L)} - R\frac{P}{P_e}\left[1 + \frac{\delta_m/L}{F_m/P_e}\frac{\partial(F_m/P_e)}{\partial(\delta_m/L)}\right]\right\} + \sum_{m=1}^{2} K_{sm}' R\frac{F_m}{P_e} \qquad (s = 1, 2) \tag{31}$$

With a given value of P/P_e, the coefficients K_{sm}, K_{sm}' can be calculated. With K_{sm} and K_{sm}' calculated and the spring characteristics given, Eq. (31) then consists of two simultaneous equations for δ_1 and δ_2. Solving, δ_1, δ_2, then F_1 and F_2 can be calculated. The Fourier coefficients a_n/L can now be determined by means of Eq. (27). The problem is thus completely solved.

The coefficients K_{sm} and K_{sm}' may be seen to be symmetrical from their definition—i.e., $K_{sm} = K_{ms}$, $K_{sms}' = K_{ms}'$. Also, they are independent of the spring characteristics. In the case of the two equally spaced springs, K_{11}, K_{22}, K_{12}, K_{11}', K_{22}', and K_{12}' can be easily summed up by well-known relations[6, 10] to be

$$\left.\begin{aligned} K_{11} &= K_{22} = \left[\frac{2}{9} + \frac{1}{4\theta}\left(3\cot\theta - \cot\frac{\theta}{3}\right)\right]\Big/\frac{P}{P_e}\left(1 - R\frac{P}{P_e}\right) \\ K_{12} &= K_{21} = \left[\frac{1}{9} - \frac{1}{4\theta}\left(3\csc\theta - \csc\frac{\theta}{3}\right)\right]\Big/\frac{P}{P_e}\left(1 - R\frac{P}{P_e}\right) \\ K_{11}' &= K_{22}' = \frac{1}{4\theta}\left(3\cot\theta - \cot\frac{\theta}{3}\right)\Big/\left(1 - R\frac{P}{P_e}\right) \\ K_{12}' &= K_{21}' = -\frac{1}{4\theta}\left(3\csc\theta - \csc\frac{\theta}{3}\right)\Big/\left(1 - R\frac{P}{P_e}\right) \end{aligned}\right\} \tag{32}$$

where $\theta = \pi\{(P/P_e)/[1 - (RP/P_e)]\}^{1/2}$.

Now assume that the deflection of the column is symmetrical. Since the two springs have the same characteristics, we have $\delta_1 = \delta_2 = \delta$ and $F_1 = F_2 = F$. Eq. (31) reduces to

$$\frac{\delta}{L} = (K_{11} + K_{12})\frac{F}{P_e}\left\{1 + \frac{R}{3}\frac{\partial(F/P_e)}{\partial(\delta/L)} - R\frac{P}{P_e}\left[1 + \frac{\delta/L}{F/P_e}\frac{\partial(F/P_e)}{\partial(\delta/L)}\right]\right\} + (K_{11}' + K_{12}')R\frac{F}{P_e} \tag{33}$$

From Eq. (32), we have

$$\left.\begin{aligned} K_{11} + K_{12} &= \left[\frac{1}{3} - \frac{1}{4\theta}\left(3\tan\frac{\theta}{2} - \tan\frac{\theta}{6}\right)\right]\Big/\frac{P}{P_e}\left(1 - R\frac{P}{P_e}\right) \\ K_{11}' + K_{12}' &= -\frac{1}{4\theta}\left(3\tan\frac{\theta}{2} - \tan\frac{\theta}{6}\right)\Big/\left(1 - R\frac{P}{P_e}\right) \end{aligned}\right\} \tag{34}$$

The load-deflection of nonlinear spring as worked out in the previous section is too complicated for the solution of δ/L when it is substituted into Eq. (33). It was found, however, that this relation can be represented with good approximation by the following power series:

$$\frac{F}{P_e} = b\left(\frac{\delta}{L}\right) + c\left(\frac{\delta}{L}\right)^2 + e\left(\frac{\delta}{L}\right)^3 \tag{35}$$

The constants b, c, and e may be determined by the initial slope and the positions of the maximum and minimum of the F vs. δ curve.

Now, as defined before,

$$u = \frac{Fl^3}{48aEI} = \frac{FL^2}{\pi^2 EI}\frac{\pi^2}{48}\frac{l}{a}\left(\frac{l}{L}\right)^2 = \frac{F}{P_e}\frac{I_b}{I}\left(\frac{\pi^2}{48}\right)\frac{K_5^2}{\sqrt{K_3}}$$

where $K_5 = l/L$. In terms of u and δ/a, Eq. (35) becomes

$$\frac{48}{\pi^2}\left(\frac{a}{l}\right)\left(\frac{L}{l}\right)^2\left(\frac{I_b}{I}\right)u = b\left(\frac{\delta}{a}\right)\left(\frac{a}{l}\right)\left(\frac{l}{L}\right) + c\left(\frac{\delta}{a}\right)^2\left(\frac{a}{l}\right)^2\left(\frac{l}{L}\right)^2 + e\left(\frac{\delta}{a}\right)^3\left(\frac{a}{l}\right)^3\left(\frac{l}{L}\right)^3$$

or

$$\frac{48}{\pi^2}\left(\frac{I_b}{I}\right)u = b\left(\frac{\delta}{a}\right)K_5^3 + c\left(\frac{\delta}{a}\right)^2\sqrt{K_3}\,K_5^4 + e\left(\frac{\delta}{a}\right)^3 K_3 K_5^5 \tag{36}$$

Combining Eq. (35) with Eq. (33), we obtain

$$\left(\frac{\delta}{L}\right) = B_1\left(\frac{\delta}{L}\right) + B_2\left(\frac{\delta}{L}\right)^2 + B_3\left(\frac{\delta}{L}\right)^3 + B_4\left(\frac{\delta}{L}\right)^4 + B_5\left(\frac{\delta}{L}\right)^5 \tag{37}$$

where

$$B_1 = \{[1-(2RP/P_e)](K_{11}+K_{12}) + R(K_{11}' + K_{12}')\}\, b' + [R(K_{11}+K_{12})b'^2/3]$$

$$B_2 = \{[1-(3RP/P_e)](K_{11}+K_{12}) + R(K_{11}'+K_{12}')\}c' + R(K_{11}+K_{12})b'c'$$

$$B_3 = \{[1-(4RP/P_e)](K_{11}+K_{12}) + R(K_{11}'+K_{12}')\}e' + [2R(K_{11}+K_{12})\times(2b'e'+c'^2)/3]$$

$$B_4 = 5(K_{11}+K_{12})R\,c'e'/3$$

$$B_5 = (K_{11}+K_{12})Re'^2$$

where $b' = bI/I_b$, $c' = cI/I_b$, and $e' = eI/I_b$. A trivial solution of the equation is

$$\delta/L = 0 \tag{38}$$

which represents the unbuckled straight column. Other solutions may be obtained by dividing Eq. (37) through by the common factor δ/L and then solving the resulting fourth-order equation in δ/L. For any given value of P/P_e, $(K_{11}+K_{12})$ and $(K_{11}'+K_{12}')$ can be calculated from Eq. (34) and (δ/L) can then be solved from Eq. (37).

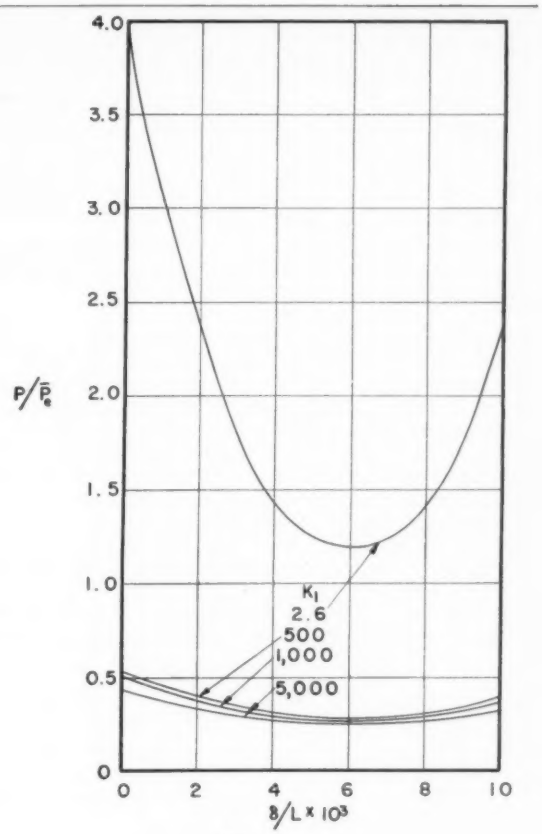

FIG. 5.

In terms of the constants defined previously, we find that

$$R = P_e/A_cG_c = \pi^2 EI/L^2A_cG_c$$
$$= \pi^2(E_fI_f + E_cI_c)/L^2A_cG_c$$
$$= \pi^2\left(\frac{h}{a}\right)^2\left(\frac{a}{l}\right)^2\left(\frac{l}{L}\right)^2\left[\frac{E_f}{G_c}\frac{A_f}{A_c} + \frac{2(1+\nu_c)}{3}\right]$$
$$= \pi^2 K_3K_4K_5^2\left\{K_1K_2 + [2(1+\nu_c)/3]\right\}$$

we shall take $K_2 = 0.1$, $K_3 = 0.0016$, $K_4 = 0.2$, $K_5 = 0.1$, and $I/I_b = 2.77 \times 10^{-4}$. For $K_1 = 2.6$, 500, 1,000, 5,000, we have $R = 3.56 \times 10^{-5}$, 1.60×10^{-3}, 3.16×10^{-2}, and 1.58×10^{-2}, respectively. From Fig. 3, the constants b, c, e are then computed. To compare the characteristics of the P vs. δ curves, we plot $P/\bar{P}_e$ against δ/L in Fig. 5, where $\bar{P}_e = \pi^2\bar{E}\bar{I}/L^2$, $\bar{E}\bar{I}$ being the EI of the homogeneous column.

CONCLUSIONS

From the $P/\bar{P}_e$ vs. δ/L curves, it is seen that, as the shear rigidity of the core of the sandwich structure is

reduced, influence of nonlinearity of the equations on the characteristics of the buckling decreases. Because of the decrease of shear rigidity of the column, the classical buckling load is greatly reduced, while the "valley" in the P vs. δ curve due to retaining the nonlinear terms does not lower as much. This explains that, for sandwich cylinders with weak cores, the buckling loads as calculated by the small deflection theory check well with those found by experiments; whereas for sandwich cylinders with strong core, this agreement cannot be expected.

References

[1] Teichmann, F. K., Wang, C. T., and Gerard, G., *Buckling of Sandwich Cylinders Under Axial Compression*, Journal of the Aeronautical Sciences, Vol. 18, No. 6, pp. 398–406, June, 1951.

[2] Teichmann, F. K., and Wang, C. T., *Finite Deflections of Curved Sandwich Plates and Sandwich Cylinders*, Sherman M. Fairchild Publication Fund Paper No. FF-4, Institute of the Aeronautical Sciences, January, 1951.

[3] von Kármán, Th., Dunn, L. G., and Tsien, H. S., *The Influence of Curvature on the Buckling Characteristics of Structures*, Journal of the Aeronautical Sciences, Vol. 7, No. 7, p. 276, May, 1940.

[4] von Kármán, Th., and Tsien, H. S., *The Buckling of Thin Cylindrical Shells Under Axial Compression*, Journal of the Aeronautical Sciences, Vol. 8, No. 8, p. 303, June, 1941.

[5] Donnell, L. H., and Wan, C. C., *Effect of Imperfections on Buckling of Thin Cylinders and Columns under Axial Compression*, J. of Appl. Mechanics, Vol. 17, No. 1, p. 73, March, 1950.

[6] Tsien, H. S., *Buckling of a Column with Non-Linear Lateral Supports*, Journal of the Aeronautical Sciences, Vol. 9, No. 4, p. 119, February, 1942.

[7] Tsien, H. S., *Lower Buckling Load in the Non-Linear Buckling Theory for Thin Shells*, Quarterly Appl. Math., Vol. V, No. 2, p. 236, July, 1947.

[8] Biezeno, C. B., and Koch, J. J., *On the Non-Linear Deflection of a Semi-Circular Ring, Clamped at Both Ends*, Proc. Koninklyke Nederlansche Akademie van Wetenschappen, Vol. XLIX, pp. 139–145, 1946.

[9] Timoshenko, S., *Theory of Elastic Stability*, p. 230; McGraw-Hill Book Company, Inc., 1936. Also J. Appl. Mech., Vol. 2, p. 17, 1935.

[10] Knopp, K., *Theory and Application of Infinite Series*, p. 207–208, Hafner Publishing Company, 1928.

On Unsteady Nonlinearized Conical Flow

(*Continued from page 92*)

[9] Bleakney and Taub, *Interaction of Shock Waves*, Review of Modern Physics, October, 1949.

[10] Taub, A. H., *Refraction of Plane Shock Waves*, Physical Review, Vol. 71, p. 51, 1947.

[11] Bleakney, Fletcher, and Weimer, *The Density Field in Mach Reflection of Shock Waves*, Phys. Rev., July 15, 1949.

[12] Liepmann, H., *The Interaction Between Boundary Layer and Shock Waves in Transonic Flow*, Journal of the Aeronautical Sciences, Vol. 13, No. 12, pp. 623–63, December, 1946.

[13] Liepmann, Ashkenas, and Cole, *Experimental Transonic Flow*, Galcit Report, June, 1947.

[14] Geiger and Mautz, *The Shock Tube as an Instrument for the Investigation of Transonic and Supersonic Flow Patterns*, Univ. of Mich. Research Report, June, 1949.

[15] Courant, R., and Friedrichs, K. O., *Supersonic Flow and Shock Waves*, p. 332; Interscience Publishers, New York, 1948.

[16] Lighthill, M. J., *The Diffraction of Blast I*, Proc. Roy. Soc. Series A, Vol. 198, 1949.

[17] Lighthill, M. J., *The Diffraction of Blast II*, Proc. Roy. Soc. Series A, Vol. 200, 1949–1950.

[18] Ferri, Antonio, *Elements of Aerodynamics of Supersonic Flows*, The Macmillan Company, New York, 1949.

[19] Vazsonyi, Andrew, *On Rotational Gas Flows*, Q.A.M., Vol. 3, p. 1, 1945.

[20] Roberts and Lin, *The Method of Characteristics in Compressible Flow, Part 2, Unsteady Flow*, Tech. Report No. F-TR-1173D-ND, Wright Field, Dayton, Ohio, December, 1947.

[21] Edmonson, Murnaghan, and Snow, *The Theory and Practice of Two Dimensional Supersonic Pressure Calculations*, A.P.L., Johns Hopkins Univ., Bumblebee Report No. 26, December, 1945.

Theoretical Investigation of Several Types of Single Degree of Freedom Flutter

HARRY L. RUNYAN,* HERBERT J. CUNNINGHAM,* AND CHARLES E. WATKINS*

Langley Aeronautical Laboratory, N.A.C.A.

SUMMARY

The possibility of an undamped oscillation of an airfoil (or aerodynamic body) with a single degree of freedom in potential flow was first noted by Glauert in 1929 but has received relatively little attention until recently. These undamped oscillations might have a direct bearing on problems of both "dynamic stability" and "flutter" of airplanes. Because of the many configurations of airplane design now being considered and because of the wide operational ranges of speed and altitude, knowledge of these single degree phenomena becomes more significant.

The present paper gives theoretically predicted effects of several primary parameters associated with single degree of freedom flutter. Specific problems dealt with are: (a) pitching oscillation of an unswept wing, oscillation of an aileron about its hinge axis, and bending oscillation of a swept wing in subsonic streams; (b) pitching of an unswept rectangular wing, pitching of a delta or triangular wing, and oscillations of an aileron about its hinge line, in supersonic streams.

Results for one series of experiments which confirm the existence of single degree of freedom pitching flutter of an unswept wing at low speeds are included.

INTRODUCTION

IT HAS BEEN RECOGNIZED for some time that the linearized aerodynamic theory for an airfoil, oscillating in a two-dimensional potential subsonic or supersonic flow, indicates that under certain conditions a single degree of freedom pitching instability is possible. The possibility of occurrence of this instability, which may be referred to as a type of single degree of freedom flutter, was first noted by Glauert[1] about 1929. Glauert, following Wagner,[2] made theoretical studies of the air forces acting on an airfoil oscillating in two-dimensional incompressible flow. Although Glauert discussed briefly the conditions under which the theory for incompressible flow indicated that such an instability might occur and went so far as to propose an experimental investigation to test the theory, it appears the problem was completely overlooked for several years.

In 1937, Possio[3] published the results of a theoretical study of air forces acting on an airfoil oscillating in steady two-dimensional supersonic flow. In his publication it was pointed out that, for certain ranges of Mach Number and location of axis of rotation, a pitching instability is indicated by linearized theory for two-dimensional supersonic flow. There followed considerable interest in the possibility of single degree of freedom flutter in supersonic flow, and a number of investigators[4–7] both in this country and in England studied the problem.

In 1946, Garrick and Rubinow[5] presented the results of a general investigation of oscillating air forces and flutter in two-dimensional supersonic flow. Their investigation was partly devoted to the problem of single degree of freedom flutter. Ranges of Mach Number and of location of axis of rotation were delineated for which single degree flutter was predicted to be possible. Furthermore, these authors pointed out again that a similar type of instability is indicated by the theory for incompressible flow. After this, Smilg[8] made a calculation study to determine the conditions, with regard to moment of inertia and location of airfoil pitch axis, under which the instability might occur in incompressible flow.

The results of Garrick and Rubinow[5] for supersonic flow and of Smilg[8] for incompressible flow may be considered as starting points for some recent[9–11] and current work on the problem of single degree of freedom flutter. In some of these investigations the possibility of undamped oscillations other than pitching of the wing has been studied.

The purpose of the present paper is to discuss some results and salient features of these investigations. Theoretically predicted effects are given of several primary parameters associated with single degree of freedom flutter. Specific problems dealt with are: (a) at subsonic speeds, pitching oscillation of an unswept wing, oscillation of an aileron about its hinge axis, and bending oscillations of a swept wing; (b) at supersonic speeds, pitching of an unswept rectangular wing, pitching of a delta or triangular wing, and oscillations of an aileron about its hinge line.

Results are included for one series of experiments which confirm the existence of single degree of freedom pitching flutter of an unswept wing at low speeds.

Until recently, whatever interest was shown in the phenomena of undamped single degree oscillations was mainly academic. However, with present-day configurations of airplane design for high speeds at high altitudes, undamped single degree oscillations even of extremely small amplitude may become important. Furthermore, calculations of single-degree flutter may

Presented at the Aeroelasticity Session, Nineteenth Annual Meeting, I.A.S., New York, January 29–February 1, 1951.

* Aeronautical Research Scientist.

be a useful easily obtained limit for cases of coupled flutter.

Symbols

a	= nondimensional distance of axis of rotation from midchord, measured in half chords, positive aft
A_0, A_1	= aerodynamic flutter coefficients
b	= airfoil half chord
B_0, B_1	= mass, inertia, and elastic force coefficients
c	= nondimensional location of control surface hinge axis, measured in half chords from the midchord, positive aft
c'	= cot Λ
C_z	= structural stiffness per unit of span length ($z = \alpha, \beta, h$)
d	= coefficient of viscous damping
d_0	= $1/E'$
d_1	= defined in section following Eq. (5-2)
E'	= complete elliptic integral of second kind
F'	= complete elliptic integral of first kind
F, G	= functions of k for oscillating plane flow
g_z	= coefficient of structural damping ($z = \alpha, \beta, h$)
h	= vertical bending displacement
I_z	= moment of inertia about axis of rotation per unit of span length ($z = \alpha, \beta$)
k	= reduced frequency parameter ($b\omega/v$)
l'	= wing semispan
M	= Mach Number
m	= mass per unit length
M_z	= complex aerodynamic moment about axis of rotation ($z = \alpha, \beta$)
M_1, M_2, M_3, M_4	= aerodynamic flutter coefficients
P_n	= aerodynamic lift force
v	= velocity, ft. per sec.
x_θ	= location of axis of rotation, based on chord, measured from leading edge, positive aft
y'	= spanwise coordinate
z	= a single degree of freedom ($z = \alpha, \beta, h$)
Z_1, Z_2, Z_3, Z_4	= aerodynamic flutter coefficients
α	= angular displacement of airfoil about axis of rotation a
β_1	= $\sqrt{M^2 - 1}$
β	= angular displacement of control surface about axis of rotation c
ω	= circular frequency
ω_z	= natural circular frequency ($z = \alpha, \beta, h$)
Λ	= sweep angle
η	= nondimensional spanwise coordinate, based on semispan l'
ρ	= air density

Subscripts

r	= reference
R	= root
h	= bending degree of freedom
z	= a single degree of freedom
α	= pitching degree of freedom
β	= control surface degree of freedom

Basic Considerations

Before discussing specific examples of single degree of freedom flutter, it may be advantageous first to review the concept of a single degree of freedom vibrating system and then to show the relation of this example to an aerodynamic system. The linear differential equation for a free system consisting of a mass m, a spring having a spring constant C_z, and a viscous damper having a coefficient d is

$$m\ddot{x} + d\dot{x} + C_z x = 0 \tag{i}$$

The motion represented by this equation is damped if d is a positive quantity, as is ordinarily the case. If d should be negative, the motion is undamped and a condition of dynamic instability exists, and, if d is zero, harmonic oscillations may exist, corresponding to a borderline condition between damped and undamped motion.

For a system such as an aircraft wing oscillating in a steady air stream, the same type of equation would apply as for the mass-spring-damper system previously mentioned. However, the coefficients m, d, and C_z of Eq. (i) will now have added components associated with the aerodynamics. A typical equation of an oscillating wing is

$$I_z\ddot{z} + (1 + ig_z)C_z z = M_z(z, \dot{z}, \ddot{z}, \ldots) \tag{ii}$$

where M_z represents the complex aerodynamic moment that is a function in part of amplitude z, velocity $\dot{z}$, acceleration $\ddot{z}$, a reduced frequency $k = \omega b/v$, location of axis of rotation, Mach Number M, and sweep angle Λ. Eq. (ii) can be separated into two components, one associated with the damping of the system (sometimes referred to as the imaginary part) and the other associated with the flutter frequency and velocity as follows (sometimes called the real part): damping (out-of-phase component)

$$-C_z g_z + Im(M_z) = 0 \tag{iii}$$

and frequency equation (in-phase component)

$$\omega^2 I_z - C_z = -Re(M_z) \tag{iv}$$

where

$$M_z = Re(M_z) + iIm(M_z)$$

Eq. (iii) is equivalent to the vanishing of the damping coefficient d of Eq. (i) and thus represents a borderline condition between damped and undamped oscillations. This is the condition sought in flutter work. The flutter frequency and air speed can then be determined from Eq. (iv).

(I) Subsonic Flow

(I) Pitching Oscillations of an Airfoil

The first example to be considered is that of an airfoil oscillating in pitch. As was pointed out in the introduction, Smilg[8] has reported some calculation studies for the Mach Number zero case in which it was shown that the axis of rotation must be ahead of the one-quarter chord. This work has recently been extended

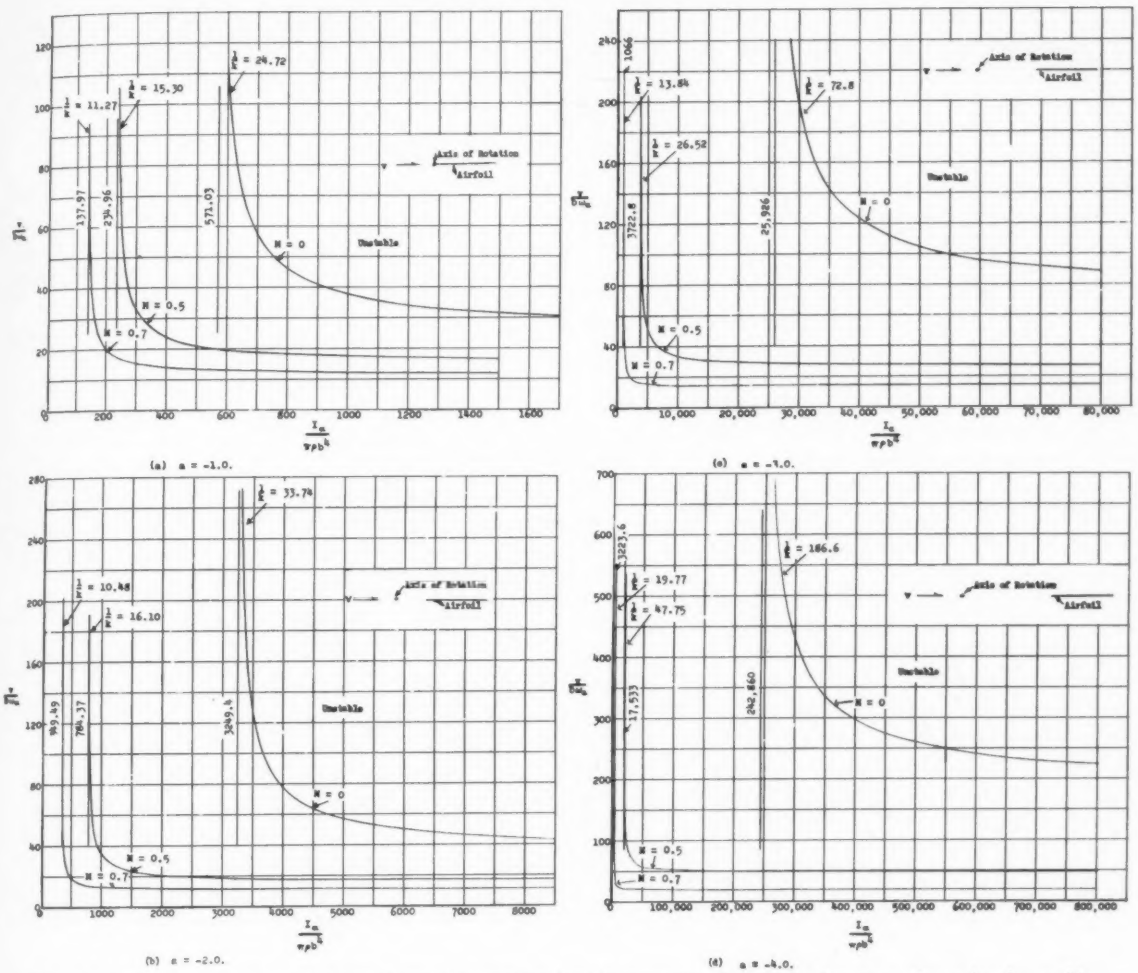

FIG. 1-1. Plot of reduced velocity coefficient $v/b\omega_\alpha$ against inertia parameter $I_\alpha/\pi\rho b^4$ for four axes of rotation ($g_\alpha = 0$).

by Runyan to include the effect of Mach Number and structural damping.

Eq. (ii) in terms of the pitching (or yawing) degree of freedom α results in

$$I_\alpha\ddot{\alpha} + (1 + ig_\alpha)C_\alpha\alpha = M_\alpha \qquad (1\text{-}1)$$

where M_α is the complex aerodynamic moment. M_α for two-dimensional flow was given analytically by Theodorsen[12] for the $M = 0$ case, and some numerical values were given by Garrick[13] for the compressible-flow case.

If Eq. (1-1) is separated into two components, there results: (out-of-phase component)

$$\frac{4}{k^2}\left[M_4 - \frac{1}{2}\left(\frac{1}{2} + a\right)\left(M_2 + Z_4 - \frac{a}{2}Z_2\right)\right] + \frac{1}{k^2}M_2 + g_\alpha\left(\frac{\omega_\alpha}{\omega}\right)^2\frac{I_\alpha}{\pi\rho b^4} = 0 \qquad (1\text{-}2)$$

(in-phase component)

$$\left[\left(\frac{\omega_\alpha}{\omega}\right)^2 - 1\right]\frac{I_\alpha}{\pi\rho b^4} + \frac{4}{k^2}\left[M_3 - \frac{1}{2}\left(\frac{1}{2} + a\right)\left(M_1 + Z_3 - \frac{a}{2}Z_1\right)\right] + \frac{1}{k^2}M_1 = 0 \qquad (1\text{-}3)$$

Eq. (1-2) represents the condition that the total damping, structural plus aerodynamic, vanishes. Because of the transcendental nature of this equation, the solution must be obtained by step-by-step or graphical methods. The calculation procedure used here is to assume values of Mach Number M, structural damping g_α, location of axis of rotation a, and the inertia parameter $I_\alpha/\pi\rho b^4$ and to solve Eq. (1-2) graphically for k. The value of reduced frequency k thus obtained, taken with the corresponding assumed parameters, then constitutes a set of parameters under which a borderline condition between damped and undamped oscillation exists. This set of conditions can thus be applied to Eq. (1-3) in

order to determine the frequency of oscillation ω and the flutter speed v associated with these conditions.

Some results of calculations based on the above procedure for $g_\alpha = 0$ are presented in Fig. 1-1 where a flutter speed coefficient $v/b\omega_\alpha$ is plotted against an inertia parameter $I_\alpha/\pi\rho b^4$ for three Mach Numbers, $M = 0$, 0.5, and 0.7 and for four locations of axis of rotation $a = -1$, -2, -3, and -4. The effect of altitude may be observed since an increase in the inertia parameter $I_\alpha/\pi\rho b^4$ may represent an increase in altitude. The region of instability for each curve is to the right or above the curve, and the vertical asymptotes to the respective curves indicate the smallest value of the inertia parameter at which the oscillation could occur. The results of Smilg[8] correspond to the curves $M = 0$. One of the more important trends to be noted by an examination of curves is the large effect that Mach Number has on the range of the inertia parameter in which the instability can occur. For instance, for the axis of rotation located at $a = -4$ (Fig. 1-1d), the minimum (asymptotes) value of the inertia parameter for $M = 0$ is 242,000 whereas for $M = 0.7$ it is reduced to 3,223. If the aircraft center of gravity is regarded as the axis of rotation and the vertical tail is considered as the airfoil, values of the inertia parameter for modern aircraft vary from 2,000 to 20,000 at sea level, which are increased by a factor of 10 for aircraft operating at 60,000 ft. It can be seen, then, that the parameters of modern aircraft may fall within the ranges of the parameter indicated here. However, it should be remembered that the calculations presented here are based on two-dimensional flow considerations and that such effects as aspect ratio and other degrees of freedom have not been considered. It is probable that these additional factors could have a great effect on the single degree of freedom instability, and the results presented in this paper must be considered as possible limit conditions for actual configurations.

The results of calculations in which structural damping coefficient g_α has been considered are shown on Fig. 1-2 for one axis of rotation location $a = -1.24$. The abscissa is the inertia parameter, and the ordinate is the flutter speed coefficient $v/b\omega_\alpha$. The type of structural damping used in flutter analysis is in phase with the velocity but is proportional to amplitude. Damping has a great effect on the flutter speed, as can be seen by an examination of Fig. 1-2. As an example, the flutter speed for zero structural damping is raised by a factor of 5, with $I_\alpha/\pi\rho b^4 = 18{,}000$ for $g_\alpha = 0.02$. If possible, the use of structural damping should be an effective method of eliminating this type of flutter.

A preliminary experimental investigation at low air speeds of single degree of freedom oscillation has been made by Runyan in which a rigid wing was hinged in front of the leading edge ($a = -1.24$) and was restrained by a coil spring. The results of the investigation are shown on Fig. 1-2. The experimental data agree with theory for $M = 0$ and $g_\alpha = 0.008$ at high values of the inertia parameter which correspond to high altitudes. However, at low values of inertia parameter the agreement between theory and experiment is poor and requires further investigation.

(2) *Control-Surface Oscillations*

By a similar analysis, a single degree of freedom oscillation can theoretically be shown to exist if the control surface degree of freedom is examined. The equilibrium of moments on a section of a control surface about its axis of rotation may be written as

$$I_\beta\ddot{\beta} + (1 + ig_\beta)C_\beta\beta = M_\beta \qquad (2\text{-}1)$$

Theodorsen[12] has given the expression for M_β for the $M = 0$ condition. Tables for M_β for subsonic flow have been given by Dietze[14] for one control-surface chord/wing-chord ratio, and these tables were extended by Turner and Rabinowitz[15] to include several control-surface chord/wing-chord ratios. Tables of M_β for supersonic flow have been published by Huckel and Durling.[16]

The results of calculations based on the values of M_β from reports mentioned above are presented in Fig. 2-1, where the abscissa is the inertia parameter $I_\beta/\pi\rho b^4$ and the ordinate is the flutter speed coefficient $v/b\omega_\beta$. One ratio of control-surface chord to wing chord of 0.15 ($c = 0.7$) is given for three Mach Numbers. These curves exhibit the same characteristics as previously noted for the pitching oscillations. A limiting (asymptotic) value of the inertia parameter for each curve is indicated below which the configuration would be stable. Therefore, a control surface that is stable at low altitudes could conceivably become unstable at high altitudes. Moreover, the effect of Mach Number is extremely great and increases the region of the inertia parameter in which the oscillation could occur. For instance, at $M = 0$, the limiting value of the inertia parameter is 15 and is reduced to 5.57 at $M = 0.7$ and is further reduced to 0.0079 for $M = 10/9$.

Recently single degree of freedom flutter of a control surface has been experienced in high-speed flight, and the explanation of the cause has not been entirely clear, although most investigators have been of the opinion that separated flow is involved. The mechanism of instability presented here, however, should provide a framework for a more complete and logical study, even though it is not necessarily a complete explanation of the cause. However, as for the pitching wing previously discussed, similar qualifications with regard to the effect of aspect ratios and other degrees of freedom apply to the control-surface oscillations.

(3) *Bending Oscillation of a Swept Wing*

This section deals with a cantilever swept wing performing only harmonic bending oscillations. The wing is shown in Fig. 3-1, and the equation of equilibrium of forces for a wing section dy', similar to Eq. (ii), is

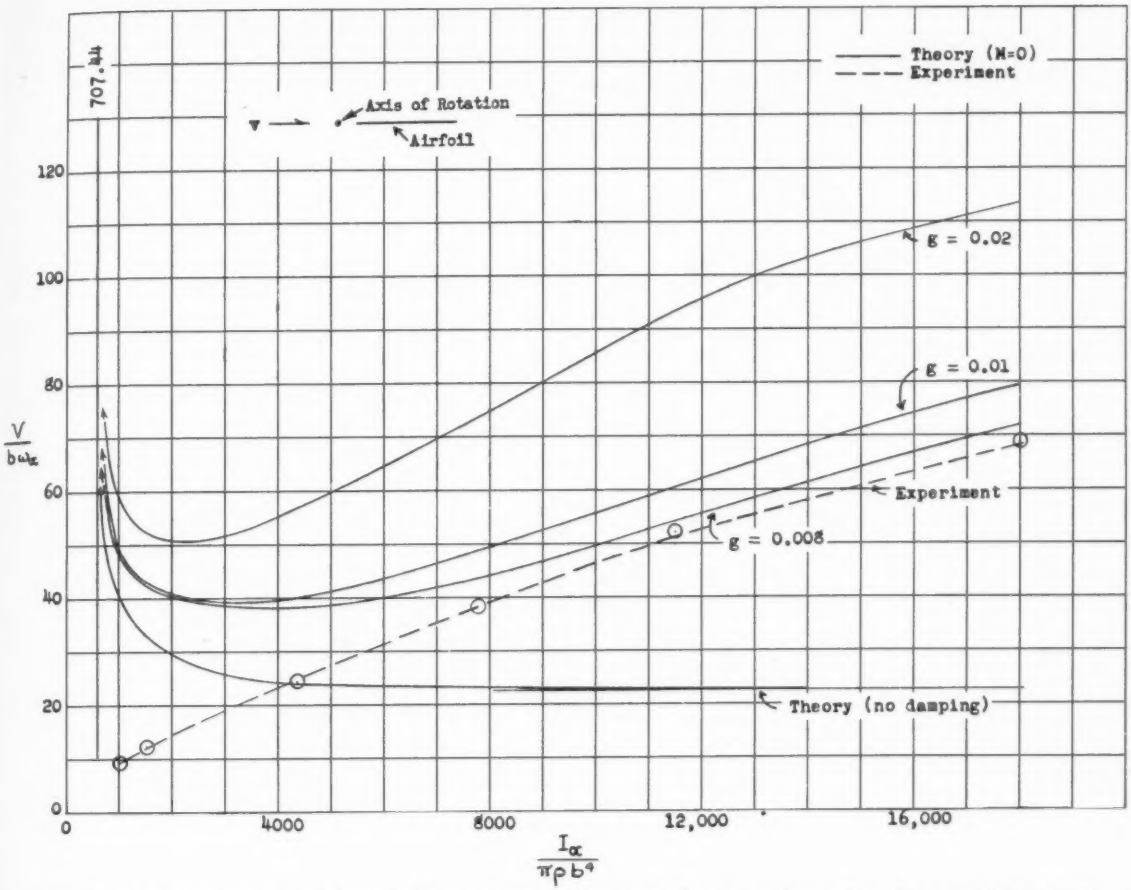

FIG. 1-2. Curves of experimental and theoretical single degree pitching oscillations for various values of structural damping ($a = -1.24$).

$$-\ddot{h}m - C_h(1 + ig_h)h = -P_h(\dot{h}, \ddot{h}, \ldots) \quad (3\text{-}1)$$

where h is vertical bending displacement of the section dy', m is mass of a unit-length section, C_h is effective elastic restraint, and g_h is structural damping coefficient for bending vibration. P_h is the aerodynamic lifting force for harmonic bending oscillation and is a function of several parameters including angle of sweep, Mach Number, and reduced frequency k_n, which is $\omega b/v \cos \Lambda$. The semichord b is for a section normal or nearly normal to the leading edge.

The case of cantilever wing bending inherently treats a wing whose different spanwise sections have different amplitudes—that is, the wing has a mode shape that is not a constant over the span. An equation of equilibrium of forces for harmonic motion, therefore, is not, in general, that of a representative section but is an equation whose elements are integrations over the wing.

The bending displacement of a section as a function of time and of span position is represented by

$$h = \boldsymbol{h}[f_h(y')] \quad (3\text{-}2)$$

where y' is the coordinate measured along the length of the swept wing, $f_h(y')$ is the shape of the bending mode, and

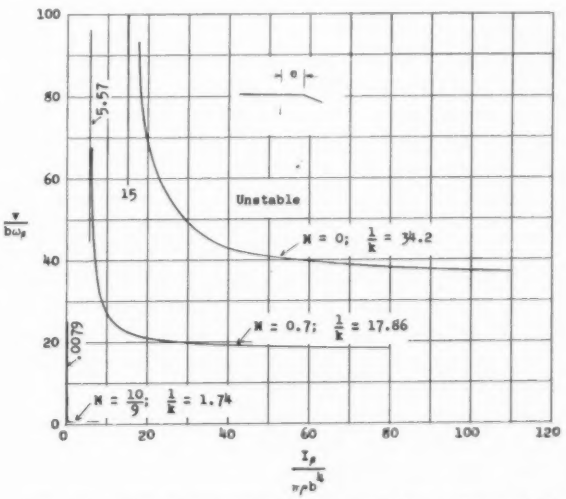

FIG. 2-1. Plot of reduced velocity coefficient $v/b\omega_\beta$ against inertia parameter $I_\beta/\pi\rho b^4$ for one location of axis of rotation $c = 0.7$ and for several Mach Numbers.

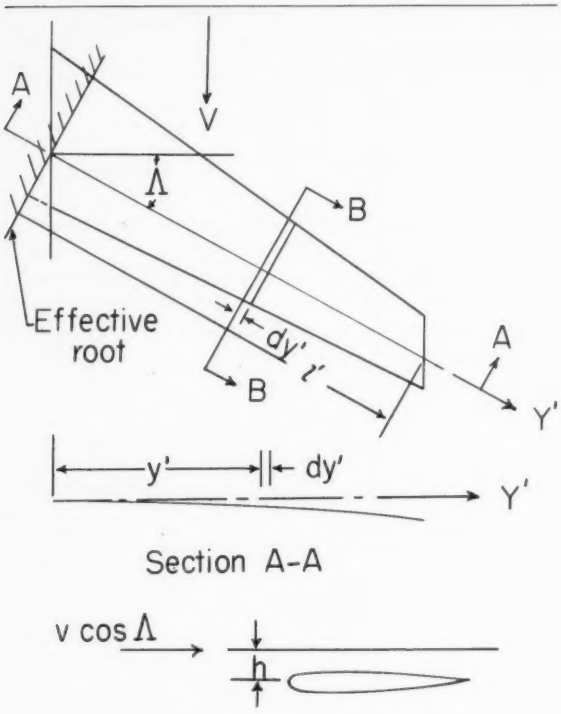

FIG. 3-1. Swept wing.

$$h = h_0 e^{i\omega t} \tag{3-3}$$

of which h_0 is a constant.

In consideration of the work done by all forces in the bending direction, the equation of equilibrium of bending forces for the entire wing is

$$-\ddot{h}\int_0^{l'} m[f_h(y')]^2 dy' - h\int_0^{l'} C_h(1 + ig_h)[f_h(y')]^2 dy' = -\int_0^{l'} P_h[f_h(y')]dy' \tag{3-4}$$

The limits 0 and l' are values of y' for wing root and tip, respectively.

Through a series of steps, Eq. (3-4) can be converted to a more useful form. The steps are: (1) Wing bending frequency ω_h is introduced to represent elastic restoring force; (2) substitute for P_h the aerodynamic forces of Eq. (10) of reference 17 which apply for bending vibration; (3) convert the lengthwise variable y' to the nondimensional η, which is zero at the root and 1.0 at the tip; (4) replace $\ddot{h}$ by $-\omega^2 h$; and (5) collect terms. The resulting equation of equilibrium of complex forces can then, as in preceding sections, be separated into two equations of component forces, expressing the simultaneous equilibrium of forces in phase with bending displacement and of forces 90° out of phase wth displacement. The two equations in symbolic form are: equilibrium of in-phase forces

$$(B_0 + A_0)\pi\rho b_r^3\omega^2 l' = 0 \tag{3-5}$$

equilibrium of forces 90° out of phase

$$(B_1 + A_1)\pi\rho b_r^3\omega^2 l' = 0 \tag{3-6}$$

where B_0 is the integrated coefficient of mass inertia and elastic forces in phase with bending displacement, B_1 is the integrated coefficient of structural damping forces, A_0 is the integrated coefficient of aerodynamic forces in phase with displacement, and A_1 is the integrated coefficient of aerodynamic damping force. The coefficients in expanded form as developed are

$$B_0 = \left[1 - \left(\frac{\omega_h}{\omega}\right)^2\right]\int_0^{1.0}\left(\frac{b}{b_r}\right)^2 \frac{1}{\kappa}[F_h(\eta)]^2 d\eta$$

$$B_1 = -g_h\left(\frac{\omega_h}{\omega}\right)^2\int_0^{1.0}\left(\frac{b}{b_r}\right)^2 \frac{1}{\kappa}[F_h(\eta)]^2 d\eta$$

$$A_0 = -\int_0^{1.0}\left(\frac{b}{b_r}\right)^2 R_{ch}[F_h(\eta)]^2 d\eta - \int_0^{1.0}\left(\frac{b}{b_r}\right)^3 \frac{\tan\Lambda}{l'/b_r}\frac{1}{k_n} I_{ch}[(F_h(\eta)]\frac{dF_h}{d\eta}d\eta - \int_0^{1.0}\left(\frac{b}{b_r}\right)^4\left(\frac{\tan\Lambda}{l'/b_r}\right)^2 \frac{1}{k_n^2}[F_h(\eta)]\frac{d^2F_h}{d\eta^2}d\eta$$

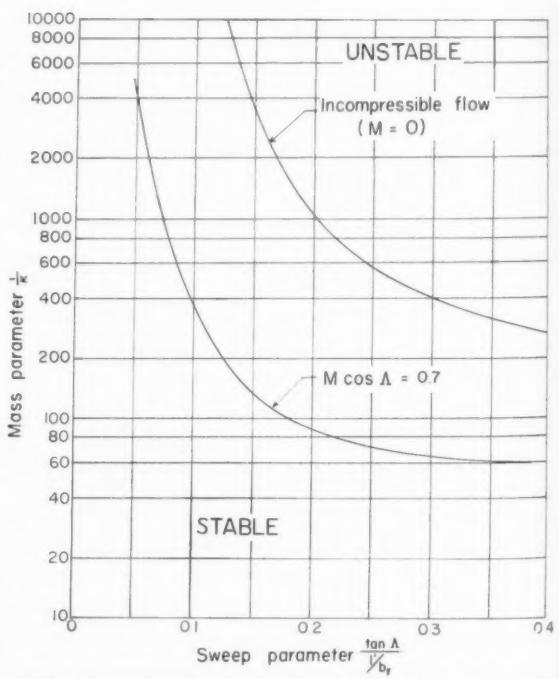

Fig. 3-2. Minimum mass parameter as a function of the sweep parameter to enable single degree bending flutter of a uniform swept wing.

$$A_1 = -\int_0^{1.0} \left(\frac{b}{b_r}\right)^2 I_{ch}[F_h(\eta)]^2\, d\eta + \int_0^{1.0} \left(\frac{b}{b_r}\right)^3 \frac{\tan\Lambda}{l'/b_r}\,\frac{1}{k_n}\,(-1 + R_{ch})\,[F_h(\eta)]\,\frac{dF_h}{d\eta}\,d\eta$$

where κ is $\pi\rho b^2/m$ mass parameter; b_r is the semichord of a section chosen as a reference,

$$F_h(\eta) = f_h(l'\eta) = f_h(y')$$

R_{ch} and I_{ch} are the real and imaginary parts, respectively, of a complex function, which accounts for part of the aerodynamic effects. The reduced frequency k_n is $\omega b/v \cos\Lambda$.

Since a dynamic instability ($\omega \neq 0$) is being treated, the quantity within the parentheses in each equation, Eqs. (3-5) and (3-6), is zero as follows:

$$B_0 + A_0 = 0 \qquad (3\text{-}7)$$

$$B_1 + A_1 = 0 \qquad (3\text{-}8)$$

For incompressible flow, the aerodynamic functions R_{ch} and I_{ch} used are those of two-dimensional incompressible flow. That is,

$$R_{ch} = -1 - (2G/k_n); \quad I_{ch} = (2F/k_n) \qquad (3\text{-}9)$$

where the transcendental functions F and G of Theodorsen account for the effects of the wing wake.

An attempt to approximate some effects of compressibility at subsonic speeds can be made by substituting, for R_{ch} and I_{ch}, values for two-dimensional subsonic compressible flow according to the normal-component Mach Number $M\cos\Lambda$. For this purpose, the functions R_{ch} and I_{ch} of Eq. (3-9) are replaced by R_{ch}' and $(1/k_n)I_{ch}'$, respectively, in the notation of Garrick.[13]

The simultaneous equations can be solved for any two quantities or parameters when the other parameters are specified. For the present problem, it is convenient to solve for the sweep parameter $\tan\Lambda/(l'/b_r)$ and an integrated mean or effective value of mass density ratio

$$\frac{1}{\kappa_e} = \frac{\displaystyle\int_0^{1.0} \left(\frac{b}{b_r}\right)^2 \frac{1}{\kappa}\,[F_h(\eta)]^2 d\eta}{\displaystyle\int_0^{1.0} \left(\frac{b}{b_r}\right)^2 [F_h(\eta)]^2 d\eta} \qquad (3\text{-}10)$$

The sweep parameter increases as the sweep angle Λ increases and as the length-to-semichord ratio l'/b_r decreases. The effective mass parameter $1/\kappa_e$ signifies also effect of altitude and increases with increased altitude for a given wing.

Fig. 3-2 for the case of a uniform cantilever swept wing shows, as ordinate, the minimum value of mass parameter $1/\kappa_e$ as a function of the sweep parameter $\tan\Lambda/(l'/b_r)$, for which single-degree bending flutter is theoretically possible in incompressible flow and in the compressible flow $M\cos\Lambda = 0.7$. Conversely, for any mass parameter, the curves show the minimum value of the sweep parameter for which single degree flutter is possible. For values above each curve single degree bending flutter of a uniform wing is possible; for values below the curves, it is not possible.

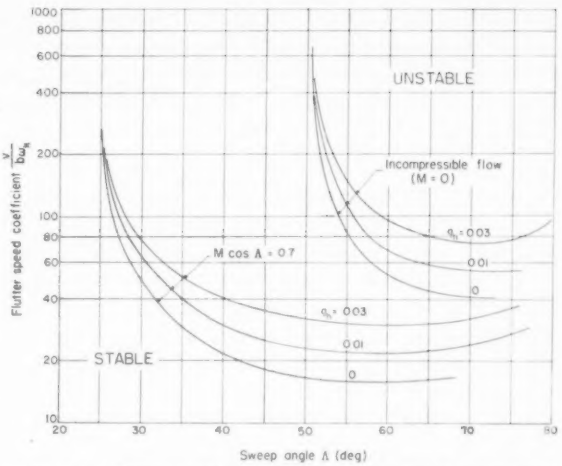

FIG. 3-3. Flutter-speed coefficient as a function of sweep angle for single degree bending flutter of a uniform swept wing of length-semichord ratio 6 and mass parameter $1/\kappa$ of 1,000.

It may be noted from Fig. 3-2 that, for a uniform wing with $\Lambda = 45°$ and length-to-semichord ratio of 5 (sweep parameter of 0.2), a wing mass parameter of at least 1,000 is necessary to enable single degree flutter in incompressible air. Such a large mass parameter is far above any contemplated value for actual aircraft. Present-day jet fighters have a wing section $1/\kappa$ of the order of 25 for sea-level air density and of 100 at high altitudes. The factor may be increased by heavier wings, higher altitudes, and weights on the wing.

It is to be noted further from Fig. 3-2 that the normal-component Mach Number $M\cos\Lambda = 0.7$ causes a marked decrease of the minimum values of mass parameter and sweep parameter to enable single degree bending flutter. A wing whose sweep parameter is 0.2 is predicted to need a mass parameter greater than only about 90, a practical combination.

Fig. 3-3 shows curves of flutter-speed coefficient as functions of sweepback angle for a uniform wing with the parameters: $1/\kappa = 1{,}000$; length-to-semichord ratio 6; and three different structural damping coefficients 0, 0.01, and 0.03 in incompressible flow and in compressible flow with $M\cos\Lambda = 0.7$.

As was noted in Fig. 3-2 and in previous sections for single degree wing pitching and aileron oscillation, compressibility is seen in Fig. 3-3 to have a marked effect on flutter characteristics. For example, for a sweep angle of 60° the flutter-speed coefficient for $M\cos\Lambda = 0.7$ flow is only about 31 per cent of that for incompressible flow. Consequently, for the two calculated flutter speeds to be the same, the wing stiffness in terms of $b\omega_h$ must in the $M\cos\Lambda = 0.7$ flow be about 327 per cent of that required for incompressible flow.

Also in Fig. 3-3 structural damping is predicted to have a large effect on single degree flutter speed for the

particular wing parameters given. At a sweep angle of 60° for an incompressible fluid, an increase of structural damping coefficient from 0 to 0.03 is predicted to increase flutter-speed coefficient by about 85 per cent. Such a large effect of structural damping is associated with the large mass parameter of 1,000.

In addition to effects of mass parameter, sweep angle, and structural damping, there is an important effect of ratio of wing length-to-semichord which is not treated here. Also of interest is the fact that single degree of freedom bending flutter is the limiting case if bending-torsion flutter as the ratio of wing bending frequency to torsion frequency approaches zero under certain conditions on mass parameter and sweep parameter. Those conditions are given for a uniform wing in Fig. 3-2. Some effects of permitting the frequency ratio ω_h/ω_α to increase from zero to finite values when the sweep parameter and mass parameter are such as to permit single degree bending flutter have been analyzed by Cunningham, but these effects are not within the scope of the present paper.

In conclusion, it should be stated of this section that the three-dimensional flow effects of finiteness of span, of mode shape, and of compressibility obviously need more exact analysis than is presented here, particularly for wings of small length-to-chord ratio. Structural effects of the root of such a wing in their relation to bending vibration also need more rigorous treatment.

(II) Supersonic Flow

The final two sections deal with wings of rectangular and triangular or delta plan forms in supersonic flow. As mentioned in the introduction, the problem of undamped pitching oscillations of wings in two-dimensional supersonic flow has been studied by a number of investigators.[4–7] In three-dimensional flow, the rectangular wing with Mach lines behind the wing diagonals has been treated by Watkins[9] and by Stewart and Li.[10] The wide delta wing—that is, one with supersonic leading edges—has been treated by Miles,[11] Watkins, Nelson, and others. The narrow delta wing—that is, with subsonic leading edges—has recently been treated by Watkins.

It is convenient to treat these cases by expanding the aerodynamic moment coefficient in terms of the reduced frequency parameter k. Considerable information regarding undamped pitching oscillations can be obtained by retaining only terms of the moment coefficient which depend on the first order of k. By such an approach one can indeed determine, with satisfactory accuracy, the range of values of such parameters as Mach Number, location of pitch axis, and aspect ratio in which the oscillations can occur. In order to study such factors as critical speed and frequency associated with the oscillations, more complete expressions for the moment coefficient are required. It is expedient here, however, to discuss only the first-order effects of the reduced frequency.

The equations to be considered are

$$(I_\alpha/\pi\rho b^4)\ [1 - (\omega_\alpha/\omega)^2] - M_3 = 0 \quad \text{(II-1)}$$

and

$$(I_\alpha/\pi\rho b^4)\ (\omega_\alpha/\omega)^2\ g_\alpha + M_4 = 0 \quad \text{(II-2)}$$

where M_3 and M_4 are the in-phase and out-of-phase components, respectively, of the moment coefficient.

(4) *Pitching Oscillation of Rectangular Wings*

For wings of rectangular plan form with Mach lines behind the wing diagonals, the components of moment coefficient, to the first order of the reduced frequency parameter, are

$$M_3 = \frac{1}{3\beta_1{}^2k^2}\left[3\beta_1(1 - 2x_0) - \frac{2 - 3x_0}{\text{A.R.}}\right] \quad \text{(4-1)}$$

$$M_4 = \frac{2}{3\beta_1{}^4k}\left[2\beta_1{}^3(1 - 3x_0 + 3x_0{}^2) - \beta_1 \times (2 - 3x_0) - \frac{2\beta_1{}^2x_0(3x_0 - 2) + 4x_0 - 3}{2\text{A.R.}}\right] \quad \text{(4-2)}$$

where x_0 is the distance, referred to wing chord, of the pitch axis from the leading edge; A.R. is aspect ratio; and β_1 is $\sqrt{M^2 - 1}$.

The range of values of M, x_0, and A.R. in which undamped oscillations can occur in this case is delineated easily by consideration of Eq. (II-2) with the damping coefficient g_α zero. The condition that M_4 vanish, as may be seen from Eq. (4-2), leads to an algebraic equation in β_1, x_0, and A.R. which may be solved readily for any one of these quantities when particular values are assigned to the other two.

Fig. 4-1 shows values of x_0 and M which satisfy this borderline condition for some selected values of aspect ratio. The curve for infinite aspect ratio corresponds to the two-dimensional flow case treated in other publications.[4–7, 9] The curves for finite aspect ratio end in the lower right portion of the figure for combinations of aspect ratio and Mach Number for which the Mach lines from the wing tips coincide with the wing diagonals.

The regions inside the different curves of Fig. 4-1 give the ranges of value of x_0 and M in which single degree pitching instability might occur—that is, in which M_4 has a negative value. It may be noted that, as the aspect ratio is decreased, the ranges of values of both M and x_0, in which the instability could occur, are decreased. For example, the curve for infinite aspect ratio indicates that the instability might occur at some Mach Number between 1 and a maximum of about 1.58 and for any pitch axis located in an unlimited range ahead of the two-thirds chord position. The curve for aspect ratio 2, however, indicates that the Mach Num-

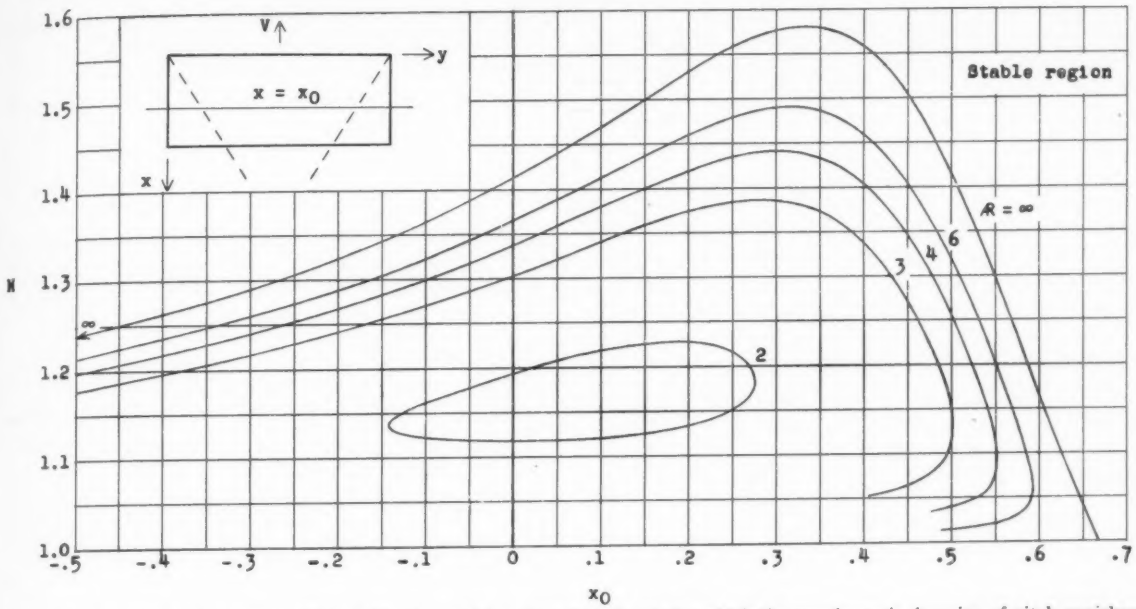

FIG. 4-1. Curves showing ranges of Mach Number and location of pitch axis for which the aerodynamic damping of pitch vanishes for rectangular wings with selected values of aspect ratio.

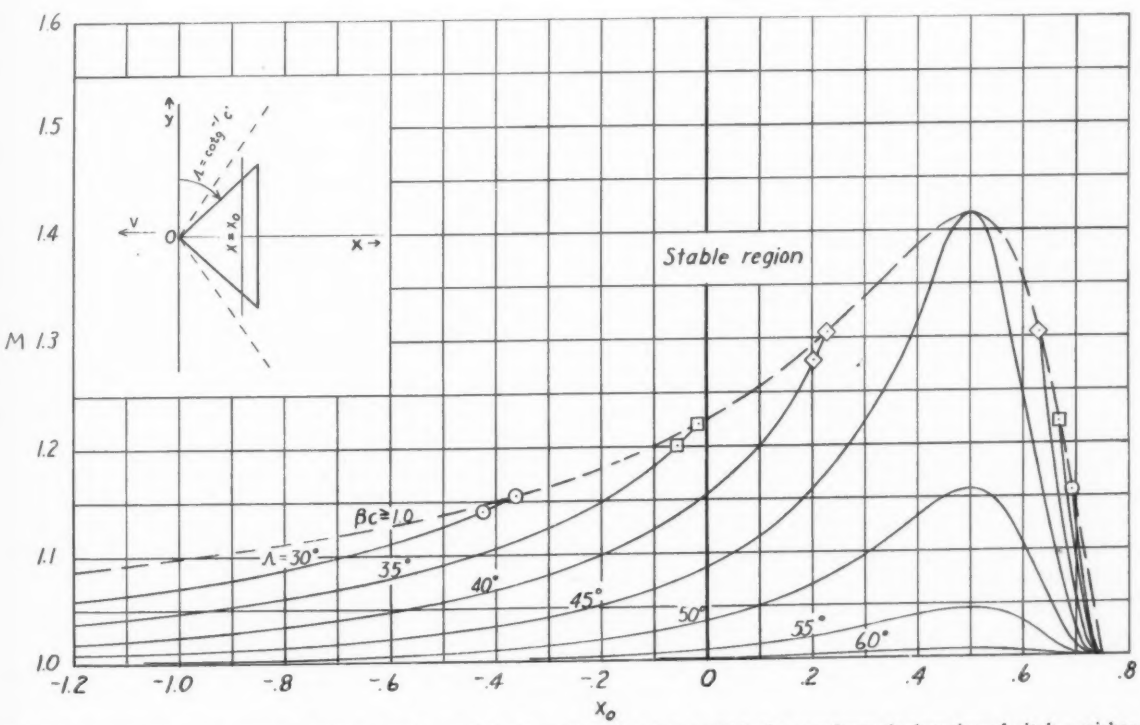

FIG. 5-1. Curves showing ranges of Mach Number and location of pitch axis for which the aerodynamic damping of pitch vanishes for delta wings with selected values of leading-edge sweep angle.

ber range is approximately only from 1.12 to 1.23 and that the location of pitch axis is limited from between 0.275 chord (behind) and −0.25 chord (ahead) relative to the leading edge. Examination of Eq. (4-2) (or of more complete expressions for M_4) will show that, as M and x_0 are held constant, the value of M_4 decreases (with x_0 not greater than about 0.67) as $^1/_2$ A.R. as A.R. decreases. Hence, decreasing the aspect ratio has a highly stabilizing effect. It may be concluded therefore that, with wings of finite aspect ratio, small values of the damping term $g_\alpha (g_\alpha \neq 0)$ could exclude the possibility of the undamped pitching oscillations.

(5) *Pitching Oscillation of Delta Wings*

For delta wings, the components of the coefficient of total moment acting about the pitch axis x_0, to the first order of the reduced frequency $k = b_R\omega/v$ (b_R is the root chord), are

$$M_3 = (\pi c'^2/3k^2)d_0(2 - 3x_0) \tag{5-1}$$

$$M_4 = \frac{\pi c'^2}{2\beta_1^2 k}\left\{3d_1(2M^2 - 1) - d_0(2M^2 + 1) + 4x_0 d_1[d_0 - (2M^2 - 1)] + 4x_0^2 d_1(M^2 - 1)\right\} \tag{5-2}$$

where c' is the cotangent of the angle of sweepback Λ,

$$d_0 = \frac{1}{E'}, \quad d_1 = \frac{1 - \beta_1^2 c'^2}{\beta_1^2 c'^2 F' + (1 - 2\beta c'^2)E'}$$

F' and E' are complete elliptic integrals of the first and second kind, respectively, with moduli $\sqrt{1 - \beta_1^2 c'^2}$. The location of pitch axis x_0 is referred to the wing root chord and is measured from the wing apex.

Fig. 5-1 shows values of Mach Number and location of pitch axis for some particular values of angle of sweepback Λ for which the condition that M_4 vanish is satisfied. As in Fig. 4-1, the regions inside the different curves give the ranges of M and x_0 for which M_4 is negative (regions of instability).

For all angles of sweepback, the range of location of pitch axis extends from the three-quarter chord to an infinite distance ahead of the wing apex ($-\infty < x_0 \leq 0.75$). The pitch-axis location at the half chord ($x_0 = 0.5$) shows an instability over the greatest range of Mach Number, from 1.0 to $\sqrt{2}$, and this range applies to a delta wing whose angle of sweepback is equal to, or less than, 45°.

As the angle of sweepback increases, the range of Mach Number of the region of instability decreases. As the sweep angle increases to about 60°, the range of Mach Number in which instability might occur, as well as the magnitude of the negative damping moment, is so small that, here again, a small amount of structural damping could eliminate the possibility of instability. This behavior is in accord with that of rectangular plan-form wings in that reducing aspect ratio has a highly stabilizing effect on single degree of freedom pitching oscillations.

It may be seen further in Fig. 5-1 that the upper-limit Mach Number for a zero damped oscillation ($M_4 = 0$) increases as the angle of sweepback decreases until the wing leading edge becomes sonic (Mach line coincides with the leading edge); but the Mach number for $M_4 = 0$ does not change with a further decrease of Λ. Thus, when the flow at the leading edges of a delta wing is sonic or supersonic ($\beta_1 c' \geq 1$), the conditions under which M_4 vanish no longer depend on the angle of sweepback. Hence, the dashed curve represents the upper limit of Mach Number for which M_4 vanish for all wide delta wings.

Concluding Remarks

The main purpose of the paper has been to direct attention to the possible loss of damping, theoretically indicated, for various single degree of freedom systems rather than to give a complete discussion of the problem. Each case considered is a limiting one of coupled flutter involving two or more degrees of freedom, and no attempt has been made to examine the effects of relaxing the condition of infinite structural stiffness in other degrees of freedom.

A study of the examples treated indicates that Mach Number has a marked influence and can cause a reduction of the stable region as defined by a mass or inertia parameter. Structural damping for all cases considered raised the flutter speed and could be an effective means of reducing or eliminating the oscillation. For the examples treated in supersonic flow, the range of variables in which the oscillation could occur was greatly reduced by a decrease in aspect ratio. The effect of aspect ratio has not been introduced in the examples calculated for subsonic flow, and it may be expected that large effects exist. This simplified treatment, however, should prove useful in connection with further experimental studies and in providing a logical grouping of variables.

References

[1] Glauert, H., *Force and Moment on an Oscillatory Aerofoil*, British A.R.C., R. & M. No. 1242 (Ac 397), London, March, 1929.

[2] Wagner, H., *Über die Entstehung des dynamischen Auftriebs von Tragflugeln*, Zeitschrift für Angewandte Mathematik und Mechanik, Vol. 5, pp. 17–35, 1925.

[3] Possio, C., *L'Azione aerodinamica sul profilo oscillante alle velocita ultrasonore*, Acta, Pont. Acad. Sci., Vol. I, No. 11, pp. 93–106, 1937.

[4] Temple, G., and Jahn, H. A., *Flutter at Supersonic Speeds. Part I—Midchord Derivative Coefficients for a Thin Aerofoil at Zero Incidence*, British A.R.C., R. & M. No. 2140, 1945.

[5] Garrick, I. E., and Rubinow, S. I., *Flutter and Oscillating Air-Force Calculations for an Airfoil in a Two-Dimensional Supersonic Flow*, N.A.C.A. Report No. 846, 1946.

[6] Jones, W. P., *Negative Torsional Aerodynamic Damping at Supersonic Speeds*, British A.R.C., R. & M. No. 2194, 1946.

[7] Cheilek, H., and Frissel, H., *Theoretical Criteria for Single-Degree-of-Freedom Flutter at Supersonic Speeds*, Report No. CAL-7A, Cornell Aero. Laboratory, Inc., May 8, 1947.

(*Continued on page 126*)

Supersonic Flow Around Cones at Large Yaw

G. B. W. YOUNG* AND C. P. SISKA†
The RAND Corporation

SUMMARY

Equations have been developed for the flow properties in the region bounded by a supersonic cone body at large angle of attack and its attached shock wave for use with the tabulations of Kopal.[1-3] A comparison of the theoretical results is made with the experimental data of Cronvich.[7] A slight discrepancy that increases with increasing Mach Number has been found in the value of K_{DYH}, the yawing head drag as tabulated by Kopal.

SYMBOLS

a	=	local velocity of sound
c	=	speed of sound in a vacuum
C_x	=	axial pressure force coefficient
C_N	=	normal pressure force coefficient
C_D	=	force pressure drag coefficient
C_L	=	lift coefficient
p	=	static pressure
u, v, w	=	orthogonal velocity components
V	=	resultant velocity
β	=	angle of velocity vector with respect to the wind axis
ϵ	=	yaw angle (equal to negative angle of attack)
ρ	=	density
barred values	=	nonyaw properties
primes	=	derivatives with respect to $\bar{\theta}$

Subscripts

1	=	free stream
r	=	rotated conical field régime
s	=	solid cone surface
w	=	shock wave surface
B	=	body axis coordinates

INTRODUCTION

THIS PRESENTATION IS INTENDED as an aid to aerodynamicists and missile designers who will utilize Kopal's tabulation of Stone's solution for supersonic flow around cones at large yaw. Relations for the flow characteristics in the conical flow field and for the normal and axial pressure force coefficients are presented in terms of the parameters used by Kopal. Since the general method of derivation is similar to that given in reference 6, many of the details are omitted.

Under the direction of Kopal,[1-3] the Computing Section of the Center of Analysis at M.I.T. has tabulated results for supersonic flow around cones at zero angle of attack, at small angles of attack, and at large angles of attack. The presentation of the results for nonyaw cones is complete, and the analysis of the problem by Taylor and Maccoll[4] is generally available. The tabulations for cones at small and large yaws contain all the essential results but are not in the form whereby the flow characteristics in the conical flow field are readily obtainable. Stone's analysis[5] for slightly yawing cones, which is employed by Kopal, has been published and has been elaborated upon by Young.[6] The analysis for cones at large yaw is only briefly reviewed in the introduction in reference 3. A brief résumé of the present paper has been published in this journal.[8] The purpose of the résumé was to draw early attention to the proper use of the M.I.T. tables.

Received May 17, 1951. Revised and received August 16, 1951.

* Research Engineer.
† Aerodynamicist.

GENERAL DISCUSSION

Stone[5] obtained a second-order solution to the problem of a supersonic cone at large yaw by assuming the following expressions for the flow properties, as the nonyaw variables ($\bar{u}$, $\bar{v}$, $\bar{p}$, and $\bar{\rho}$) are perturbed by the effects of angle of attack. See Fig. 1a for the wind coordinates as used in references 2, 3, and 5.

$$\left.\begin{aligned}
u(\bar{\theta}) &= \bar{u} + \epsilon \sum_{n=0}^{\infty} x_n \cos n\varphi + \epsilon^2 \sum_{m=0}^{\infty} u_m \cos m\varphi \\
v(\bar{\theta}) &= \bar{v} + \epsilon \sum_{n=0}^{\infty} y_n \cos n\varphi + \epsilon^2 \sum_{m=0}^{\infty} v_m \cos m\varphi \\
w(\bar{\theta}) &= \epsilon \sum_{n=0}^{\infty} z_n \sin n\varphi + \epsilon^2 \sum_{m=0}^{\infty} w_m \sin m\varphi \\
p(\bar{\theta}) &= \bar{p} + \epsilon \sum_{n=0}^{\infty} \eta_n \cos n\varphi + \epsilon^2 \sum_{m=0}^{\infty} p_m \cos m\varphi \\
\rho(\bar{\theta}) &= \bar{\rho} + \epsilon \sum_{n=0}^{\infty} \xi_n \cos n\varphi + \epsilon^2 \sum_{m=0}^{\infty} \rho_m \cos m\varphi
\end{aligned}\right\} \quad (1)$$

Kopal[2, 3] evaluated the coefficients in the following corresponding expressions

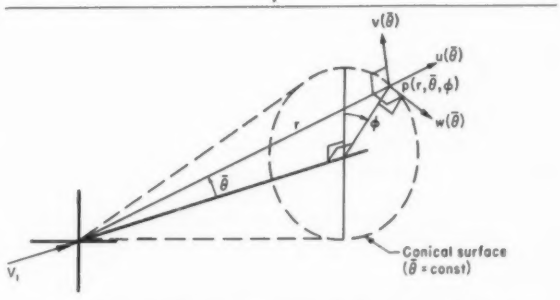

Fig. 1a — Perturbed velocity components, Eq. (2), in the non-yawed conical flow field with wind axis coordinate system ($r, \bar{\theta}, \phi$)

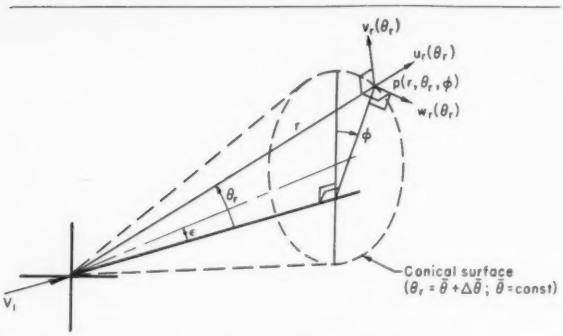

Fig. 1b — Velocity components, Eq. (3), in yawed conical flow field with wind axis coordinate system (r, θ, ϕ)

$$\left.\begin{aligned} u(\bar{\theta}) &= \bar{u} + \epsilon x \cos\varphi + \epsilon^2(u_0 + u_2 \cos 2\varphi) \\ v(\bar{\theta}) &= \bar{v} + \epsilon y \cos\varphi + \epsilon^2(v_0 + v_2 \cos 2\varphi) \\ w(\bar{\theta}) &= \epsilon z \sin\varphi + \epsilon^2 w_2 \sin 2\varphi \\ p(\bar{\theta}) &= \bar{p} + \epsilon\eta \cos\varphi + \epsilon^2(p_0 + p_2 \cos 2\varphi) \\ \rho(\bar{\theta}) &= \bar{\rho} + \epsilon\xi \cos\varphi + \epsilon^2(\rho_0 + \rho_2 \cos 2\varphi) \end{aligned}\right\} \quad (2)$$

The coefficients x, u_0, u_2, etc., are tabulated for various $\bar{\theta}$ with cone angles and Mach Numbers as parameters. The determination of these coefficients essentially completes the problem. However, upon examination of the manner in which the boundary conditions were formulated, it becomes evident that the properties $u(\bar{\theta})$, $v(\bar{\theta})$, etc., apply only in the conical field of the nonyaw cone[6] (see reference 6). In order to obtain the flow properties in the conical field of the yawed cone, a Taylor series expansion is required, this being equivalent to rotating the nonyaw conical field to a yawed position. The expansion is as follows:

$$\left.\begin{aligned} u_r(\theta_r) &= u(\bar{\theta} + \Delta\bar{\theta}) = \\ &\quad u(\bar{\theta}) + u'(\bar{\theta})\Delta\bar{\theta} + u''(\bar{\theta})(\Delta\bar{\theta}^2/2) + \ldots \\ v_r(\theta)_r &= v(\bar{\theta} + \Delta\bar{\theta}) = \\ &\quad v(\bar{\theta}) + v'(\bar{\theta})\Delta\bar{\theta} + v''(\bar{\theta})(\Delta\bar{\theta}^2/2) + \ldots \\ w_r(\theta_r) &= w(\bar{\theta} + \Delta\bar{\theta}) = \\ &\quad w(\bar{\theta}) + w'(\bar{\theta})\Delta\bar{\theta} + w''(\bar{\theta})(\Delta\bar{\theta}^2/2) + \ldots \\ p_r(\theta_r) &= p(\bar{\theta} + \Delta\bar{\theta}) = \\ &\quad p(\bar{\theta}) + p'(\bar{\theta})\Delta\bar{\theta} + p''(\bar{\theta})(\Delta\bar{\theta}^2/2) + \ldots \\ \rho_r(\theta_r) &= \rho(\bar{\theta} + \Delta\bar{\theta}) = \\ &\quad \rho(\bar{\theta}) + \rho'(\bar{\theta})\Delta\bar{\theta} + \rho''(\bar{\theta})(\Delta\bar{\theta}^2/2) + \ldots \end{aligned}\right\} \quad (3)$$

where u_r, v_r, etc., are the flow properties for the yawed field and are functions of θ_r, the yawed conical surface variable (see Fig. 1b).

The expressions θ_r and $\Delta\bar{\theta}$ for the solid cone surface and the shock wave surface are well defined by Kopal.[3] They are

$$\theta_{r_s} = \bar{\theta}_s + \Delta\bar{\theta}_s = \bar{\theta}_s + \epsilon \cos\varphi - (1/2)\epsilon^2 \cot\bar{\theta}_s \sin^2\varphi \quad (4a)$$

and

$$\theta_{r_w} = \bar{\theta}_w + \Delta\bar{\theta}_w = \bar{\theta}_w + \epsilon\alpha \cos\varphi + \epsilon^2(\beta_0 + \beta_2 \cos 2\varphi) \quad (4b)$$

Now the disturbing element is how to evaluate $\Delta\bar{\theta}$ for the intermediate conical surfaces. For small angles of attack, good results can be obtained by considering the intermediate surfaces to be rotated an amount ϵ [see Eq. (5)]; these surfaces remain circular cones, as does the solid cone surface. However, at high angles of attack, in the region of the bottom plane ($\varphi = 180°$), the properties directly behind the shock wave assume a discontinuity in slope. Also, the properties in a considerable range of θ_r, in the region of the top plane ($\varphi = 0°$), cannot be computed. To circumvent this situation an alternate method is proposed. The intermediate conical surfaces are considered to be distorted linearly, from the circular cone body to the distorted shock wave. Both methods are illustrated in the next section, and a comparison of the flow properties are shown in Figs. 6, 7, and 8.

Flow Characteristics in the Yawed Conical Flow Field with Wind Axis Coordinates (r, θ_r, φ)

(1) *Method A*

In this method it is assumed that all intermediate surfaces remain circular cones and are rotated an amount ϵ. The equation for these surfaces therefore is

$$\theta_r = \bar{\theta} + \epsilon \cos\varphi - 1/2\epsilon^2 \cot\bar{\theta} \sin^2\varphi \qquad (\text{for } \bar{\theta}_s \leq \bar{\theta} < \bar{\theta}_w) \quad (5)$$

Carrying out the operation indicated by Eq. (3) and using Eq. (5) and the first line of Eq. (2), for an example, the radial velocity component in the yawed conical flow field is given by

$$\begin{aligned} u_r(\theta_r) &= u(\bar{\theta}) + u'(\bar{\theta})\Delta\bar{\theta} + u''(\bar{\theta})(\Delta\bar{\theta}^2/2) + \ldots \\ &= \bar{u} + \epsilon x \cos\varphi + \epsilon^2(u_0 + u_2 \cos 2\varphi) + \\ &\quad [\bar{u}' + \epsilon x' \cos\varphi + \epsilon^2(u_0' + u_2' \cos 2\varphi)] \times \\ &\quad [\epsilon \cos\varphi - (1/2)\epsilon^2 \cot\bar{\theta} \sin^2\theta] + \\ &\quad [\bar{u}'' + \epsilon x'' \cos\varphi + \epsilon^2(u_0'' + u_2'' \cos 2\varphi)] \times \\ &\quad [(1/2)\epsilon^2 \cos^2\varphi + \ldots] \end{aligned}$$

Upon expansion and collection of terms it becomes, to the order ϵ^2,

$$\begin{aligned} u_r(\theta_r) &= \bar{u} + (x + \bar{u}')\epsilon \cos\varphi + \\ &\quad [u_0 - (1/4)\bar{u}' \cot\bar{\theta} + (1/2)x' + (1/4)\bar{u}'']\epsilon^2 + \\ &\quad [u_2 + (1/4)\bar{u}' \cot\bar{\theta} + (1/2)x' + (1/4)\bar{u}'')\epsilon^2 \cos 2\varphi \end{aligned}$$

This equation for u_r would hold for the flow field from the surface up to the shock wave.

For the radial velocity immediately behind the shock wave, Eq. (4b) is employed, yielding

$$\begin{aligned} u_{r_w}(\theta_{r_w}) &= u(\bar{\theta}_w) + u'(\bar{\theta}_w)\Delta\bar{\theta}_w + u''(\bar{\theta}_w)(\Delta\bar{\theta}_w^2/2) + \ldots \\ &= \bar{u}_w + \epsilon x_w \cos\varphi + \epsilon^2(u_{0_w} + u_{2_w} \cos 2\varphi) + \\ &\quad [\bar{u}_w' + \epsilon x_w' \cos\varphi + \epsilon^2(u'_{0_w} + u_{2_w}' \cos 2\varphi)] \times \\ &\quad [\epsilon\alpha \cos\varphi + \epsilon^2(\beta_0 + \beta_2 \cos 2\varphi)] + \\ &\quad [\bar{u}_w'' + \epsilon x_w'' \cos\varphi + \epsilon^2(u_{0_w}'' + u_{2_w}'' \cos 2\varphi)] \times \\ &\quad [(1/2)\epsilon^2\alpha^2 \cos^2\varphi + \ldots] \end{aligned}$$

Again, after expanding and collecting terms,

$$u_{r_w}(\theta_{r_w}) = \bar{u}_w + (x_w + \alpha\bar{u}_w')\epsilon\cos\varphi + [u_{0_w} + (1/2)\alpha x_w' + \beta_0\bar{u}_w' + (1/4)\alpha^2\bar{u}_w'']\epsilon^2 + [u_{2_w} + (1/2)\alpha x_w' + \beta_2\bar{u}_w' + (1/4)\alpha^2\bar{u}_w'']\epsilon^2\cos 2\varphi$$

In a similar manner all the necessary flow relations in the conical field at angle of attack can be obtained. The primed quantities in the equations are derivatives with respect to the variable $\bar{\theta}$ and can be found in explicit form in the latter part of this section. Since the equations of the flow properties at the solid cone surface simplify when the boundary conditions are inserted, this special set of equations is included with those of the general flow field and at the shock wave as follows:

At the yawed solid cone surface θ_{r_s},

$$\left.\begin{aligned}
u_{r_s} &= \bar{u}_s + \epsilon x_s\cos\varphi + \epsilon^2[u_{0_s} + (1/2)\bar{u}_s] + \epsilon^2\cos 2\varphi[u_{2_s} + (1/2)\bar{u}_s]\\
v_{r_s} &= \epsilon^2[v_{0_s} - x_s - (1/2)z_s\csc\bar{\theta}_s] + \epsilon^2\cos 2\varphi[v_{2_s} - \bar{u}_s\cot\bar{\theta}_s - x_s - (1/2)z_s\csc\bar{\theta}_s]\\
w_{r_s} &= \epsilon z_s\sin\varphi + \epsilon^2\sin 2\varphi[w_{2_s} - \bar{u}_s\csc\bar{\theta}_s - (1/2)z_s\cot\bar{\theta}_s]\\
p_{r_s} &= \bar{p}_s\left[1 + \epsilon\cos\varphi\left(\frac{\eta}{\bar{p}}\right)_s + \epsilon^2\left(\frac{p_0}{\bar{p}} + \frac{\gamma\bar{u}^2}{2\bar{a}^2}\right)_s + \epsilon^2\cos 2\varphi\left(\frac{p_2}{\bar{p}} + \frac{\gamma\bar{u}^2}{2\bar{a}^2}\right)_s\right]\\
\rho_{r_s} &= \bar{\rho}_s\left[1 + \epsilon\cos\varphi\left(\frac{\xi}{\bar{\rho}}\right)_s + \epsilon^2\left(\frac{\rho_0}{\bar{\rho}} + \frac{\bar{u}^2}{2\bar{a}^2}\right)_s + \epsilon^2\cos 2\varphi\left(\frac{\rho_2}{\bar{\rho}} + \frac{\bar{u}^2}{2\bar{a}^2}\right)_s\right]
\end{aligned}\right\} \quad (6)$$

At the yawed shock wave surface θ_{r_w},

$$\left.\begin{aligned}
u_{r_w} &= \bar{u}_w + \epsilon\cos\varphi(x + \alpha\bar{v})_w + \epsilon^2[u_0 + (1/2)\alpha y + \beta_0\bar{v} + (1/4)\alpha^2\bar{u}'']_w + \epsilon^2\cos 2\varphi[u_2 + (1/2)\alpha y + \beta_2\bar{v} + (1/4)\alpha^2\bar{u}'']_w\\
v_{r_w} &= \bar{v}_w + \epsilon\cos\varphi(y + \alpha\bar{u}'')_w + \epsilon^2[v_0 + (1/2)\alpha y' + \beta_0\bar{u}'' + (1/4)\alpha^2\bar{u}''']_w + \epsilon^2\cos 2\varphi[v_2 + (1/2)ay' + \beta_2 u'' + (1/4)\alpha^2\bar{u}''']_w\\
w_{r_w} &= \epsilon z_w\sin\varphi + \epsilon^2\sin 2\varphi[w_2 + (1/2)\alpha z']_w\\
p_{r_w} &= \bar{p}_w\left[1 + \epsilon\cos\varphi\left(\frac{\eta}{\bar{p}} + \alpha\frac{\bar{p}'}{\bar{p}}\right)_w + \epsilon^2\left(\frac{p_0}{\bar{p}} + \frac{\alpha}{2}\frac{\eta'}{\bar{p}} + \beta_0\frac{\bar{p}'}{\bar{p}} + \frac{\alpha^2}{4}\frac{\bar{p}''}{\bar{p}}\right)_w + \epsilon^2\cos 2\varphi\left(\frac{p_2}{\bar{p}} + \frac{\alpha}{2}\frac{\eta'}{\bar{p}} + \beta_2\frac{\bar{p}'}{\bar{p}} + \frac{\alpha^2}{4}\frac{\bar{p}''}{\bar{p}}\right)_w\right]\\
\rho_{r_w} &= \bar{\rho}_w\left[1 + \epsilon\cos\varphi\left(\frac{\xi}{\bar{\rho}} + \alpha\frac{\bar{\rho}'}{\bar{\rho}}\right)_w + \epsilon^2\left(\frac{\rho_0}{\rho} + \frac{\alpha}{2}\frac{\xi'}{\bar{\rho}} + \beta_0\frac{\bar{\rho}'}{\bar{\rho}} + \frac{\alpha^2}{4}\frac{\bar{\rho}''}{\bar{\rho}}\right)_w + \epsilon^2\cos 2\varphi\left(\frac{\rho_2}{\bar{\rho}} + \frac{\alpha}{2}\frac{\xi}{\bar{\rho}} + \beta_0\frac{\bar{\rho}'}{\bar{\rho}} + \frac{\alpha^2}{4}\frac{\bar{\rho}''}{\bar{\rho}}\right)_w\right]
\end{aligned}\right\} \quad (7)$$

At the yawed intermediate conical surfaces $\theta_{r_s} \le \theta_r < \theta_{r_w}$

$$\left.\begin{aligned}
u_r &= \bar{u} + \epsilon\cos\varphi(x + \bar{v}) + \epsilon^2[u_0 - (1/4)\bar{v}\cot\bar{\theta} + (1/2)y + (1/4)\bar{u}''] + \epsilon^2\cos 2\varphi[u_2 + (1/4)\bar{v}\cot\bar{\theta} + (1/2)y + (1/4)\bar{u}'']\\
v_r &= \bar{v} + \epsilon\cos\varphi(y + \bar{u}'') + \epsilon^2[v_0 - (1/4)\bar{u}''\cot\bar{\theta} + (1/2)y' + (1/4)\bar{u}'''] + \epsilon^2\cos 2\varphi[v_2 + (1/4)\bar{u}''\cot\bar{\theta} + (1/2)y + (1/4)\bar{u}''']\\
w_r &= \epsilon z\sin\varphi + \epsilon^2\sin 2\varphi[w_2 + (1/2)z']\\
p_r &= \bar{p}\left[1 + \epsilon\cos\varphi\left(\frac{\eta}{\bar{p}} + \frac{\bar{p}'}{\bar{p}}\right) + \epsilon^2\left(\frac{p_0}{\bar{p}} - \frac{1}{4}\frac{\bar{p}'}{\bar{p}}\cot\bar{\theta} + \frac{1}{2}\frac{\eta'}{\bar{p}} + \frac{1}{4}\frac{\bar{p}''}{\bar{p}}\right) + \epsilon^2\cos 2\varphi\left(\frac{p_2}{\bar{p}} + \frac{1}{4}\frac{\bar{p}'}{\bar{p}}\cot\bar{\theta} + \frac{1}{2}\frac{\eta'}{\bar{p}} + \frac{1}{4}\frac{\bar{p}''}{\bar{p}}\right)\right]\\
\rho_r &= \bar{\rho}\left[1 + \epsilon\cos\varphi\left(\frac{\xi}{\bar{\rho}} + \frac{\bar{\rho}'}{\bar{\rho}}\right) + \epsilon^2\left(\frac{\rho_0}{\bar{\rho}} - \frac{1}{4}\frac{\bar{\rho}'}{\bar{\rho}}\cot\bar{\theta} + \frac{1}{2}\frac{\xi'}{\bar{\rho}} + \frac{1}{4}\frac{\bar{\rho}''}{\bar{\rho}}\right) + \epsilon^2\cos 2\varphi\left(\frac{\rho_2}{\bar{\rho}} + \frac{1}{4}\frac{\bar{\rho}'}{\bar{\rho}}\cot\bar{\theta} + \frac{1}{2}\frac{\xi}{\bar{\rho}} + \frac{1}{4}\frac{\bar{\rho}''}{\bar{\rho}}\right)\right]
\end{aligned}\right\} \quad (8)$$

It must be remembered that the barred quantities and first- and second-order coefficients are tabulated as a function of $\bar{\theta}$, the nonyaw conical variable.[1-3] Thus $\bar{\theta}$ is employed as a parameter relating the flow properties given by Eqs. (6), (7), and (8) to the spatial positions, in the yawed conical flow field as given by Eqs. (4a), (4b), or (5). A typical calculation scheme is given in Table 1.

(2) *Method B*

This method assumes that the intermediate conical surfaces are distorted linearly in shape from that of the solid cone surface to that of the shock wave at angle of attack. It is evident that Eqs. (4a) and (4b) have the same form, and therefore a linear variation between the two can be achieved by linearly varying the coefficients of the φ terms. That is,

$$\theta_r = \bar{\theta} + \epsilon k_1\cos\varphi + \epsilon^2(k_2 + k_3\cos 2\varphi) \text{ (for } \theta_{r_s} \le \theta_r \le \theta_{r_w}) \quad (9a)$$

where

$$\left.\begin{aligned}
k_1 &= 1 - (1 - \alpha)\left[\frac{\bar{\theta} - \bar{\theta}_s}{\bar{\theta}_w - \bar{\theta}_s}\right]\\
k_2 &= -\frac{1}{4}\cot\bar{\theta}_s + \left(\frac{1}{4}\cot\bar{\theta}_s + \beta_0\right)\left[\frac{\bar{\theta} - \bar{\theta}_s}{\bar{\theta}_w - \bar{\theta}_s}\right]\\
k_3 &= \frac{1}{4}\cot\bar{\theta}_s - \left(\frac{1}{4}\cot\bar{\theta}_s - \beta_2\right)\left[\frac{\bar{\theta} - \bar{\theta}_s}{\bar{\theta}_w - \bar{\theta}_s}\right]
\end{aligned}\right\} \quad (9b)$$

The results of carrying out the operation indicated in Eq. (3) and using Eq. (9a) are

TABLE 1
Calculation of Static Pressure Ratio p_r/p_1 in $\varphi = 0°$ Plane (Method A)

$\theta_s = 15°$
$M_r = 1.9541$
$\epsilon = -12°$

1	2	3	4	5	6	7
$\bar{\theta}$ (deg.)	$\Delta\theta$ (rad.)	$\Delta\theta$ (deg.)	θ_r (deg.)	$\bar{a}^2$	$\bar{u}$	$\bar{v}$
...	See Eq. (5)	$\frac{180}{\pi}$ **2**	**1 + 3**	Ref. 1	Ref. 1	Ref. 1
15	−0.20944	−12	3	0.12960	0.60000	0
17°	−0.20944	−12	5	0.12945	0.59930	−0.03954

8	9	10	11	12	13	14
$\bar{v}^2$	$\cot\theta$	$\bar{v}\cot\theta$	$\bar{u} + \bar{v}\cot\theta$	$\bar{a}^2 - \bar{v}^2$	$(\bar{u} + \bar{u}'')$	$\csc\theta$
7²	**cot 1**	**7 × 9**	**6 + 10**	**5 − 8**	$-\frac{5 \times 11}{12}$	**csc 1**
0	3.7321	0	0.6000	0.12960	0.6000	3.8637
0.00156	3.2709	−0.1293	0.4700	0.12789	−0.4757	3.4203

15	16	17	18	19	20	21
$\csc^2\theta$	$\bar{v}\csc^2\theta$	$-2\bar{v}$	$\bar{u}''$	$-\bar{u}''\cot\theta$	**16 + 17 + 19**	**5 × 20**
14²	**7 × 15**	**−2 × 7**	**13 − 6**	**−9 × 18**	...	...
14.928	0	0	−1.2000	4.479	4.479	0.5805
11.698	−0.4625	−0.07908	−1.0750	3.516	3.133	0.4056

22	23	24	25	26	27	28
$2\bar{v}\bar{u}''(\bar{u} + \bar{u}'')$	$\bar{v}^3$	$(\gamma - 1)\frac{\bar{v}^2}{\bar{a}^2}$	$(\bar{u} + \bar{u}'')^2$	**24 × 25**	$\frac{\mathbf{21 + 22 + 23}}{\mathbf{26}} +$	$\bar{u}'''$
−13 × 17 × 18	**7 × 8**	$0.405\,\frac{\mathbf{23}}{5}$	**13²**	...	...	$\frac{\mathbf{27}}{\mathbf{12}}$
0	0	0	0.3600	0	0.5805	4.479
−0.04044	−0.0000617	−0.000193	0.2263	0	0.3651	2.855

29	30	31	32	33	34	35
$\frac{\gamma}{\bar{a}^2}$	$\frac{\bar{p}'}{\bar{p}}$	$-\frac{\gamma\bar{u}''}{\bar{a}^2}(\bar{u} + \bar{u}'')$	$\frac{\gamma\bar{v}^2}{\bar{a}^4}$	**32 × 25**	$(v + \bar{u}''')$	$-\frac{\gamma\bar{v}}{\bar{a}^2}(v + \bar{u}''')$
$\frac{1.405}{5}$	**−7 × 13 × 29**	**−13 × 18 × 29**	$\frac{\mathbf{29 \times 8}}{5}$	...	**7 + 28**	**−7 × 29 × 34**
10.84	0	−7.805	0	0	4.479	0
10.85	−0.2041	−5.548	0.1308	0.0296	2.815	1.208

36	37	38	39	40	41	42
$\frac{\bar{p}''}{\bar{p}}$	y	$-y\cot\theta$	$2\frac{\bar{v}y}{\bar{a}^2}$	$2\frac{\bar{v}y}{\bar{a}^2}(\bar{u} + \bar{u}'')$	x	$\frac{\bar{v}^2}{\bar{a}^2}$
31 + 33 + 35	Ref. 2	**−9 × 37**	$\frac{\mathbf{-17 \times 37}}{5}$	**13 × 39**	Ref. 2	$\frac{\mathbf{8}}{\mathbf{5}}$
−7.805	1.2000	−4.479	0	0	−0.2503	0
−4.310	0.9833	−3.216	−0.6007	0.2858	−0.2124	0.01205

43	44	45	46	47	48	49
$2 - \frac{\bar{v}^2}{\bar{a}^2}$	$-x\left(2 - \frac{\bar{v}^2}{\bar{a}^2}\right)$	z	$-z\csc\theta$	$\bar{u}x$	$\bar{v}y$	$(\bar{u}x + \bar{v}y)$
2 − 42	**−41 × 43**	Ref. 2	**−14 × 45**	**6 × 41**	**7 × 37**	**47 + 48**
2.000	0.5006	0.9803	−3.788	−0.1502	0	−0.1502
1.988	0.4223	0.7352	−2.515	−0.1273	−0.03888	−0.1662

50	51	52	53	54	55	56
$(\gamma - 1)\frac{\bar{v}^2}{\bar{a}^4}$	**13 × 49 × 50**	**38 + 40 + 44 + 46 + 51**	y'	$-\frac{\eta}{\bar{p}}$	$-\frac{(\gamma - 1)}{\bar{a}^2} \times$ **49**	$-\frac{x + y'}{\bar{u} + \bar{u}''}$
$0.405\,\frac{\mathbf{42}}{5}$	...	...	$\frac{\mathbf{5 \times 52}}{\mathbf{12}}$	Ref. 2	$-0.405\,\frac{\mathbf{49}}{\mathbf{5}}$	$-\frac{\mathbf{41 + 53}}{\mathbf{13}}$
0	0	−7.766	−7.766	−1.6055	0.4694	−13.361
0.03770	0.0030	−5.020	−5.081	−1.7813	0.5200	−11.128

TABLE 1

Calculation of Static Pressure Ratio p_r/p_l in $\varphi = 0°$ Plane (Method A) (*Continued from page 114*)

57	58	59	60	61	62	63
54 + 55 + 56	**−30 × 57**	$-\frac{\gamma y}{\bar{a}^2}(\bar{u} + \bar{u}'')$	$\frac{\eta'}{\bar{p}}$	$\left(\frac{\eta}{\bar{p}} + \frac{\bar{p}'}{\bar{p}}\right)$	$\epsilon \cos \varphi$ **61**	$\frac{p_0}{\bar{p}}$
...	...	**−13 × 29 × 37**	**58 + 59**	**30 − 54**	−0.20944 × **61**	Ref. 3
−14.497	0	7.805	7.805	1.6055	−0.3633	−5.070
−12.389	−2.529	5.075	2.546	1.5772	−0.3303	−2.679

64	65	66	67	68	69	70
$\frac{1}{4}\frac{\bar{p}'}{\bar{p}}\cot\bar{\theta}$	$\frac{1}{2}\frac{\eta'}{\bar{p}} + \frac{1}{4}\frac{\bar{p}''}{\bar{p}}$	**63 + 65 − 64**	ϵ^2 **66**	$\frac{p_2}{\bar{p}}$	**64 + 65 + 68**	$\epsilon^2 \cos 2\varphi$ **69**
$\frac{9 \times 30}{4}$	$\frac{1}{2}$ **60** + $\frac{1}{4}$ **36**	...	0.04386 × **66**	Ref. 3	...	0.04386 × **69**
0	1.9512	−3.119	−0.1368	3.370	5.321	0.2334
−0.1669	0.1955	−2.317	−0.1016	4.419	4.448	0.1951

71	72	73	74	75	76	
$\frac{p_r}{\bar{p}}$	$\frac{\bar{p}_2}{p_1}$	$\frac{\bar{a}^2}{\bar{a}_s^2}$	**73**$^{\gamma/(\gamma-1)}$	$\frac{\bar{p}}{p_1}$	$\frac{p_r}{p_1}$	...
1 + **62** + **67** + **70**	Ref. 1	$\frac{5}{0.12960}$	**73**$^{3.469}$	**72** × **74**	**71** × **75**	...
0.7603	1.5488	1.0000	1.0000	1.5488	1.1776	...
0.7632	1.5488	0.9988	0.9959	1.5424	1.1772	...

$$
\left.\begin{aligned}
u_r &= \bar{u} + \epsilon \cos\varphi(x + k_1\bar{v}) + \epsilon^2\left(u_0 + k_2\bar{v} + \frac{1}{2}k_1 y + \frac{1}{4}k_1^2\bar{u}''\right) + \epsilon^2\cos 2\varphi\left(u_2 + k_3\bar{v} + \frac{1}{2}k_1 y + \frac{1}{4}k_1^2\bar{u}''\right)\\
v_r &= \bar{v} + \epsilon\cos\varphi(y + k_1\bar{u}'') + \epsilon^2\left(v_0 + k_2\bar{u}'' + \frac{1}{2}k_1 y' + \frac{1}{4}k_1^2\bar{u}'''\right) + \epsilon^2\cos 2\varphi\left(v_2 + k_3\bar{u}'' + \frac{1}{2}k_1 y' + \frac{1}{4}k_1^2\bar{u}'''\right)\\
w_r &= \epsilon z \sin\varphi + \epsilon^2 \sin 2\varphi\,[w_2 + (1/2)\,k_1 z']
\end{aligned}\right\} \quad (10)
$$

$$
\left.\begin{aligned}
p_r &= \bar{p}\left[1 + \epsilon\cos\varphi\left(\frac{\eta}{\bar{p}} + k_1\frac{\bar{p}'}{\bar{p}}\right) + \epsilon^2\left(\frac{p_0}{\bar{p}} + k_2\frac{\bar{p}'}{\bar{p}} + \frac{1}{2}k_1\frac{\eta'}{\bar{p}} + \frac{1}{4}k_1^2\frac{\bar{p}''}{\bar{p}}\right) + \epsilon^2\cos 2\varphi\left(\frac{p_2}{\bar{p}} + k_3\frac{\bar{p}'}{\bar{p}} + \frac{1}{2}\frac{\eta'}{\bar{p}} + \frac{1}{4}k_1^2\frac{\bar{p}''}{\bar{p}}\right)\right]\\
\rho_r &= \bar{\rho}\left[1 + \epsilon\cos\varphi\left(\frac{\xi}{\bar{\rho}} + k_1\frac{\bar{p}'}{\bar{p}}\right) + \epsilon^2\left(\frac{\rho_0}{\bar{\rho}} + k_2\frac{\bar{p}'}{\bar{p}} + \frac{1}{2}k_1\frac{\xi'}{\bar{\rho}} + \frac{1}{4}k_1^2\frac{\bar{p}''}{\bar{p}}\right) + \epsilon^2\cos 2\varphi\left(\frac{\rho_2}{\bar{\rho}} + k_3\frac{\bar{p}'}{\bar{p}} + \frac{1}{2}\frac{\xi'}{\bar{\rho}} + \frac{1}{4}k_1^2\frac{\bar{p}''}{\bar{p}}\right)\right]
\end{aligned}\right\} \quad (10)\ \textit{Cont.}
$$

When $\theta_r = \theta_{r_s}$ and $\theta_r = \theta_{r_w}$, Eq. (10) reduces to Eqs. (6) and (7), respectively.

The derivatives with respect to $\bar{\theta}$ are obtained in explicit form from Eqs. (5)–(12) in reference 2, and are as follows:*

$$
\left.\begin{aligned}
\bar{u}' &= \bar{v}\\
\bar{u}'' &= [\bar{a}^2(2\bar{u} + \bar{v}\cot\bar{\theta}) - \bar{u}\bar{v}^2]/(\bar{a}^2 - \bar{v}^2)
\end{aligned}\right\} \quad (11)
$$

[*Eq. (11) continued on page 116*]

* Eqs. (11) can be reduced at the body surface by means of the boundary conditions [reference 2, Eq. (13)].

$$\bar{v}_s = 0, \qquad y_s = 2\bar{u}_s$$

In the evaluation of z' at the body surface, use must be made of L'Hospital's rule, giving

$$z_s' = -2\bar{u}_s \csc\bar{\theta}_s - z_s\cos\bar{\theta}_s$$

$$
\left.
\begin{aligned}
\bar{u}''' &= \frac{1}{\bar{a}^2 - \bar{v}^2}\left[\bar{a}^2(\bar{v}\csc^2\bar{\theta} - 2\bar{v} - \bar{u}''\cot\bar{\theta}) + 2\bar{v}\bar{u}''(\bar{u} + \bar{u}'') + \bar{v}^3 + \frac{(\gamma-1)\,\bar{v}^2}{\bar{a}^2}(\bar{u} + \bar{u}'')^2\right] \\
y &= x' \\
y' &= \frac{\bar{a}^2}{\bar{a}^2 - \bar{v}^2}\left[-y\cot\bar{\theta} + 2\frac{\bar{v}y}{\bar{a}^2}(\bar{u} + \bar{u}'') - x\left(2 - \frac{\bar{v}^2}{\bar{a}^2}\right) - z\csc\bar{\theta} + (\gamma-1)\frac{\bar{v}^2}{\bar{a}^4}(\bar{u} + \bar{u}'')(\bar{u}x + \bar{v}y)\right] \\
z' &= -y\csc\bar{\theta} - z\left(\cot\bar{\theta} + \frac{\bar{u}}{\bar{v}}\right) - \frac{\csc\bar{\theta}}{\bar{v}}\left[\bar{u}x + \frac{\bar{a}^2 d}{\gamma(\gamma-1)}\right] \\
\bar{p}'/\bar{p} &= -(\gamma\bar{v}/\bar{a}^2)(\bar{u} + \bar{u}'') \\
\frac{\bar{p}''}{\bar{p}} &= -\frac{\gamma\bar{u}''}{\bar{a}^2}(\bar{u} + \bar{u}'') + \frac{\gamma\bar{v}^2}{\bar{a}^4}(\bar{u} + \bar{u}'')^2 - \frac{\gamma\bar{v}}{\bar{a}^2}(\bar{v} + \bar{u}''') \\
\frac{\bar{\rho}'}{\bar{\rho}} &= -(\bar{v}/\bar{a}^2)(\bar{u} + \bar{u}'') \\
\frac{\bar{\rho}''}{\bar{\rho}} &= -\frac{\bar{u}''}{\bar{a}^2}(\bar{u} + \bar{u}'') - \frac{\bar{v}}{\bar{a}^2}(\bar{v} + \bar{u}''') + (2-\gamma)\left(\frac{\bar{v}^2}{\bar{a}^4}\right)(\bar{u} + \bar{u}'')^2 \\
\frac{\eta'}{\bar{p}} &= \frac{\gamma\bar{v}(\bar{u} + \bar{u}'')}{\bar{a}^2}\left[-\frac{\eta}{\bar{p}} - \frac{(\gamma-1)}{\bar{a}^2}(\bar{u}x + \bar{v}y) - \frac{x + y'}{\bar{u} + \bar{u}''}\right] - \frac{\gamma y(\bar{u} + \bar{u}'')}{\bar{a}^2} \\
\frac{\xi'}{\bar{\rho}} &= \frac{\bar{v}(\bar{u} + \bar{u}'')}{\bar{a}^2}\left[-\frac{\xi}{\bar{\rho}} - \frac{(\gamma-1)}{\bar{a}^2}(\bar{u}x + \bar{v}y) - \frac{x + y'}{\bar{u} + \bar{u}''}\right] - \frac{y(\bar{u} + \bar{u}'')}{\bar{a}^2}
\end{aligned}
\right\} \quad (11)\ \textit{Cont.}
$$

Cone Surface Characteristics with Body Axis Coordinates (r, Ⓗ, ψ)

For the purpose of obtaining and integrating surface distributions, it is more convenient to obtain the cone surface characteristics in body axis coordinates. Using Eq. (4a) for the body surface, the unit surface vectors are, to the order ϵ^2,

$$
\left.
\begin{aligned}
n &= [0,\ 1 - (1/2)\epsilon^2\csc^2\bar{\theta}_s\sin^2\varphi,\ \epsilon\csc\bar{\theta}_s\sin\varphi] \\
t_1 &= (1,\ 0,\ 0) \\
t_2 &= (t_1 \times n) = [0,\ -\epsilon\csc\bar{\theta}_s\sin\varphi,\ 1 - (\epsilon^2/2)\csc^2\bar{\theta}_s\sin^2\varphi]
\end{aligned}
\right\} \quad (12)
$$

And so, the velocity components normal and tangential to the body surface become

$$
\left.
\begin{aligned}
u_{B_s} &= t_1 \cdot V_{r_s}(u_{r_s}, v_{r_s}, w_{r_s}) \\
v_{B_s} &= n \cdot V_{r_s}(u_{r_s}, v_{r_s}, w_{r_s}) \\
w_{B_s} &= t_2 \cdot V_{r_s}(u_{r_s}, v_{r_s}, w_{r_s})
\end{aligned}
\right\} \quad (13)
$$

The directions of u_{B_s}, v_{B_s}, and w_{B_s} are those given by an increasing spherical coordinate system with reference to the body axis, as shown in Fig. 2. Substituting Eqs. (6) and (12) into Eqs. (13), one obtains

$$
\left.
\begin{aligned}
u_{B_s} &= \bar{u}_s + \epsilon x_s\cos\varphi + \epsilon^2[u_{0_s} + (1/2)\bar{u}_s] + \epsilon^2\cos 2\varphi[u_{2_s} + (1/2)\bar{u}_s] \\
v_{B_s} &= \epsilon^2(v_{0_s} - x_s) + \epsilon^2\cos 2\varphi(v_{2_s} - \bar{u}_s\cot\bar{\theta}_s - x_s - z_s\csc\bar{\theta}_s) \\
w_{B_s} &= \epsilon z_s\sin\varphi + \epsilon^2\sin 2\varphi \times [w_{2_s} - \bar{u}_s\csc\bar{\theta}_s - (1/2)z_s\cot\bar{\theta}_s]
\end{aligned}
\right\} \quad (14)
$$

Now, one of the relations between the coordinate systems (r, θ_r, φ) and $(r,$ Ⓗ, $\psi)$ is

$$\cot\varphi = \cos\epsilon\cot\psi + \sin\epsilon\cot Ⓗ\csc\psi \quad (15)$$

From this, the following relations can be obtained:

$$
\left.
\begin{aligned}
\epsilon\cos\varphi &= \epsilon\cos\psi + (1/2)\epsilon^2\cot Ⓗ - (1/2)\epsilon^2\cot Ⓗ\cos 2\psi \\
\epsilon\sin\varphi &= \epsilon\sin\psi - (1/2)\epsilon^2\cot Ⓗ\sin 2\psi \\
\epsilon^2\sin 2\varphi &= \epsilon^2\cos 2\psi \\
\epsilon^2\sin 2\varphi &= \epsilon^2\sin 2\psi
\end{aligned}
\right\} \quad (16)
$$

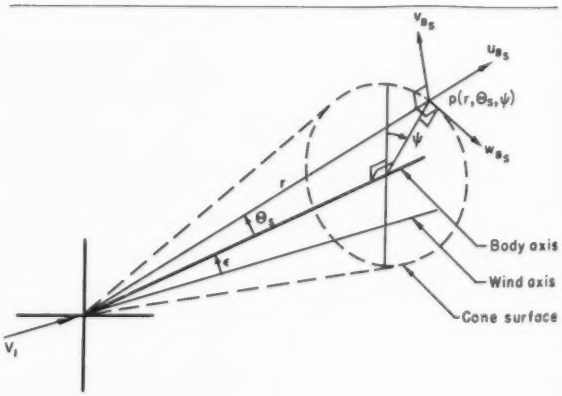

Fig. 2 — Velocity components, Eq. (17), in body axis coordinate system (r, Θ_s, ψ)

Substituting Eqs. (16) into Eqs. (14) and since $\Theta_s = \bar{\theta}_s$, the relations for the surface velocity components are

$$\left.\begin{aligned} u_{B_s} &= \bar{u}_s + \epsilon x_s \cos\psi + \\ &\quad \epsilon^2[u_{0_s} + (1/2)x_s \cot\bar{\theta}_s + (1/2)\bar{u}_s] + \\ &\quad \epsilon^2 \cos 2\psi[u_{2_s} - (1/2)x_s \cot\bar{\theta}_s + (1/2)\bar{u}_s] \\ v_{B_s} &= \epsilon^2(v_{0_s} - x_s) + \epsilon^2 \cos 2\psi \times \\ &\quad (v_{2_s} - \bar{u}_s \cot\bar{\theta}_s - x_s - z_s \csc\bar{\theta}_s) = 0 \\ w_{B_s} &= \epsilon z_s \sin\psi + \\ &\quad \epsilon^2 \sin 2\psi(w_{2_s} - \bar{u}_s \csc\bar{\theta}_s - z_s \cot\bar{\theta}_s) \end{aligned}\right\} \quad (17)$$

In Eq. (17), since v_{B_s} is the normal velocity to the surface, v_{B_s} should equal zero; that this is satisfied can be seen from Eqs. (31), (22), and (21) in reference 3.

In the case of the pressure and density on the solid cone surface, only a transformation of variables is necessary. Therefore, using Eqs. (6) and (16) and remembering that $\Theta_s = \bar{\theta}_s$, the surface pressure and density relations in a body axis coordinate system are

$$\left.\begin{aligned} p_{B_s} &= \bar{p}_s\left[1 + \epsilon\cos\psi\left(\frac{\eta}{\bar{p}}\right)_s + \right. \\ &\quad \epsilon^2\left(\frac{p_0}{\bar{p}} + \frac{\gamma\bar{u}^2}{2\bar{a}^2} + \frac{1}{2}\frac{\eta}{\bar{p}}\cot\bar{\theta}\right)_s + \\ &\quad \left.\epsilon^2\cos 2\psi\left(\frac{p_2}{\bar{p}} + \frac{\gamma\bar{u}^2}{2\bar{a}^2} - \frac{1}{2}\frac{\eta}{\bar{p}}\cot\bar{\theta}\right)_s\right] \\ \rho_{B_s} &= \bar{\rho}_s\left[1 + \epsilon\cos\psi\left(\frac{\xi}{\bar{\rho}}\right)_s + \right. \\ &\quad \epsilon^2\left(\frac{\rho_0}{\rho} + \frac{\bar{u}^2}{2\bar{a}^2} + \frac{1}{2}\frac{\xi}{\bar{\rho}}\cot\bar{\theta}\right)_s + \\ &\quad \left.\epsilon^2\cos 2\psi\left(\frac{\rho_2}{\bar{\rho}} + \frac{\bar{u}^2}{2\bar{a}^2} - \frac{1}{2}\frac{\xi}{\bar{\rho}}\cot\bar{\theta}\right)_s\right] \end{aligned}\right\} \quad (18)$$

Normal and Axial Pressure Force Coefficients

Referring to Fig. 3, the axial and normal forces on the surface element dS are

$$dF_X = (p_{B_s} - p_1)x \tan^2\Theta_s\, dx\, d\psi$$

and

$$dF_N = -(p_{B_s} - p_1)x \tan\Theta_s \cos\psi\, dx\, d\psi$$

Introducing the pressure relation from Eq. (18) and integrating gives

$$F_X = \pi l^2 \tan^2\Theta_s \times \left\{\bar{p}_s\left[1 + \epsilon^2\left(\frac{p_0}{\bar{p}} + \frac{1}{2}\frac{\eta}{\bar{p}}\cot\bar{\theta} + \frac{\gamma\bar{u}^2}{2\bar{a}^2}\right)_s\right] - p_1\right\}$$

and

$$F_N = (\pi/2)l^2 \tan\theta_s \bar{p}_s \epsilon(\eta/\bar{p})_s$$

Thus, the pressure coefficients are given by

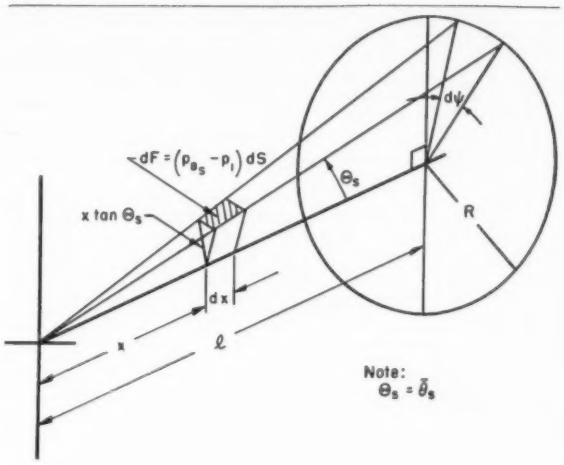

Fig. 3 — Definition of cone body geometry

$$C_X = \frac{4F_X}{\pi D^2 q_1} = \frac{\bar{p}_s/p_1}{\gamma/2M_1^2} \times \left[1 + \epsilon^2\left(\frac{p_0}{\bar{p}} + \frac{1}{2}\frac{\eta}{\bar{p}}\cot\bar{\theta} + \frac{\gamma\bar{u}^2}{2\bar{a}^2}\right)_s\right] - \frac{1}{\gamma/2M_1^2} \quad (19)$$

and

$$C_N = \frac{4F_N}{\pi D^2 q_1} = -\frac{\epsilon}{2}\frac{(\bar{p}_s/p_1)(\eta/\bar{p})_s \cot\bar{\theta}_s}{\gamma/2M_1^2} \quad (20)$$

The drag and lift coefficient to the order ϵ^2 can be obtained as follows (where positive angle of attack is $-\epsilon$):

$$C_D = C_X[1 - (\epsilon^2/2)] - \epsilon C_N$$
$$C_L = C_N[1 - (\epsilon^2/2)] + \epsilon C_X$$

Employing Eqs. (19) and (20) gives

$$C_D = \frac{\bar{p}_s/p_1}{\gamma/2M_1^2}\left[1 + \epsilon^2\left(\frac{p_0}{\bar{p}} + \frac{\gamma\bar{u}^2}{2\bar{a}^2} + \frac{\eta}{\bar{p}}\cot\bar{\theta} - \frac{1}{2}\right)_s\right] - \frac{[1 - (\epsilon^2/2)]}{\gamma/2M_1^2} \quad (21)$$

and

$$C_L = -\frac{\epsilon/2(\bar{p}/p_1)_s(\eta/\bar{p})_s \cot\bar{\theta}_s}{\gamma/2M_1^2} + \frac{\epsilon[(\bar{p}_s/p_1) - 1]}{\gamma/2M_1^2} \quad (22)$$

The above aerodynamic coefficients are related to Kopal's parameters (K_N, K_D, and K_{DYH}) in the following manner:

$$C_N = -(8\epsilon/\pi)K_N$$

$$C_X = AK_D + \epsilon^2\left\{\left(AK_D + \frac{2}{\gamma M_1^2}\right)\left[K_{DYH} - \frac{\gamma\bar{u}_s x_s d}{2\bar{a}_s^2(\gamma - 1)} + \frac{1}{2}\right] - \frac{8}{\pi}K_N\right\}$$

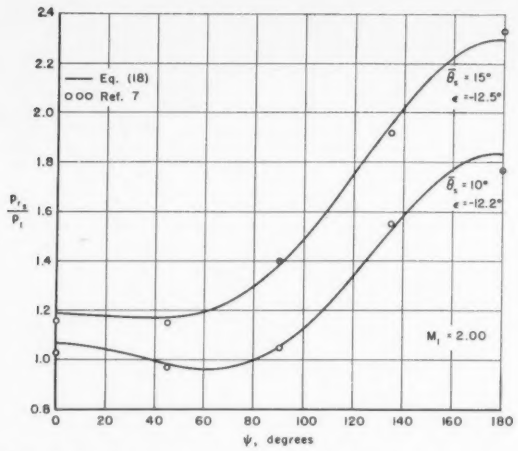

Fig. 4—Surface static pressure variation around cone at $M_1 = 2.00$

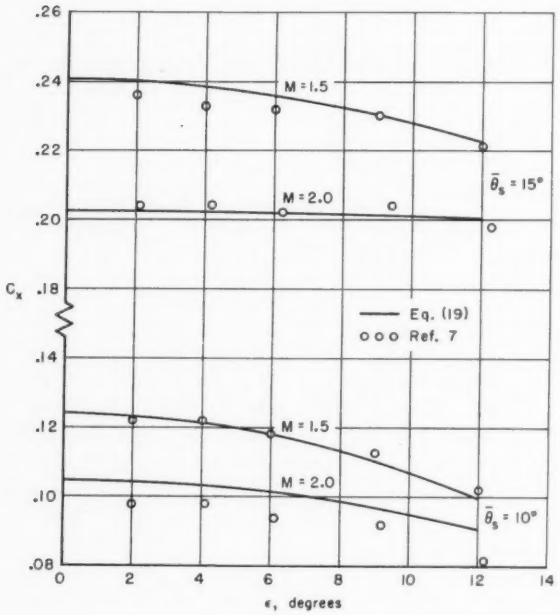

Fig. 5—Variation of axial force coefficient with angle of attack

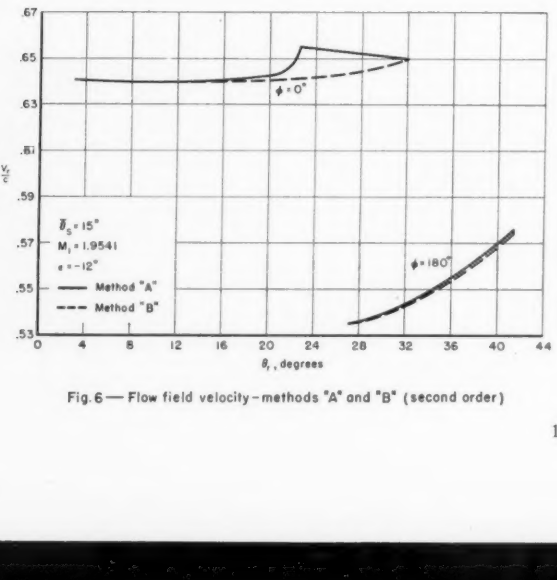

Fig. 6—Flow field velocity—methods "A" and "B" (second order)

$$C_L = -\epsilon\,[(8/\pi)K_N - AK_D] \tag{23}$$

$$C_D = AK_D + \epsilon^2\left\{\left[K_{DYH} - \frac{\gamma\bar{u}_s x_s d}{2\bar{a}_s^2(\gamma-1)}\right]\left(AK_D + \frac{2}{\gamma M_1^2}\right) + \frac{1}{\gamma M_1^2}\right\}$$

where $A = 2$ if K_D is taken from reference 1 and $A = 8/\pi$ if K_D is taken from references 2 and 3. The term $\gamma\bar{u}_s x_s d/2\bar{a}_s^2(\gamma - 1)$ appears in the above equation because Eqs. (41) and (42) in references 3 are incompatible. However, the tabulated values correspond to Eq. (42). Thus, in order to use the tabulated values of K_{DYH}, Eq. (41) should be corrected from

$$K_D = K_{D_0}[1 + \epsilon^2 K_{DYH} + \ldots]$$

to

$$K_D = K_{D_0}\left[1 + \epsilon^2\left(K_{DYH} - \frac{\gamma\bar{u}_s x_s d}{2\bar{a}_s^2(\gamma-1)}\right) + \ldots\right]$$

The effect of this term on the drag coefficient is small at moderate Mach Number but increases with increasing Mach Number as shown in Table 2.

TABLE 2
Calculation of Drag Coefficients, Eq. (23)

θ_s	M_1	ϵ	C_D*	C_D†	$\left(\frac{C_D\dagger - C_D*}{C_D*}\right)\%$
5°	4.8602	5°	0.03722	0.03724	0.05
		10°	0.07903	0.07911	0.10
	13.196	5°	0.03116	0.03797	21.85
		10°	0.07147	0.09871	38.11
10°	4.0748	5°	0.09476	0.09542	0.70
		10°	0.14217	0.14479	1.84
25°	2.0665	5°	0.47519	0.47682	0.34
		10°	0.49929	0.50585	1.31

* Eq. (23) without the term $\gamma\bar{u}_s x_s d/2\bar{a}_s^2(\gamma - 1)$.
† Eq. (23).

Concluding Remarks

The theoretical results for the pressure distribution around the cone and for the angle of attack variation in the axial force coefficient are compared with the experimental data of Cronvich[7] in Figs. 4 and 5. The indication is that the method presented for use with Kopal's tabulations is satisfactory both in regard to magnitudes and trends of variation. In these comparisons the theoretical results were linearly interpolated with Mach Number to correspond to the experimental Mach Number. It must be remarked that the experimental values given in Fig. 5 are integrated surface pressures from experimental values[7] averaged for a series of test runs. In Figs. 6, 7, and 8 are presented the comparisons of flow field properties as described by methods A and B. It is believed that method B is superior for establishing the initial conditions for a characteristic solution of the flow field for a pointed body of revolution. The comparisons of the first- and second-order solutions for some flow properties are shown in Figs. 9 and 10.

It should be mentioned that Stone's solutions yield the following information on the entropy distribution in the yawed conical flow field: In the first-order analysis the entropy is constant in each meridian plane. In the second-order analysis the entropy is constant only in the

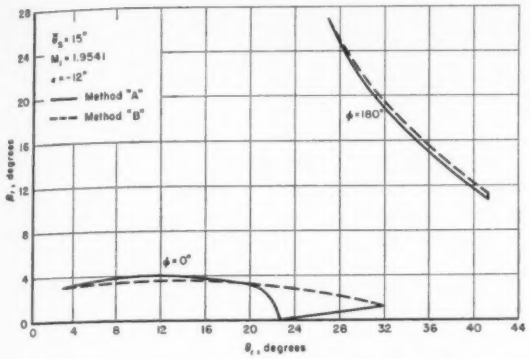

Fig. 7 — Velocity vector angle – methods "A" and "B" (second order)

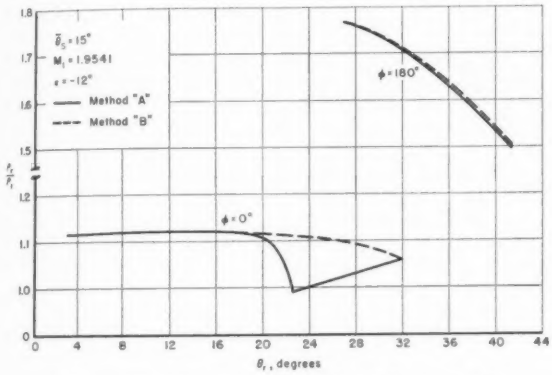

Fig. 8 — Flow field density – methods "A" and "B" (second order)

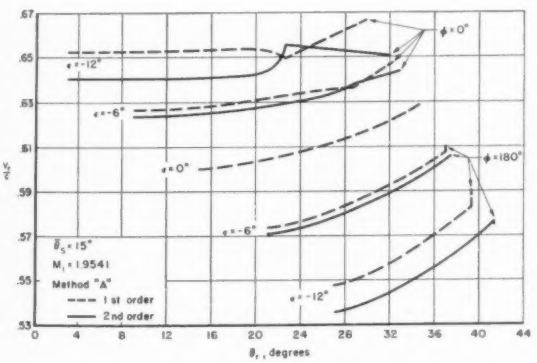

Fig. 9 — Flow field velocity for first and second order theory

top and bottom meridian planes. The true entropy distribution should be such that the entropy along each stream line is constant. This dictates the method of distorting the intermediate conical surfaces (see method B above). Thus with the proper distortion of these surfaces, the second-order solution should approach the physical conditions. Method B is only a first attempt in this direction. When properly interpreted, Stone's results for the second-order flow characteristics on the solid cone surface are not affected by the method of distortion and should be exact to the order of analysis. In view of the first-order results of constant entropy in each meridian plane, Ferri[9] has introduced a vortical layer through which the entropy can vary and has developed a method of using the first-order results of Stone-Kopal.[2] A comparison of the experimental and analytical results given by Ferri[9] for the pressure coefficients over a 10° cone at $M = 6.86$ are made with Stone-Kopal's second-order values in Figs. 11 and 12.

The authors are indebted to Dr. M. D. Van Dyke for the many constructive discussions and to Miss B. Dodge for computational assistance.

References

[1] Kopal, Z., *Tables of Supersonic Flow Around Cones*, M.I.T. Tech. Report No. 1, 1947.

(*Continued on page 142*)

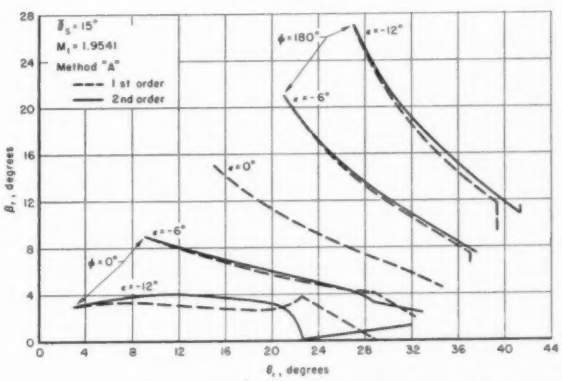

Fig. 10 — Velocity vector angle with respect to the wind axis for first and second order solutions

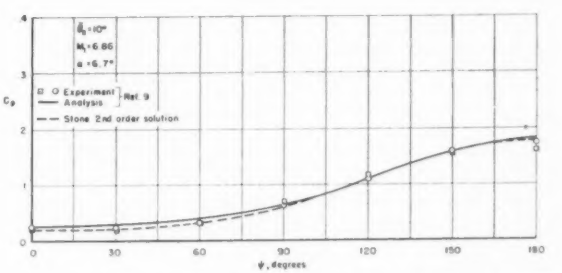

Fig. 11 — The comparison of pressure coefficient at large angle of attack ($\alpha = 6.7°$)

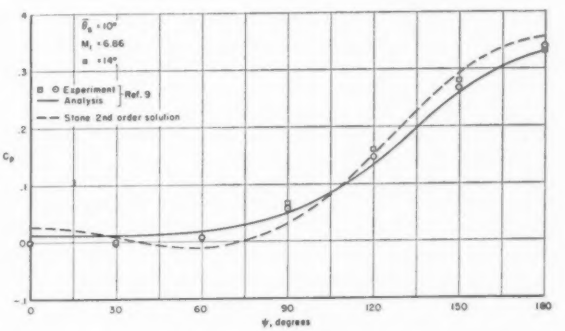

Fig. 12 — The comparison of pressure coefficient at large angle of attack ($\alpha = 14°$)

Heat Transfer by Laminar Flow from a Rotating Plate*

KNOX MILLSAPS† AND KARL POHLHAUSEN‡

Wright Air Development Center

ABSTRACT

An exact solution of the heat-transfer problem for the von Kármán example of the laminar flow of a viscous fluid over a rotating plate is given in dimensionless form and physically discussed. The solution is explicitly given for a constant temperature on the plate with viscous dissipation included. The numerical results are given for Prandtl Numbers from 0.5 to 10.

INTRODUCTION

THERE ARE ONLY A FEW CASES KNOWN where the mathematical structure of the flow of a viscous fluid can be rigorously determined without simplifying the basic hydrodynamic equations by neglecting the effects of certain terms in the differential system describing the motion. One of these few solutions for the case of the laminar flow of a fluid over a plate rotating at a constant velocity is due to von Kármán.[1] It is the purpose of this paper to show that the associated heat-transfer problem for the von Kármán example can also be solved exactly.**, [2]

It should be noted that the physical significance of these exact solutions for the rotating plate lies not in their engineering importance, since in practical cases the motion rapidly becomes turbulent,††, [3] but rather in the possibilities of making critical comparisons with approximate methods.

(I) THE BASIC EQUATIONS

The equation of continuity, the Navier-Stokes equations, and the energy equation for the steady motion of an incompressible fluid (density ρ is constant) when expressed in cylindrical coordinates (r, ϑ, z) with velocity components (u_r, u_ϑ, u_z) and kinematic viscosity ν are, respectively,‡‡, [4]

$$\frac{\partial u_r}{\partial r} + \frac{u_r}{r} + \frac{1}{r}\frac{\partial u_\vartheta}{\partial \vartheta} + \frac{\partial u_z}{\partial z} = 0 \tag{1.1}$$

$$u_r\frac{\partial u_r}{\partial r} + \frac{u_\vartheta}{r}\frac{\partial u_r}{\partial \vartheta} - \frac{u_\vartheta^2}{r} + u_z\frac{\partial u_r}{\partial z} = -\frac{1}{\rho}\frac{\partial p}{\partial r} + \nu\left(\frac{\partial^2 u_r}{\partial r^2} + \frac{1}{r}\frac{\partial u_r}{\partial r} - \frac{u_r}{r^2} + \frac{1}{r^2}\frac{\partial^2 u_r}{\partial \vartheta^2} - \frac{2}{r^2}\frac{\partial u_\vartheta}{\partial \vartheta} + \frac{\partial^2 u_r}{\partial z^2}\right) \tag{1.2}$$

$$u_r\frac{\partial u_\vartheta}{\partial r} + \frac{u_\vartheta}{r}\frac{\partial u_\vartheta}{\partial \vartheta} + \frac{u_r u_\vartheta}{r} + u_z\frac{\partial u_\vartheta}{\partial z} = -\frac{1}{\rho r}\frac{\partial p}{\partial \vartheta} + \nu\left(\frac{\partial^2 u_\vartheta}{\partial r^2} + \frac{1}{r}\frac{\partial u_\vartheta}{\partial r} - \frac{u_\vartheta}{r^2} + \frac{1}{r^2}\frac{\partial^2 u_\vartheta}{\partial \vartheta^2} + \frac{2}{r^2}\frac{\partial u_r}{\partial \vartheta} + \frac{\partial^2 u_\vartheta}{\partial z^2}\right) \tag{1.3}$$

$$u_r\frac{\partial u_z}{\partial r} + \frac{u_\vartheta}{r}\frac{\partial u_z}{\partial \vartheta} + u_z\frac{\partial u_z}{\partial z} = -\frac{1}{\rho}\frac{\partial p}{\partial z} + \nu\left(\frac{\partial^2 u_z}{\partial r^2} + \frac{1}{r}\frac{\partial u_z}{\partial r} + \frac{1}{r^2}\frac{\partial^2 u_z}{\partial \vartheta^2} + \frac{\partial^2 u_z}{\partial z^2}\right) \tag{1.4}$$

and, denoting the temperature of the fluid by t,

$$c_v\left(u_r\frac{\partial t}{\partial r} + \frac{u_\vartheta}{r}\frac{\partial t}{\partial \vartheta} + u_z\frac{\partial t}{\partial z}\right) = \frac{k}{\rho}\left(\frac{\partial^2 t}{\partial r^2} + \frac{1}{r}\frac{\partial t}{\partial r} + \frac{1}{r^2}\frac{\partial^2 t}{\partial \vartheta^2} + \frac{\partial^2 t}{\partial z^2}\right) + \nu\,(2e_{rr}^2 + 2e_{\vartheta\vartheta}^2 + 2e_{zz}^2 + e_{r\vartheta}^2 + e_{\vartheta z}^2 + e_{rz}^2) \tag{1.5}$$

where c_v is the specific heat expressed in mechanical mass units, k is the thermal conductivity, and

$$\left.\begin{aligned} e_{rr} &= \frac{\partial u_r}{\partial r}, & e_{\vartheta\vartheta} &= \frac{1}{r}\frac{\partial u_\vartheta}{\partial \vartheta} + \frac{u_r}{r} \\ e_{zz} &= \frac{\partial u_z}{\partial z}, & e_{\vartheta z} &= \frac{1}{r}\frac{\partial u_z}{\partial \vartheta} + \frac{\partial u_\vartheta}{\partial z} \\ e_{rz} &= \frac{\partial u_r}{\partial z} + \frac{\partial u_z}{\partial r}, & e_{r\vartheta} &= \frac{1}{r}\frac{\partial u_r}{\partial \vartheta} + \frac{\partial u_\vartheta}{\partial r} - \frac{u_\vartheta}{r} \end{aligned}\right\} \tag{1.6}$$

As shown in the schematic diagram in Fig. 1, the problem of an infinite plate being rotated about a point in its plane at a constant angular velocity ω and being heated to a constant temperature t_w with the fluid hav-

Received August 13, 1951.

* The authors wish to express their thanks to Frank W. Bubb, Chief Scientist, Flight Research Laboratory, for making this investigation possible and to Mrs. Olga Kay Francis for her help in performing the tedious numerical calculations.

† Now, Professor of Physics, Alabama Polytechnic Institute.

‡ Research Scientist, Applied Mechanics Research Group.

** Two further cases of fluid flow, together with the associated heat-transfer problem that can be solved exactly, are the Hamel-Jeffery examples of flow in convergent and divergent channels. The explicit solution of the hydrodynamic problem in terms of elliptic functions was given by Jeffery[2] and Hamel.[2] The solution of the energy equation in terms of elliptic functions arising from a generalized inhomogeneous Lamé equation will be given in a forthcoming paper by the present authors.

†† A summary of the results from experimental investigations is given in Goldstein.[3]

‡‡ These forms of the continuity and dynamical equations are given by Hopf.[4] This form of energy equation may be inferred from Goldstein.[4]

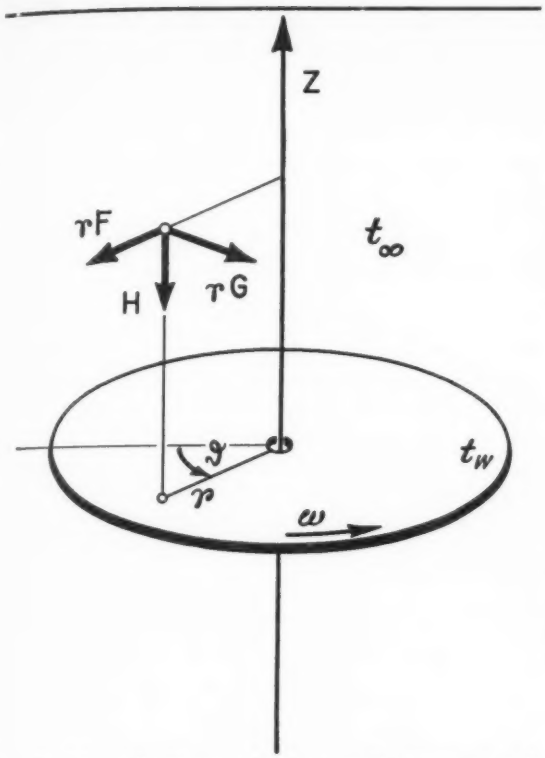

FIG. 1. Schematic diagram showing coordinate system and velocity components.

ing an ambient temperature t_∞ is characterized by the boundary conditions

$$\left.\begin{array}{ll} t(r,\vartheta,0) = t_w & t(r,\vartheta,\infty) = t_\infty \\ u_r(r,\vartheta,0) = 0 & u_r(r,\vartheta,\infty) = 0 \\ u_\vartheta(r,\vartheta,\infty) = 0 & u_z(r,\vartheta,0) = 0 \\ u_\vartheta(r,\vartheta,0) = r\omega & \end{array}\right\} \quad (1.7)$$

Since the angular velocity is assumed to be constant, the physical problem is axially symmetric, and, consequently, the partial derivatives with respect to ϑ vanish. Accordingly, the partial differential system [Eqs. (1.1)–(1.5)] may be reduced for laminar flow to a set of ordinary nonlinear differential equations by assuming

$$\left.\begin{array}{l} u_r = rf(z), \quad u_\vartheta = rg(z), \quad u_z = h(z) \\ \text{for the velocity components,} \\ p = p(z) \\ \text{for the pressure, and} \\ t = r^2 s(z) + q(z) + t_\infty \\ \text{for the thermal distribution.} \end{array}\right\} \quad (1.8)$$

The reduced equations are

$$2f + h' = 0 \quad (1.9)$$

$$f^2 - g^2 + hf' = \nu f'' \quad (1.10)$$

$$2fg + hg' = \nu g'' \quad (1.11)$$

$$hh' = -(p'/\rho) + \nu h'' \quad (1.12)$$

$$2c_r fs + c_v hs' = (k/\rho)s'' + \nu(f'^2 + g'^2) \quad (1.13)$$

$$c_v hq' = (k/\rho)(4s + q'') + 12\nu f^2 \quad (1.14)$$

where the primes denote differentiation with respect to z.

The equations may be made dimensionless by introducing the following variables:

$$\left.\begin{array}{l} f = \omega F, \quad g = \omega G, \quad h = (\nu\omega)^{1/2} H \\ p = \rho\nu\omega P, \quad s = \dfrac{\omega^2}{c_v} S, \quad q = \dfrac{\nu\omega}{c_v} Q \\ r = \left(\dfrac{\nu}{\omega}\right)^{1/2} R, \quad z = \left(\dfrac{\nu}{\omega}\right)^{1/2} \xi, \quad \sigma = \dfrac{\rho\nu c_v}{k} \\ t = (\nu\omega/c_v)T \end{array}\right\} \quad (1.15)$$

where σ is a modified Prandtl Number in which the specific heat at constant volume has been used instead of the specific heat at constant pressure. (In the case of incompressible fluids the distinction vanishes.) The dimensionless equations resulting from the application of these transformations are

$$H' + 2F = 0 \quad (1.16)$$

$$F'' - HF' - F^2 = -G^2 \quad (1.17)$$

$$G'' - HG' + 2FG = 0 \quad (1.18)$$

$$P' - H'' + HH' = 0 \quad (1.19)$$

$$S'' - \sigma HS' + \sigma H'S = -\sigma(F'^2 + G'^2) \quad (1.20)$$

$$Q'' - \sigma HQ' = -(4S + 12\sigma F^2) \quad (1.21)$$

where the primes now denote differentiation with respect to ξ. The boundary conditions for the velocity components have been transformed into

$$F(0) = 0, \qquad F(\infty) = 0 \quad (1.22)$$

$$G(0) = 1, \qquad G(\infty) = 0 \quad (1.23)$$

$$H(0) = 0 \quad (1.24)$$

One obtains the thermal distribution by combining S and Q into

$$T = R^2 S + Q + T_\infty \quad (1.25)$$

with the boundary conditions becoming

$$S(0) = 0, \qquad S(\infty) = 0 \quad (1.26)$$

$$Q(0) = T_w - T_\infty, \qquad Q(\infty) = 0 \quad (1.27)$$

(II) SOLUTION OF THE EQUATIONS

The first four equations [Eqs. (1.16)–(1.19)] with the boundary conditions [Eqs. (1.22)–(1.24)] constitute the hydrodynamic part of the problem and have been integrated numerically by Cochran,[5] who used a process of continuous joining of power expansions from

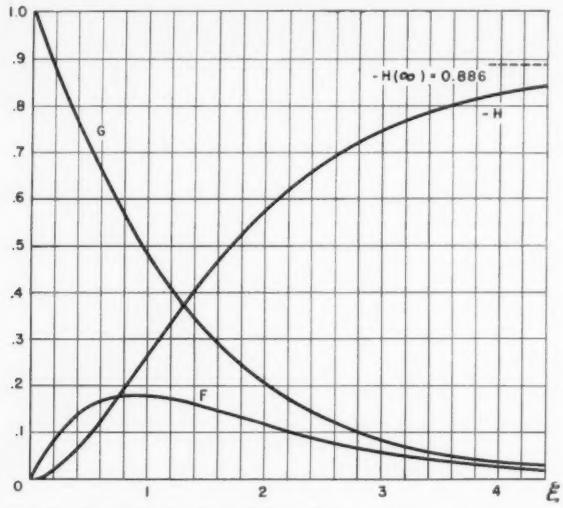

FIG. 2. Numerical values of the velocity components calculated by Cochran.

FIG. 3. Three-dimensional model of the flow over a rotating plate.

the origin with asymptotic expansions from infinity. The numerical results of Cochran are given in Fig. 2.

The three-dimensional composition of the velocity components shows that a spiral fanlike motion of the fluid occurs in the von Kármán example. A photograph of a three-dimensional model of this fluid motion is given in Fig. 3.

One should note that the spiral motion shown in Fig. 3 is an exact solution of the hydrodynamic equations, and, if a comparison with the Prandtl boundary-layer hypothesis is made, one finds a boundary layer of approximately constant thickness over the entire plate, provided the small influence of flow toward the plate is neglected. This interesting conclusion, first noted by von Kármán, may be drawn from the following elementary considerations: The magnitude of the fluid velocity $\bar{V}(R, \xi)$ divided by $(\vartheta\omega)^{1/2}$ is given by

$$(R^2F^2 + R^2G^2 + H^2)^{1/2} \tag{2.1}$$

and for large R this expression becomes

$$R[F^2 + G^2]^{1/2} \tag{2.2}$$

Eq. (2.1) clearly shows that a boundary layer consistent with the Prandtl hypothesis does exist in the von Kármán example, and Eq. (2.2) shows that it is one of approximately constant thickness, since in almost any particular physical example $(\omega/\nu)^{1/2}$ is quite large. For a physically significant definition of the thickness of the boundary layer δ, an equalization of areas in the velocity profile is perhaps to be recommended, and, in symbolism, this definition is

$$\delta(R) = \frac{\displaystyle\int_0^\infty \Big|\,|\bar{V}(R, \xi)| - |\bar{V}(R, \infty)|\,\Big|\, d\xi}{\displaystyle\max_{0 \le \xi \le \infty} \Big|\,|\bar{V}(R, \xi)| - |\bar{V}(R, \infty)|\,\Big|} \tag{2.3}$$

Fig. 4 is an application of the definition to the case of the rotating plate with flow toward the plate neglected.

FIG. 4. Approximate velocity profile showing thickness of the boundary layer.

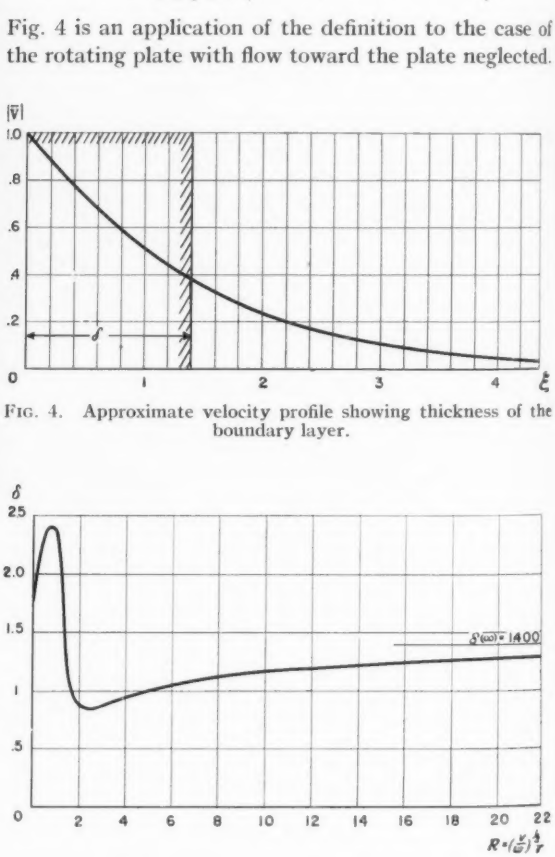

FIG. 5. Thickness of the boundary layer as function of R.

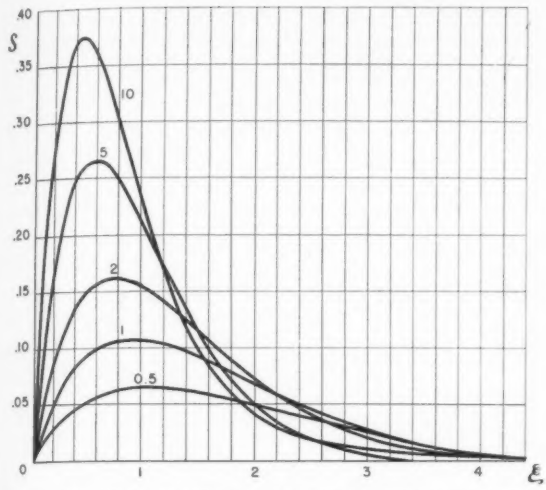

FIG. 6. Numerical values of S with Prandtl Number as a parameter.

Fig. 5 shows the thickness of the boundary layer δ as a function of R with flow toward the plate taken into account.

Somewhat similar to the hydrodynamic problem, the temperature field in the fluid due to a heated rotating plate is characterized by the dimensionless functions S and Q which are solutions of Eqs. (1.20)–(1.21) satisfying the boundary conditions (1.26)–(1.27). The differential system [Eqs. (1.20)–(1.21)] is composed of two inhomogeneous linear equations of the second order, with variable coefficients that are functions of the hydrodynamic variables and the Prandtl Number σ.

An analytical solution of the equation for $S(\xi)$ is unknown; hence, it appears necessary to obtain solutions for parametric values of σ by numerical methods. The straightforward method of obtaining the required numerical solution would be to assume initial values of $S'(\xi)$ and to integrate the differential equation for $S(\xi)$ by some numerical method and by subsequent interpolations to obtain a correct value for $S'(0)$ such that the boundary condition at infinity is satisfied. However, since the equation is linear and one of the second order, the following simple method may be applied without the necessity of trial integrations:[6]

The first-order term, $-\sigma HS'$, in Eq. (1.20) may be eliminated by the substitution

$$y = S(\xi) \exp\left[-(\sigma/2)\int H\, d\xi\right] \tag{2.4}$$

The resulting normal equation is

$$y'' + \left(\frac{3\sigma H'}{2} - \frac{\sigma^2 H^2}{4}\right) y = -\sigma(F'^2 + G'^2) \exp\left(-\frac{\sigma}{2}\int H\, d\xi\right) \equiv M(\xi) \tag{2.5}$$

If $y_1(\xi)$ is a numerical solution of the homogeneous normal equation for arbitrary nonvanishing initial values of the function and its first derivative, which is obtained by the Runge-Kutta method (for instance), a second fundamental integral is given by

$$y_2(\xi) = y_1 \int_{\xi_1}^{\xi} \frac{d\xi}{y_1^2} \tag{2.6}$$

and the particular integral is given by

$$y_p(\xi) = y_1 \int_{\xi_1}^{\xi} \frac{1}{y_1^2} \int_{\xi_1}^{\xi} M(\xi)\, y_1\, d\xi\, d\xi \tag{2.7}$$

Since superposition is a valid procedure, the general solution is given by

$$y = Ay_1 + By_2 + y_p \tag{2.8}$$

where A and B are arbitrary constants to be determined by the boundary conditions. If the boundary conditions are

$$y(\xi_1) = a, \qquad y(\xi_2) = b \tag{2.9}$$

then

$$A = a/y_1(\xi_1) \tag{2.10}$$

$$B = \frac{by_1(\xi_1) - ay_1(\xi_2) - y_p(\xi_2)y_1(\xi_1)}{y_1(\xi_1)\, y_2(\xi_2)} \tag{2.11}$$

For the case under consideration, it is seen from Eqs. (1.26) and (2.4) that Eqs. (2.9) reduce to

$$y(0) = 0, \qquad y(\infty) = 0 \tag{2.12}$$

and the particular values of the constants are

$$A = 0, \qquad B = -\int_0^{\infty} \frac{1}{y_1^2} \int_0^{\xi} M(\xi) y_1\, d\xi\, d\xi \Big/ \int_0^{\infty} \frac{d\xi}{y_1^2} \tag{2.13}$$

Therefore, the required numerical solution is

$$S(\xi) = y_1(\xi) \left\{ \int_0^{\xi} \frac{1}{y_1^2} \int_0^{\xi} M(\xi) y_1\, d\xi\, d\xi - \frac{\displaystyle\int_0^{\xi} \frac{d\xi}{y_1^2} \int_0^{\infty} \frac{1}{y_1^2} \int_0^{\xi} M(\xi) y_1\, d\xi\, d\xi}{\displaystyle\int_0^{\infty} \frac{d\xi}{y_1^2}} \right\} \exp\left(\frac{\sigma}{2}\int H\, d\xi\right) \tag{2.14}$$

where $M(\xi)$ is defined in Eq. (2.5) and $y_1(\xi)$ is an arbitrary nonvanishing solution of the homogeneous normal

equation. Since it was necessary to assign a definite value to the upper limit of integration in the infinite integrals, this numerical method was checked for the indicated Prandtl Numbers by the conventional Runge-Kutta method using interpolation to determine the initial slope satisfying the boundary condition at infinity. Fig. 6 shows the numerical results for parametric values of σ up to 10.

The equation for Q,

$$Q'' - \sigma HQ' = -(4S + 12\sigma F^2) \equiv N(\xi) \tag{2.15}$$

does not contain the dependent variable explicitly; hence, the equation may be reduced to a first-order linear equation for which the solution is well known. The resulting Q may then be obtained by an additional integration.

In terms of quadratures the solution of Eq. (2.15) is

$$Q = \int_0^\xi [\exp(\sigma \int H d\xi)] \left[\int_0^\xi N(\xi) \exp(-\sigma \int H\, d\xi)\, d\xi + C_1 \right] d\xi + C_2 \tag{2.16}$$

where C_1 and C_2 are integration constants to be determined from conditions (1.27) and are given by

$$C_2 = T_w - T_\infty \tag{2.17}$$

$$C_1 = -[I_2 + (T_w - T_\infty)]/I_1 \tag{2.18}$$

where

$$\left.\begin{aligned} I_1 &= \int_0^\infty \exp(\sigma \int H\, d\xi)\, d\xi \\ I_2 &= \int_0^\infty \exp(\sigma \int H\, d\xi) \int_0^\xi N(\xi) \exp(-\sigma \int H\, d\xi)\, d\xi\, d\xi \end{aligned}\right\} \tag{2.19}$$

It is then seen that the solution for Q may be written as

$$Q = [T_w - T_\infty]\left[1 - \frac{\int_0^\xi \exp(\sigma \int H\, d\xi)\, d\xi}{I_1}\right] - \frac{I_2}{I_1}\int_0^\xi \exp(\sigma \int H\, d\xi)\, d\xi + \int_0^\xi \exp(\sigma \int H\, d\xi) \int_0^\xi N(\xi) \exp(-\sigma \int H\, d\xi)\, d\xi\, d\xi \tag{2.20}$$

Now, it is clear that Q may be divided into two parts, Q_1 and Q_2, one being a factor times the temperature difference $T_w - T_\infty$ and the other being only a function of the viscous dissipation and independent of the temperature difference. Accordingly, one has

$$Q = Q_1(T_w - T_\infty) + Q_2 \tag{2.21}$$

Figs. 7 and 8 give the numerical results for Q_1 and Q_2 for parametric values of σ up to 10.

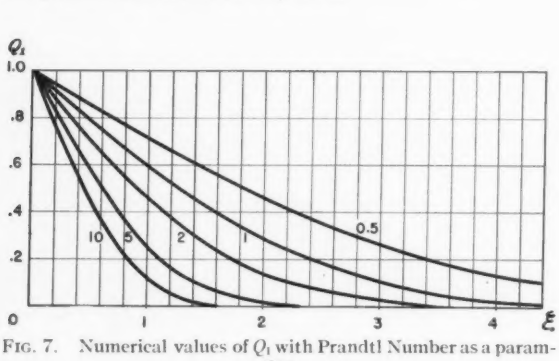

FIG. 7. Numerical values of Q_1 with Prandtl Number as a parameter.

Combining Eqs. (1.25) and (2.21) one obtains the dimensionless thermal distribution

$$T = R^2 S + Q_1(T_w - T_\infty) + Q_2 + T_\infty \tag{2.22}$$

Replacing T by $(c_v/\nu\omega)t$ and R by $(\omega/\nu)^{1/2}r$, one has the final result

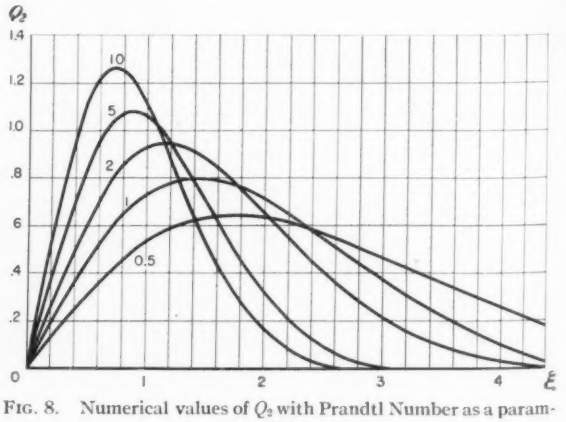

FIG. 8. Numerical values of Q_2 with Prandtl Number as a parameter.

$$t = t_\infty + Q_1(t_w - t_\infty) + \frac{\nu\omega}{c_v}\left[\frac{\omega r^2}{\nu} S + Q_2\right] \quad (2.23)$$

It is interesting to note that in the cases where viscous dissipation can be neglected—i.e., $N(\xi) = 0$, Eq. (2.23) reduces to

$$t = t_\infty + Q_1(t_w - t_\infty)$$

where t is given in degrees centigrade and, of course, $\omega r^2/\nu$ is the Reynolds Number for a given value of r.

The foregoing determination of the thermal distribution enables one to calculate the amount of heat that is transferred to the fluid. This calculation may be made by noting that the amount of heat transferred by conduction per unit area and unit time is given by $-k(\partial t/\partial z)_{z=0}$ and that the total heat flow per unit time from one side of a plate of radius r_0 is

$$e = -k \int_0^{2\pi} \int_0^{r_0} \left(\frac{\partial t}{\partial z}\right)_{z=0} r\, dr\, d\vartheta \quad (2.24)$$

By using transformations (1.15), Eq. (2.24) may be put into the dimensionless form

$$E \equiv \frac{e}{\rho\nu^{1/2}\omega^{1/2}} = -\frac{1}{\sigma} \int_0^{2\pi} \int_0^{R_0} \left(\frac{\partial T}{\partial \xi}\right)_{\xi=0} R\, dR\, d\vartheta \quad (2.25)$$

and, after substituting from Eq. (2.22) and performing the indicated integrations, one deduces that

$$E = -\frac{\pi R_0^2}{\sigma}\left[\frac{R_0^2}{2} S'(0) + (T_w - T_\infty)Q_1'(0) + Q_2'(0)\right] \quad (2.26)$$

In Eq. (2.26), $S'(0)$ may be calculated from Eq. (2.14), and $Q_1'(0)$ and $Q_2'(0)$ may be easily obtained from Eq. (2.20). Fig. 9 gives their numerical values as functions of σ, and one sees that the dimensionless heat flow is inversely proportional to the Prandtl Number and approximately proportional to the Reynolds Number.

It will be shown later that in most practical cases the term containing $T_w - T_\infty$ as a factor is extremely large when compared to the remaining two terms. Consequently, since Eq. (2.20) shows that

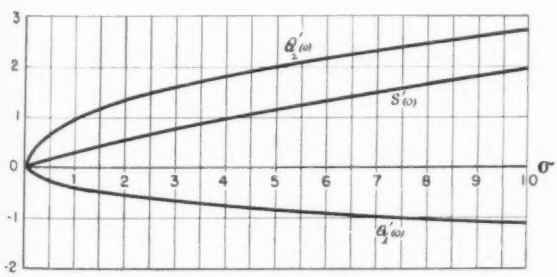

FIG. 9. Initial slopes of S, Q_1, and Q_2 as functions of the Prandtl Number.

$$Q_1'(0) = -(1/I_1) \quad (2.27)$$

one has the approximations

$$E \approx (\pi R_0^2/\sigma I_1)(T_w - T_\infty) \quad (2.28)$$

and, in dimensional form,

$$e \approx \pi k \omega^{1/2} r_0^2 (t_w - t_\infty)/\nu^{1/2} I_1 \quad (2.29)$$

where I_1 is given by Eq. (2.19).

(III) EXAMPLES

A. *Water*

A plate heated so that $t_w = 35°$C. rotates at 30 revolutions per min. ($\omega = 2\pi(30)/60 = 3.14$ rad. per sec.) in water in which $t_\infty = 30°$C. It is assumed that for the temperature range under consideration the necessary physical constants have the following values:[7]

ν	(kinematic viscosity)	= 0.0075 sq.cm. per sec.
k	(thermal conductivity)	= 0.00149 cal. per cm. sec. °C.
c_v	(specific heat)	= 0.997 cal. per Gm. °C.
ρ	(density)	= 0.996 Gm. per cu.cm.

With these basic physical constants and the value of the mechanical equivalent of heat (4.184×10^7 ergs per cal.) it may be shown that

$$\sigma = 5.0$$
$$\omega/\nu = 42 \times 10 \text{ per sq.cm.}$$
$$\frac{\nu\omega}{c_v} = \frac{(0.0075)(3.14)}{(4.184 \times 10^7)(0.997)} = 5.6 \times 10^{-10} \text{ °C.}$$

Also, since the critical Reynolds Number $(Re)_c$ for transition from laminar to turbulent flow is approximately 4.7×10^{4},[3] the critical radius r_c is found by

$$r_c = [\nu(Re)_c/\omega]^{1/2} = 10 \text{ cm.}$$

The thermal distribution is given by Eq. (2.23) and, with the particular values of the present example, takes the form

$$t = 30° + (5.6 \times 10^{-10})°[(42 \times 10)r^2 S + Q_2] + 5°Q_1$$

in which S, Q_1, and Q_2 for the parametric value $\sigma = 5$ are given in Figs. 6, 7, and 8, respectively, and the value of r ranges from 0 cm. to 10 cm. (critical radius). Since $\max.[(42 \times 10)r^2 S] = 11 \times 10^3$, the radial dependence of the thermal distributions is negligible. Hence, it is clearly seen that $5°Q_1$ is the decidingly predominant term in determining the temperature profiles and that

$$t \approx 30° + 5°Q_1$$

For the heat flow from one side of the rotating plate of 10 cm. radius, one obtains from Eq. (2.29)

$$e \approx \frac{\pi k \omega^{1/2} r_0^2 (t_w - t_\infty)}{\nu^{1/2} I_1} = \frac{(3.14)\ (0.00149)\ (3.14)^{1/2}(10)^2\ (5)}{(0.0075)^{1/2}\ (1.172)}$$

$$e \approx 41 \frac{\text{cal.}}{\text{sec.}}$$

B. Argon

If one desires to observe the radial variations in the thermal distributions, the observable magnitudes of $(t_w - t_\infty)Q_1$ and $(\nu\omega/c_r)\ (r^2\omega/\nu)\ S$ must be comparable and physically significant. A heated plate rotating in argon at low pressures appears to offer definite possibilities for making experimental investigations on the radial dependence of the temperature profiles. These possibilities can be attributed to the distinctive physical properties of argon.

If a plate heated so that $t_w = 2°C.$ is rotating at 287×10 revolutions per min. ($\omega = 2\pi(287 \times 10)/60 = 300$ rad. per sec.) in argon at 5.00×10^{-2} atmospheres so that $t_\infty = -2°C.$, the pertinent physical constants have the following values:[8]

ν $= 2.57$ sq.cm. per sec.
k $= 3.89 \times 10^{-5}$ cal. per cm. sec. °C.
C_v $= 7.45 \times 10^{-2}$ cal. per Gm. °C.
ρ $= 8.18 \times 10^{-5}$ Gm. per cu.cm.

and it may be shown that

σ $= 0.400$
ω/ν $= 117$ per sq.cm.
$\nu\omega/c_v$ $= 2.47 \times 10^{-4}$ °C.

If the critical Reynolds Number is assumed to remain approximately the same for the proposed experiment as in air at normal pressures, then

$$r_c = \left[\frac{\nu(Re)_c}{\omega}\right]^{1/2} = \left[\frac{(2.57)\ (4.7 \times 10^4)}{300}\right]^{1/2} = 20 \text{ cm.}$$

Therefore, since $\nu\omega/c_r$ max.$[(\omega r^2/\nu)\ S] \approx 1.2°C.$ is clearly measurable and roughly of the same order of magnitude as $4°Q_1$, it seems that measurements determining the radial dependence might be taken on plates rotating in argon at low pressures. Furthermore, the suggested experiment has additional features in that the turbulence level in the argon flowing toward the plate may be kept extremely low and in that, as has been previously recognized, the determinations of the critical Reynolds Number and the curve of neutral stability would appear to have particular significance, since the velocity and temperature profiles of the laminar flow can be determined exactly.

References

[1] Theodore von Kármán, Z. angew. Math. Mech., Vol. 1, p. 245, 1921.

[2] Jeffery, G. B., Phil. Mag., Ser. 6, Vol. 29, p. 455, 1915; Hamel, G., Jahresbericht der Deut. Math. Verein., Vol. 25, p. 34, 1916.

[3] Goldstein, S., et al., *Modern Developments in Fluid Dynamics*, Vol. 2, p. 368, Fig. 111; Oxford, 1938.

[4] Hopf, L., *Handbuch der Physik*, Vol. 7, Mechanik der flüssigen und gasförmigen Körper, p. 95; Julius Springer, Berlin, 1927; Goldstein, S., et al., *op. cit.*, Vol. 1, p. 104 and Vol. 2, p. 606.

[5] Cochran, W. G., Proc. Camb. Phil. Soc., Vol. 30, p. 635, 1934.

[6] Levy, H., and Baggott, E. A., *Numerical Solutions of Differential Equations*, p. 182; Dover, New York, 1950.

[7] ten Bosch, M., *Die Warmeübertragung*, p. 260; Julius Springer, Berlin, 1936.

[8] Jeans, James, *An Introduction to the Kinetic Theory of Gases*, pp. 56, 181, 189; Cambridge, 1948.

Theoretical Investigation of Several Types of Single Degree of Freedom Flutter

(*Continued from page 110*)

[8] Smilg, B., *The Instability of Pitching Oscillations of an Airfoil in Subsonic Incompressible Potential Flow*, Journal of the Aeronautical Sciences, Vol. 16, No. 11, p. 691, November, 1949.

[9] Watkins, Charles E., *Effect of Aspect Ratio on Undamped Torsional Oscillations of a Thin Rectangular Wing in Supersonic Flow*, N.A.C.A. T.N. No. 1895, 1949.

[10] Stewart, H. J., and Li, Ting-Yi, *Periodic Motions of a Rectangular Wing Moving at Supersonic Speed*, Journal of the Aeronautical Sciences, Vol. 17, No. 9, p. 529, September, 1950.

[11] Miles, John W., *On Damping in Pitch for Delta Wings*, Journal of the Aeronautical Sciences, Vol. 16, No. 9, p. 574, September, 1949.

[12] Theodorsen, Theodore, *General Theory of Aerodynamic Instability and the Mechanism of Flutter*, N.A.C.A. Report No. 496, 1935.

[13] Garrick, I. E., *Bending-Torsion Flutter Calculations Modified by Subsonic Compressibility Corrections*, N.A.C.A. Report No. 836, 1946.

[14] Dietze, F., *Die Luftkraefte des Harmonisch Schwingenden Fluegels im Kompressiblen Medium bei Unterschallgeschwindigkeit (Ebenes Problem) Teil II: Zahlen-und Kurventafeln*, Zentrale für Wissenschaftliches Berichtswesen der Luftfahrtforschung, Berlin, FB/Re/1733-2 (Translation No. F-TS-948-RE, Air Materiel Command).

[15] Turner, M. J., and Rabinowitz, S., *Aerodynamic Coefficients for an Oscillating Airfoil with Hinged Flap, with Tables for a Mach Number of 0.7*, N.A.C.A. T.N. No. 2213, 1950.

[16] Huckel, Vera, and Durling, Barbara J., *Tables of Wing-Aileron Coefficients of Oscillating Air Forces for Two-Dimensional Supersonic Flow*, N.A.C.A. T.N. No. 2055, 1950.

[17] Barmby, J. G., Cunningham, H. J., and Garrick, I. E., *Study of Effects of Sweep on the Flutter of Cantilever Wings*, N.A.C.A. T.N. No. 2121, 1950.

An Experimental Investigation of the Isothermal Laminar Boundary Layer on a Porous Flat Plate*

PAUL A. LIBBY,† LAWRENCE KAUFMAN,‡ AND R. PAUL HARRINGTON**

Polytechnic Institute of Brooklyn

SUMMARY

The transition Reynolds Numbers and velocity profiles of the laminar isothermal boundary layer on a porous flat plate with suction or injection have been measured and compared with the laminar boundary-layer analyses that have been carried out in the past several years. The results indicate that porous plates closely approximating the mathematical or ideal porous plates can be realized and that the theoretical velocity profiles are in good agreement with experiment.

SYMBOLS

A	=	surface area of the porous plate in turbulence channel wall
A, A', B, B'	=	constants depending on the physical properties of the fluid medium and of the wire and on the distance from the wall
E	=	voltage drop across the hot wire
E_0	=	voltage drop across the hot wire when $u \equiv 0$
E_1	=	voltage drop across the hot wire when $u = U$
Q	=	total volume of injected or withdrawn fluid flowing per unit time
R_x	=	Reynolds Number based on x
R_{x_i}	=	Reynolds Number based on x_i
$R_{x_{tr}}$	=	transition Reynolds Number based on x
u	=	local velocity in the x direction
U	=	free-stream velocity in the x direction
v	=	local velocity in the y direction
v_0	=	velocity in the y direction at the wall, positive for injection, negative for suction
x	=	distance along the plate, positive downstream measured from leading edge of imaginary flat plate (see Fig. 8)
x_i	=	distance along the plate from the leading edge of the imaginary plate to the leading edge of the porous section (see Fig. 8)
y	=	distance from and normal to plane of the plate
η	=	Blasius variable $= (y/x)\sqrt{R_x}$
μ	=	coefficient of viscosity
ν	=	coefficient of kinematic viscosity
ξ	=	suction or injection parameter $= (v_0/U)^2 R_x$
ξ_i	=	suction or injection parameter for the partially porous plate $= (v_0/U)^2 R_{x_i}$
ρ	=	mass density of the fluid

Received April 19, 1951.

* This research was conducted under the auspices of Project Squid, jointly sponsored by the Office of Naval Research and the Office of Air Research under Contract N6 ori-98 T. O. II. The authors gratefully acknowledge the assistance of Stanley Bernstein and Robert Sauer in the conduct of the experiments reported here and the preparation of the photomicrograph of the porous plate (Fig. 4) by Lambert H. Mott and Donald P. Ferriss of the Powder Metallurgy Laboratory of Stevens Institute of Technology.

† Associate Professor of Aeronautical Engineering.

‡ Formerly Research Assistant; now, Aeronautical Engineer, Guided Missiles Division, Fairchild Engine and Airplane Corporation.

** Formerly Professor and Head of Department; now, Professor and Head of Department, Rensselaer Polytechnic Institute.

INTRODUCTION

THE PURPOSE OF THIS INVESTIGATION is (1) to obtain experimental data on the characteristics of the isothermal laminar boundary layer on a porous flat plate subjected to homogeneous suction or injection of the same fluid as that of the main stream and (2) to compare these characteristics with the predictions of the laminar boundary-layer theory. This represents the first of a series of experimental investigations of boundary-layer characteristics on porous walls, with and without heat transfer.

The characteristics of the boundary layer on walls made of porous material with suction or injection are of considerable interest. Suction applied through such walls inhibits boundary-layer separation in the presence of adverse pressure gradients[1] and laminar boundary-layer transition.[2] By injecting a coolant through a porous wall, a thick heat-insulating boundary layer can be established to protect the wall from high-temperature gases such as exist in combustion chambers and around turbine blades.[3]

In addition to the cited references, which present the results of experimental investigation on these uses of porous materials, several theoretical investigations of the characteristics of the laminar boundary layer over a flat plate with suction or injection have been carried out. Schlichting,[4] Iglisch,[5] and Schlichting and Bussmann,[6] have determined the characteristics of the incompressible boundary layer over a flat plate subjected to uniform suction and to suction or injection varying as $1/\sqrt{x}$, where x is the space variable along the plate. Yuan[7] has calculated the laminar boundary-layer velocity and temperature characteristics for incompressible flow over a flat plate subject to uniform injection. Yuan[8] and Lew et al.[9–11] have calculated the characteristics of the compressible laminar boundary layer with uniform suction and injection, with and without heat transfer. References

FIG. 1. Turbulence channel showing adjustable side wall and hot-wire probe.

12–15 give the characteristics of the compressible laminar boundary layer with partial injection and suction.

Moreover, the laminar boundary-layer stability theory that has been developed by many investigators for the flow over impermeable walls has been applied without modification to the theoretical laminar boundary-layer velocity and temperature profiles presented in some of the references cited above. Although this application of the stability theory has not been justified rigorously, it has been assumed that the stability theory will give at least the qualitative influence of suction and injection on laminar boundary-layer stability.* Thus, Ulrich[16] has shown that suction greatly increases and injection decreases the stability of the incompressible laminar boundary layer. Lees[17] has shown that for small Mach Numbers ($M \ll 1$) laminar boundary-layer stability with injection varying as $1/\sqrt{x}$ depends on the opposing effects of the injection, which is destabilizing, and on the cooling, which is stabilizing, and that for $\xi \leq 0.25$ the cooling predominates. Libby, Lew, and Romano[18] applied the stability theory to the profiles obtained by the integral methods in reference 11. Their results thus indicated, at least qualitatively, the simultaneous effects of compressibility, uniform suction or injection, and heat transfer.

Despite the interest in the characteristics of the boundary layer on porous walls as indicated by the number of experimental and theoretical investigations in the cited references, there appears to have been no experimental investigation of the details of the actual boundary layer subjected to homogeneous suction and injection. There is need for such research; the theoretical analyses of the laminar flow should be substantiated by careful tests as the impermeable wall boundary-layer theory has been. In addition, the question arises as to whether extensive regions of laminar flow can exist with even small rates of injection over actual porous plates with their inherent roughness and with their large but finite number of pores. There exists the possibility that the injected fluid may issue from these pores in the form of discrete jets that would not permit laminar flow to exist. (That suction can maintain an indefinitely stable laminar layer has been clearly indicated by reference 2.)

In addition, a detailed examination of turbulent boundary layers on porous walls, especially with injection, is necessary to establish a theory for such boundary layers. With the present state of knowledge regarding turbulence such a theory must be semi-empirical. Measurement of the mean velocity profiles and of the skin friction can supply the required data.

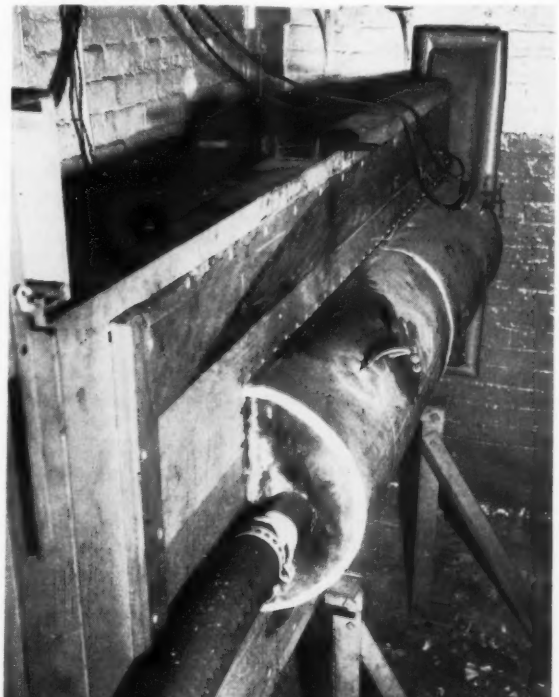

FIG. 2. Turbulence channel showing injection bell and connection to flowmeter and supercharger.

* The authors have recently been informed by Prof. Lester Lees that this application can be rigorously justified for ξ on the order of unity.

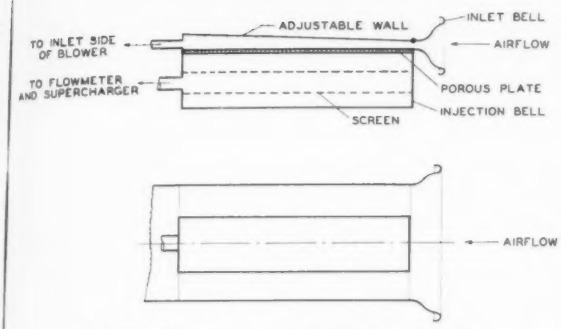

FIG. 3. Flow diagram of turbulence channel.

This report presents the results of an experimental investigation of the characteristics of these boundary layers under the simplest conditions—namely, isothermal laminar flow over a flat plate. Investigations of the isothermal turbulent boundary layer with injection and of the laminar and turbulent boundary layer with heat transfer and injection are under way and will be reported upon subsequently.

EXPERIMENTAL EQUIPMENT AND MEASUREMENT TECHNIQUE

The investigation was conducted in the 30- × 2-in. turbulence channel at PIBAL. A porous plate $^3/_{16} \times 14$ in. $\times$ 5 ft. was mounted flush with the inner surface along the centerline of one 30-in. wall immediately downstream of the inlet bell. Behind the porous plate was an injection air bell that was connected through a flowmeter to a supercharger. By changing the connections to the supercharger inlet and exhaust, either suction or injection through the porous plate could be applied by the supercharger. A 5-ft. section of the other 30-in. wall was hinged at the inlet bell so that the pressure gradient caused by skin friction and mass exchange through the porous plate could be effectively eliminated. Special care was exercised so that the pressure gradient from the leading edge of the porous plate to the measuring station was negligibly small, the deviations of the static pressure being made less than ± 1 per cent of the dynamic pressure. Although this care resulted in larger deviations downstream of the measuring station, the pressure drop properties of the porous plate were such that deviations of the injection or suction velocity from the average were negligibly small throughout the length of the porous plate. Thus, the assumptions of a flat plate with uniform suction or injection were satisfactorily achieved. Figs. 1, 2, and 3 show the two sides and a flow diagram of the channel.

The turbulence factor σ[19] in the free stream at the inlet of the channel has been assumed sufficiently small so that the free-stream turbulence would have no effect on transition. This is believed justified because the maximum velocity at the inlet to the channel during these tests was small, approximately 3 ft. per sec., and because the air flow through the channel was discharged outside the building and therefore not continuously circulated within the test room.*

Because the results of these tests must be associated with the particular porous plate used or with porous plates closely related in porosity, permeability, and grain size, the characteristic of the plate will be discussed in some detail. The plate was made from sintered bronze by the Wel-Met Company of Kent, Ohio. Fig. 4 shows a photomicrograph of the porous material in a section normal to the plane of the plate. The pores have been filled with plastic under pressure, and the surface has been heavily etched to make the pores and grains distinct. The pores are black and the bronze is white.

Several facts of interest may be established by inspection of Fig. 4. The microstructure of the porous plate used here is complex. No simple flow passages are evident. Moreover, the surface conditions are such that no discrete jets could be expected from the low pressure side of the plate. The airflow through this plate would appear to be more of a percolation than a flow through small discrete channels. This characteristic implies that the porous plate used here provides a satisfactory approximation to the ideal or mathematically porous plate assumed in the theory of the laminar boundary layer with injection—namely, one for which the injection velocity v_0 is either a constant or a smooth function of distance along the plate. This implication has been verified experimentally by placing a hot-wire at several wire diameters from the wall with only injection air flowing through the plates ($U = 0$, $v_0 > 0$). The velocity indicated by the hot-wire was steady and independent of small changes in the position of the wire in a plane parallel to the porous wall. Moreover, during measurements of the velocity profiles, the fluctuation of the wire associated with the laminar boundary-layer velocity oscillations decreased as the wall was approached. Near the wall the indications were comparatively steady.

* At the time of these tests, a suitable instrument for the qualitative determination of σ was not available. However, one is under construction and will be used to check this assumption in the near future.

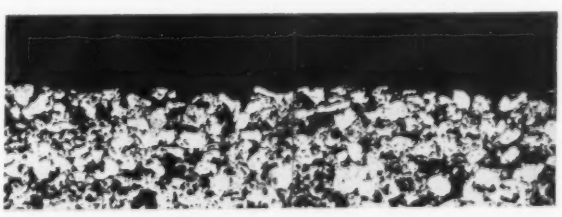

FIG. 4. Photomicrograph of a section of the porous plate. The injection or suction flow is parallel to the short side of the photograph. Magnification is 20 times.

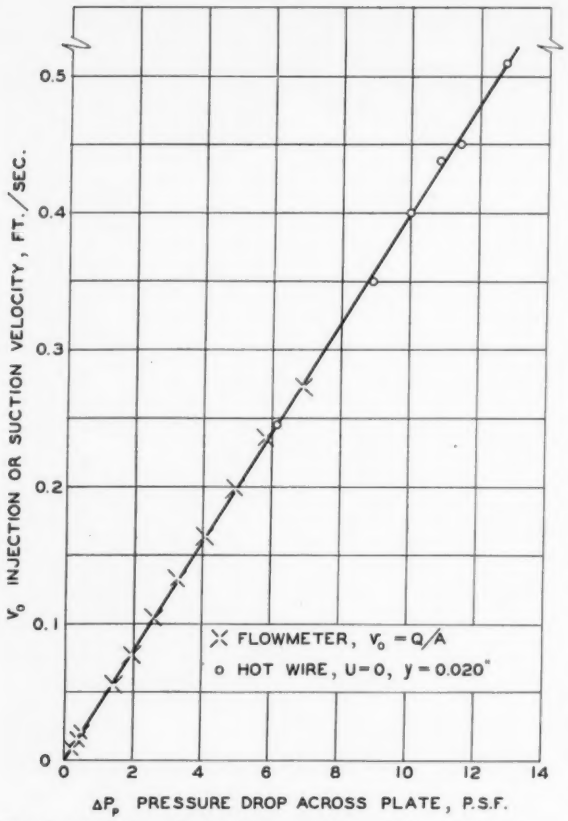

FIG. 5. Variation of injection or suction velocity with pressure drop across porous plate.

A further verification of the closeness of the approximation to the ideally porous plate may be seen from Fig. 5, which shows the variation of velocity v_0 with the pressure drop across the porous plate as determined by two different methods: by a calibrated hot-wire located 0.020 in. from the porous plate with $U = 0$ and by the ratio Q/A, where Q is the volume of injection air flowing per unit time and A is the total porous plate area. It will be seen that the agreement between the two velocities is good even at this small distance from the wall. Also indicated by Fig. 5 is the clearly viscous pressure drop across the plate for low rates of flow.

From Fig. 4 it may also be seen that the surface of the plate is comparatively rough. This roughness is greater than that associated with the usual boundary-layer investigations. However, with porous plates made of sintered metals, such surface roughness must be expected, since the surface cannot be smoothed without damaging the pores and, therefore, the permeability of the material. The aerodynamic effect of this roughness can be established only experimentally.

In order to eliminate the effect of contamination from the sides of the porous plate parallel to the free stream, all the measurements with injection were made within the most upstream 24-in. section of the plate and along its centerline. Thus, even if turbulence is assumed, because of the effect of the injection, to spread from these edges toward the centerline of the plate at a greater angle than that shown by Charters,[20] no transverse contamination could be expected.

FIG. 6. Hot-wire probe and associated electric equipment.

A hot-wire anemometer was used to make the velocity measurements. The wires, which were made of platinum either 0.001 or 0.002 in. in diameter, were mounted in the probe shown in Fig. 6. A constant resistance type of circuit was used in order that the effects of the wall on the hot-wire response could be calibrated at zero flow velocity and could be applied independently of the flow velocity. The circuit used is shown in Fig. 7.

In carrying out the tests, essentially four quantities had to be measured or chosen. These variables are the distance from the plate y, the velocity parallel to the plate u, the injection velocity v_0, and the distance along the plate x. The techniques used to measure or to determine each may be of interest. The distance of the wire from the wall was determined by moving the wire mounted in the probe slowly toward the plate until a simple d.c. circuit connecting the micrometer barrel and the porous plate was closed by the contact of the wire on the plate. The micrometer dial was then set to zero and the wire backed off the desired distance, which then was considered to be the value of y.

In determining the values of the velocity u, the indications of the hot-wire, which are really proportional to the resultant velocity, were interpreted as being due to the u velocity component only. This is justified by the smallness of the v velocity components even at the highest rates of injection considered here. The technique used to obtain the u data is suggested by a consideration of King's formula for heat transfer from a cylinder at low Mach Numbers. The heat balance between the electrical energy input and the heat convected to the fluid and inducted to the wall from the wire can be written as

$$E^2 = R(T_w - T_1)(A\sqrt{u} + B) \tag{1}$$

where

R = resistance of the wire
E = voltage drop across the wire
T_w = temperature of the wire
T_1 = temperature of the fluid stream and of the wall
A, B = constants depending on the physical properties of the fluid medium and of the wire and on the distance from the wall

For a constant resistance (constant temperature) hot-wire circuit, Eq. (1) becomes

$$E^2 = A'\sqrt{u} + B' \tag{2}$$

or

$$u = [(E^2 - B')/A']^2 \tag{3}$$

To determine the constants A' and B' for a particular wire, the following technique was used: With the turbulence channel sealed at both ends and the air therein allowed to become quiescent, a heating current giving a value of $T_w - T_1$ of approximately 50° to 150°F. above ambient was passed through the wire. At various values of y, the voltage drop required to maintain the wire at constant temperature was recorded and denoted by $E_0 = E_0(y)$. Then from Eq. (2) since $u = 0$,

$$B' = E_0^2 \tag{4}$$

If the actual magnitude of u was of interest in a particular test, the value A' was determined by recording the values of E in a stream of known velocity. By plotting the results in the form of E^2 versus $\sqrt{u}$, A' was easily determined from the slope of the resulting straight line. However, for most tests, only the ratio u/U had to be determined by the hot-wire; therefore, the constant A' did not have to be explicitly determined. By applying Eqs. 3 and 4 at two points in the flow with velocities of u and U, one finds

$$u/U = [(E^2 - E_0^2)/(E_1^2 - E_0^2)]^2 \tag{5}$$

where E_1 is the voltage drop across the wire in the free stream of known velocity U. Because of the simplicity of applying Eq. (5), it was possible to calibrate the wire immediately prior to each test so that daily effects, such as wire aging and fluid temperature changes, were minimized.

In the determination of the injection velocity v_0, the pressure drop across the porous plate was measured. Fig. 5 was used to determine and to fix the value of v_0.

Because of the boundary layer that develops on the inner wall of the inlet nozzle, the effective distance along the plate could not be measured from the be-

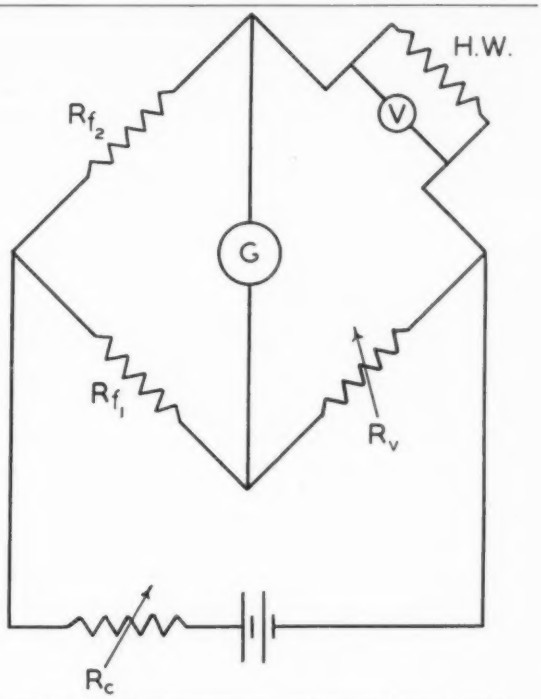

FIG. 7. Hot-wire anemometer, constant resistance circuit.

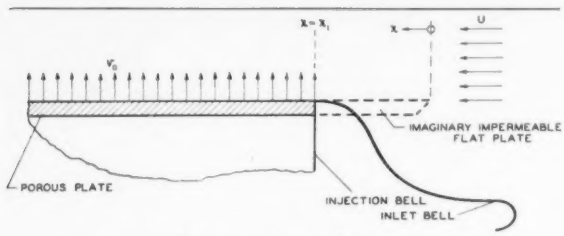

FIG. 8. Inlet conditions.

ginning of the porous section. The effect of the inlet bell with its accelerating pressure gradient was considered to be equivalent to an impermeable flat plate section of length x_1 as shown in Fig. 8. The length x_i was determined as follows: With the smallest injection rate that could be realized, without reversing the supercharger and using it as a suction pump, the impermeable plate conditions were closely approximated ($\xi \ll 1$). A velocity profile close to the leading edge of the porous plate was measured under these conditions. The value of x in the Blasius variable $\eta = (y/x)\sqrt{R_x} = y\sqrt{U/x\nu}$ was chosen so that the slope of the velocity profile at the wall $(\partial u/\partial y)_0$ was equal to the theoretical value of Blasius. The value of x_i was then simply determined by subtracting the location of the wire with respect to the leading edge of the porous plate from the value of x so determined. This same value of x_1 (4.57 in.) was then used for all subsequent tests.

The validity of using this effective inlet length is established by Fig. 9, where, for several Reynolds Numbers and several values of x_i/x (including the one used to determine x_i), the velocity profiles are compared with the classical Blasius profile. Good agreement is seen even for large values of η and for value of x_i/x close to unity. Thus, during the tests with injection and suction, the boundary layer was considered to be that over a partially porous plate with an impermeable section of length x_i and a permeable section of length $(x - x_i)$. All values of x used here are therefore measured from the leading edge of an imaginary plate x_i ahead of the leading edge of the porous plate.

Two types of data were collected in these tests. The effect of injection or suction on the transition Reynolds Number R_{xtr} for two values of x_i/x was established, and suction and injection velocity profiles were determined. The transition data were compared with the theoretical laminar boundary-layer stability limits, while the velocity profiles were compared with theoretical calculations. The transition Reynolds Number was determined by placing the wire close to the wall (y = 0.005 in. − 0.010 in.). With a fixed injection velocity, the free-stream velocity was gradually increased. A plot of u/U for the given value of y increased smoothly until some value of U was reached at which u/U would change disproportionately. The Reynolds Number corresponding to this sudden change was called the transition Reynolds Number. A clear indication of the onset of transition was obtained in this way. The extent of the transition region downstream of the point corresponding to these values of R_{xtr} can be determined only by an investigation of the turbulent boundary layer, and it is not shown by the tests reported here.

Test Results and Comparison with Theory

Fig. 10 shows the effect of suction and injection on the transition Reynolds Number R_{xtr} for two values of x_i/x. Although most of the transition data has been collected for x_i/x = 0.381, three values of R_{xtr} corresponding to x_i/x = 0.190 have been measured. Since these fall on the same curve as those for x_i/x = 0.381, it has been concluded that the transition curve can be considered to be the transition curve for the completely porous plate (x_i/x = 0).

Several comments may be made with respect to the comparison between the transition Reynolds Numbers shown on Fig. 10 and the results of laminar boundary-layer stability theory. It is seen that with suction the boundary layer is stabilized. Moreover, the effect

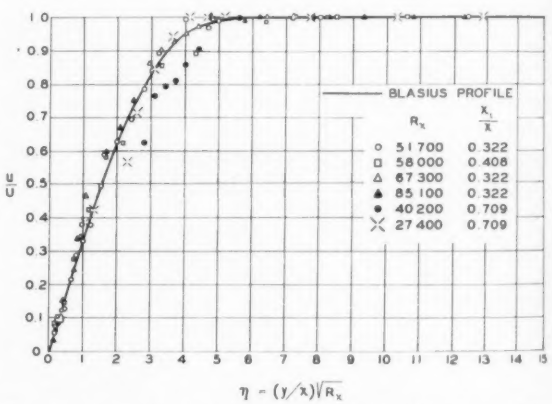

FIG. 9. Comparison of theoretical and experimental velocity profiles for $\xi \sim 0$.

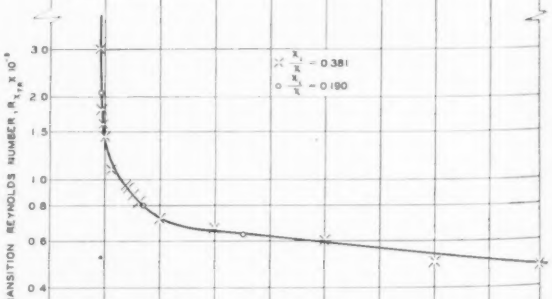

FIG. 10. Transition Reynolds Numbers for various rates of suction and injection.

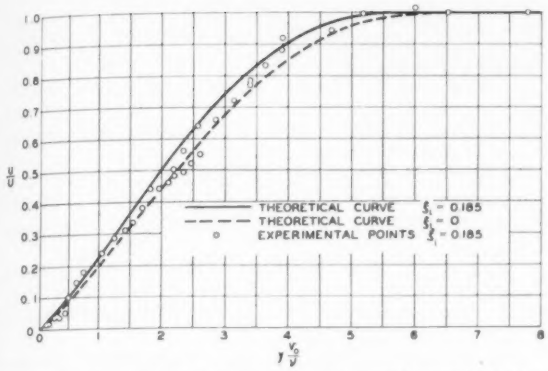

FIG. 11a. Comparison of theoretical and experimental velocity profiles with injection for $\xi = 0.518$.

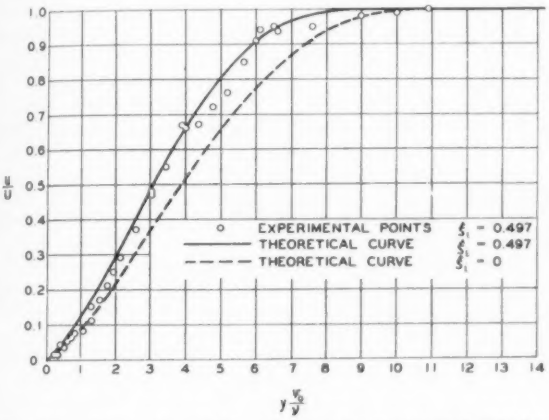

FIG. 11b. Comparison of theoretical and experimental velocity profiles with injection for $\xi = 1.0$.

of injection is to reduce the stability and to cause earlier transition. It will be noted that the stability theory appears to predict accurately the suction ratio for which the laminar boundary layer is indefinitely stable, since the results of reference 16 give -11.8×10^{-5} for this value and Fig. 10 indicates a rapid rise in $R_{x_{tr}}$ in the neighborhood of $v_0/U = -10 \times 10^{-5}$. Moreover, it indicates qualitatively the effect of suction and injection on boundary-layer stability.

Figs. 11a and 11b show the agreement for two different values of ξ between the measured velocity profiles and those of Yuan.[7] The theoretical results have been corrected for the partial injection in accordance with Eq. 17 of reference 7. It will be noted that the agreement is good and, therefore, that Yuan's analysis of the effect of injection on skin friction is experimentally substantiated. Thus, it can be expected that heat-transfer data based on the analysis of reference 7 will be accurate for at least low rates of heat transfer where the assumption of constant gas properties is satisfactory. Moreover, the range of validity of these data can probably be increased if the fluid properties (ρ, μ) are evaluated at the wall temperature. The effect of heat transfer on the stability of the laminar layer can be estimated by application of the method given in reference 18.

Fig. 12 shows the agreement for one value of ξ corresponding to suction between the measured and the theoretical profiles of Yuan. It is pointed out that the same agreement would have been achieved if the comparison had been made with the profiles calculated according to Romano.[15]

CONCLUSIONS

From the experimental investigation reported here the following conclusions may be drawn:

(1) Porous plates that satisfactorily approximate the ideal or mathematical porous plate—that is, one providing continuous normal velocities at the wall—can be realized. The microstructure of such plates will probably be complex, and, at low rates of flow, the pressure drop will be proportional to the velocity.

(2) Regions of laminar flow with injection can exist despite the inherent roughness and the finite number of pores of real porous plates. The laminar boundary-layer stability theory predicts qualitatively the effect of suction and injection on the transition Reynolds Number.

(3) The isothermal laminar boundary layer on a flat plate can be stabilized to an indefinitely high Reynolds Number if suction corresponding to approximately $(-v_0/U) = 10^{-4}$ is applied. This is in good agreement with the predictions of laminar boundary-layer stability theory of Ulrich,[16] of Libby, Lew, and Romano,[18] and of Romano.[15]

(4) The laminar boundary-layer analysis of Yuan[7] and Romano[15] for the flow over partially porous flat plates can be verified experimentally. Good agreement between theory and experiment is found. The heat-transfer data of Yuan can, therefore, be con-

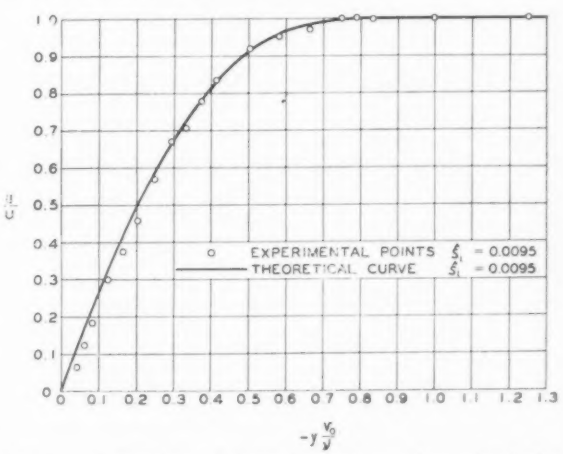

FIG. 12. Comparison of theoretical and experimental velocity profiles with suction for $\xi = 0.025$.

sidered to have been verified, at least, for low rates of heat transfer.

References

[1] Nuber, R. J., and Needham, J. R., Jr., *Exploratory Wind-Tunnel Investigation of the Effectiveness of Area Suction in Eliminating Leading-Edge Separation over an NACA 64,A212 Airfoil*, N.A.C.A. T.N. No. 1741, November, 1948.

[2] von Doenhoff, A. E., and Loftin, L. K., Jr., *Present Status of Research on Boundary-Layer Control*, Journal of the Aeronautical Sciences, Vol. 16, No. 12, p. 727, December, 1949.

[3] Duwez, P., and Wheeler, H. L., Jr., *Experimental Study of Cooling by Injection of a Fluid Through a Porous Material*, Journal of the Aeronautical Sciences, Vol. 15, No. 9, p. 509, September, 1948.

[4] Schlichting, H., *Die Grenzschicht mit Absaugung und Ausblasen*, Luftfahrtforschung, S. 179, 1942.

[5] Iglisch, R., *Exakte Lösungen für die laminare Grenzschicht der längsangeströmten ebenen Platte mit homogener Absaugung*, Bericht 43/22 des Aerodyn, Instituts der T. H. Braunschweig, UM 2061.

[6] Schlichting, H., and Bussmann, K., *Exakte Lösungen für die laminare Grenzschicht mit Absaugung und Ausblasen*, Schriften der Deutschen Akademie der Luftfahrtforschung, Bd. 7B, Heft 2, 1943.

[7] Yuan, S. W., *A Theoretical Investigation of the Temperature Field in the Laminar Boundary Layer on a Porous Flat Plate with Fluid Injection*, Project Squid Technical Report No. 4, Polytechnic Institute of Brooklyn, September, 1947.

[8] Yuan, S. W., *Heat Transfer in Laminar Compressible Boundary Layer on a Porous Flat Plate with Fluid Injection*, Journal of the Aeronautical Sciences, Vol. 16, No. 12, p. 741, December, 1949.

[9] Lew, H., *On the Compressible Boundary Layer over a Flat Plate with Uniform Suction*, contribution to Applied Mechanics, H. Reissner Anniversary Volume, p. 43; Edward Brothers, 1949.

[10] Lew, H., *The Cooling of a Flat Plate in a Laminar Compressible Flow by Uniform Fluid Injection*, PIBAL Report No. 131, Polytechnic Institute of Brooklyn, September, 1948.

[11] Lew, H., and Romano, F., *The Compressible Laminar Boundary Layer over a Flat Plate with Uniform Suction and Heat Transfer at the Wall*, PIBAL Report No. 132, Polytechnic Institute of Brooklyn, September, 1948.

[12] Lew, H., *The Compressible Laminar Boundary Layer over a Flat Plate with Partial or Variable Suction at the Wall*, PIBAL Report No. 151, Polytechnic Institute of Brooklyn, September, 1949.

[13] Yuan, S. W., and Chin, C., *Heat Transfer in a Laminar Compressible Boundary Layer on a Partially Sweat-Cooled Plate*, Project Squid Technical Report No. 13, Polytechnic Institute of Brooklyn, August, 1949.

[14] Yuan, S. W., and Ness, N., *Heat Transfer in a Laminar Compressible Boundary Layer on a Porous Flat Plate with Variable Fluid Injection*, Project Squid Technical Memorandum PIB-15, Polytechnic Institute of Brooklyn, September, 1950.

[15] Romano, F. J., *An Investigation of the Effect of Partial Suction on the Flow Characteristics and Stability of Compressible Laminar Boundary Layers over a Flat Plate*, PIBAL Report No. 174, Polytechnic Institute of Brooklyn, August, 1950.

[16] Ulrich, A., *Theoretische Untersuchungen über die Widerstandsersparnis durch Laminarhaltung mit Absaugung*, Aerodyn. Institut der Technischen Hochschule Braunschweig, Bericht Nr. 44/8 (Translated as N.A.C.A. T.M. No. 1121, June, 1947).

[17] Lees, L., *Stability of the Laminar Boundary Layer with Injection of Cool Gas at the Wall*, Princeton University Aeronautical Engineering Laboratory Report No. 139, May, 1948.

[18] Libby, P., Lew, H., and Romano, F., *On the Stability of a Laminar Compressible Boundary Layer over a Flat Plate Subject to Uniform Suction and Injection*, PIBAL Report No. 133, Polytechnic Institute of Brooklyn, October, 1948.

[19] Kuethe, A. M., and Schetzer, J. D., *Foundations of Aerodynamics*, p. 242; John Wiley and Sons, Inc., New York, 1950.

[20] Charters, A. C., Jr., *Transition Between Laminar and Turbulent Flow by Transverse Contamination*, N.A.C.A. T.N. No. 891, March, 1943.

Changes of Address

Since the Post Office Department does not as a rule forward magazines to forwarding addresses, it is important that the Institute be notified of changes in address 30 days in advance of publishing date to ensure receipt of every issue of the JOURNAL and REVIEW.

Notices should be printed legibly and sent directly to:

Institute of the Aeronautical Sciences, Inc.

2 East 64th Street, New York 21, New York

Readers' Forum

BRIEF REPORTS of investigations in the aeronautical sciences and discussions of papers published in the JOURNAL are presented in this special department. The publication will be completed approximately 8 to 10 weeks after receipt of the material. The Editorial Committee does not hold itself responsible for the opinions expressed by the correspondents. Contributions should not exceed 800 words in length.

Effect of Wind-Tunnel Nozzle on Steady-Flow Nonuniformities*

Stanley Corrsin

Associate Professor, Aeronautics Department, The Johns Hopkins University, Baltimore

November 12, 1951

Introduction

SINCE PRANDTL'S DISCUSSION on the attainment of uniform flow in a low-speed, constant density, wind tunnel,[1] designers have been acutely conscious of the benefit of high contraction ratio as a means of reducing the dimensionless measure of steady-flow irregularity in the working section.

Two simple generalizations are of practical interest: (a) the effect of upstream density ($\sim$ temperature^{-1}) irregularities on working section velocity irregularities in a low-speed tunnel; and (b) extension to compressible flow of Prandtl's rough estimate for the effect of upstream irregularities, now in both mean velocity and stagnation temperature.

The analyses are restricted to small irregularities in velocity, with resulting linearization. Velocity irregularities are considered only in the mean-flow direction.

The simplifying assumptions are (1) inviscid (isentropic) flow in the nozzle and (2) constant static pressure across the duct both before and after the nozzle.

Low-Speed Flow ($M \to 0$)

We write two Bernoulli equations between Section No. 1, well ahead of the contraction, in the "pressure box," and Section No. 2 in the working section.

$$p_1 + (1/2)\rho U_1^2 = p_2 + (1/2)\rho U_2^2 \tag{1}$$

$$p_1 + \frac{1}{2}(\rho + \delta)(U_1 + u_1)^2 = p_2 + \frac{1}{2}(\rho + \delta)(U_2 + u_2)^2 \tag{2}$$

where

p = static pressure
ρ = unperturbed density
δ = density irregularity
U = unperturbed velocity
u = velocity irregularity

Eq. (1) applied to an unperturbed streamline, Eq. (2) to a perturbed one.

We are interested in finding u_2/U_2 as a function of u_1/U_1, δ/ρ and the contraction area ratio, $A_1/A_2 = U_2/U_1$. With u_1/U_1, $u_2/U_2 \ll 1$, the difference between Eqs. (1) and (2) yields the linearized result

$$\frac{u_2}{U_2} = \left(\frac{A_2}{A_1}\right)^2\left(\frac{u_1}{U_1}\right) - \frac{1}{2}\left[1 - \left(\frac{A_2}{A_1}\right)^2\right]\frac{\delta/\rho}{1 + (\delta/\rho)} \tag{3}$$

which reduces to Prandtl's result for $\delta/\rho = 0$. If the density irregularity is due to temperature irregularity in a perfect gas—the usual case—then,

$$\frac{u_2}{U_2} = \left(\frac{A_2}{A_1}\right)^2\left(\frac{u_1}{U_1}\right) + \frac{1}{2}\left[1 - \left(\frac{A_2}{A_1}\right)^2\right]\frac{\vartheta}{T} \tag{4}$$

where T is undisturbed absolute temperature and ϑ is the irregularity. There is no restriction to $\vartheta \ll T$.

A numerical example is rather startling: Suppose $A_2/A_1 = 0.05$, $u_1/U_1 = 0.03$, and $\vartheta/T = 0.005$. Then Eq. (4) gives $u_2/U_2 = 0.000075 + 0.0025$, and the 1.5°C. temperature irregularity causes 33 times as much trouble as the 3 per cent upstream velocity irregularity!

Compressible Flow

The energy equations for unperturbed and perturbed streamlines are, with c_p assumed constant,

$$c_pT_0 = c_pT_1 + (1/2)U_1^2 = c_pT_2 + (1/2)U_2^2 \tag{5}$$

$$c_p(T_0 + \vartheta_0) = c_p(T_1 + \vartheta_1) + (1/2)(U_1 + u_1)^2 = c_p(T_2 + \vartheta_2) + (1/2)(U_2 + u_2)^2 \tag{6}$$

where

T_0 = stagnation temperature
ϑ_0 = stagnation temperature irregularity
T_1, T_2 = flow temperatures
ϑ_1, ϑ_2 = flow temperature irregularities
c_p = specific heat at constant pressure

With the assumptions of isentropy and constant pressure across Section Nos. 1 and 2,

$$\frac{p_1}{p_2} = \left(\frac{T_1}{T_2}\right)^{\gamma/(\gamma-1)} = \left(\frac{T_1 + \vartheta_1}{T_2 + \vartheta_2}\right)^{\gamma/(\gamma-1)}$$

where γ is the ratio of specific heat. Thus,

$$\vartheta_2/T_2 = \vartheta_1/T_1 \tag{7}$$

Linearization of the difference between the right-hand equalities of Eqs. (5) and (6) for (for u_1/U_1, $u_2/U_2 \ll 1$) gives, with Eq. (7), an expression for the working section velocity irregularity

$$\frac{u_2}{U_2} = \left(\frac{U_1}{U_2}\right)^2\left(\frac{u_1}{U_1}\right) + \frac{c_p\vartheta_1}{U_2^2}\left(1 - \frac{T_2}{T_1}\right) \tag{8}$$

A convenient final form is in terms of Mach Numbers (M_1, M_2) and stagnation temperature. For this we note that

$$(U_1/U_2)^2 = (M_1/M_2)^2(T_2/T_1) \tag{9}$$

From Eq. (5) it is observed that

$$U_2^2 = 2c_p(T_0 - T_2) \tag{5a}$$

* Acknowledgement is made to R. Smelt, of Sverdrup and Parcel, for his helpful criticism.

and from the (velocity perturbation) linearized difference between the left-hand equalities of Eqs. (5) and (6),

$$\frac{c_p\vartheta_1}{U_2^2} = \frac{c_p\vartheta_0}{U_2^2} - \left(\frac{U_1}{U_2}\right)^2\left(\frac{u_1}{U_1}\right) \tag{10}$$

Using Eqs. (9), (10), and (5a) in Eq. (8), we arrive at a simple form of the final result

$$\frac{u_2}{U_2} = \left(\frac{M_1}{M_2}\right)^2\left(\frac{u_1}{U_1}\right) + \frac{1}{2}\left[1 - \left(\frac{M_1}{M_2}\right)^2\right]\left(\frac{\vartheta_0}{T_0}\right) \tag{11}$$

which reduces to Eq. (4) as $M_1, M_2 \to 0$.

A nonlinearized result, involving only somewhat more algebra, is perhaps not justifiable in view of the isentropy approximation.

With the additional restriction of $\vartheta_1/T_1, \vartheta_2/T_2 \ll 1$ (but not negligible), Eq. (11) can be transformed to a simple relation

$$m_2/M_2 = (M_1/M_2)^2(m_1/M_1) \tag{12}$$

where m is Mach Number irregularity.

It is noteworthy that, for heat removal by rods or vanes in Section No. 1 ($u_1 < 0$; $\vartheta_0 < 0$), the effects in Eqs. (4) and (11) are additive, while for heat addition rods ($u_1 < 0$; $\vartheta_0 > 0$) they are opposite.

Reference

[1] Prandtl, L., *Herstellung Einwandfreier Luftströme (Windkanäle)*, Handbuch der Exp. Phys., Vol. IV, Part 2, Heraus. v. L. Schiller, Akad. Verlag. M.B.H. Leipzig 1932. (Translation as N.A.C.A. T.M. No. 726.)

On Nonplanar Surfaces of Very Low Aspect Ratio

H. M. Voss
Graduate Student, Aeronautical Engineering Department, Massachusetts Institute of Technology

October 12, 1951

THE MOMENTUM APPROACH to the problem of determination of the air forces on a wing of very low aspect ratio was first suggested by Jones.[1] Since that time this so-called zero aspect ratio theory has been extended in various directions by Spreiter,[2] for the slender wing-body combination, by Lomax and Heaslet,[3] for specific plan forms, and by Miles[4] and others[5] in unsteady flow applications.

It is the purpose of this note to point out that the cases of a nonplanar surface in steady flow or in arbitrary unsteady motion may be treated as well, as long as the deflection, and thus the downwash, is developable in a finite Fourier series in $y/S(x)$ (see Fig. 1). Formulation of this problem by the usual momentum approach appeared unsatisfactory because of the complication of the two-dimensional virtual mass of a deformed plate, the deformation varying streamwise. However, the reduction of the linearized lifting-surface integral, requiring only that the span-to-chord ratio be small,

$$(y - \eta) << (x - \xi) \tag{1}$$

over most of the plan form, has been indicated by Lomax and Sluder.[6] Details of such a reduction are considered in reference 5, although it contains one unnecessary restriction.

A solution of the three-dimensional Laplace equation is of the form,

$$\phi(x, y, z, t) = \frac{z}{4\pi}\iint_{R_a+R_w} \frac{\gamma(\xi, \eta, t)}{[(y - \eta)^2 + z^2]} \times \left\{1 + \frac{(x - \xi)}{[(x - \xi)^2 + (y - \eta)^2 + z^2]^{1/2}}\right\} d\xi\, d\eta \tag{2}$$

where ϕ is the velocity potential, R_a the wing region, R_w the wake region, and γ the discontinuity in the streamwise component of fluid velocity from top to bottom surfaces of the plate. It should be noted that Eq. (2) holds for both steady ($\gamma = 0$ in R_w) and unsteady flow. The assumption of Eq. (1) along with z negligible compared to $(x - \xi)$ in the bracketed portion of the kernel leads to,

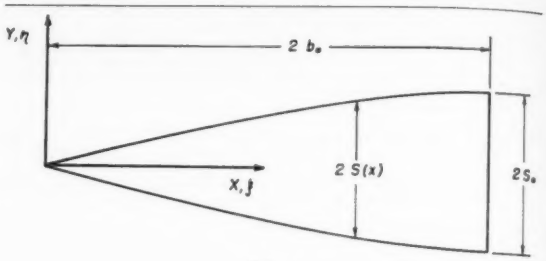

FIG. 1.

$$\phi(x, y, z, t) = \frac{z}{2\pi}\int_0^x \int_{-S(\xi)}^{S(\xi)} \frac{\gamma(\xi, \eta, t)}{[(y - \eta)^2 + z^2]} d\xi\, d\eta \tag{3}$$

Here $S(\xi)$ is the semispan as a function of the streamwise variable.

The kernel of the integral of Eq. (3) is seen to be a solution of the Laplace equation in two dimensions; the integral of γ over the chord serves as a distribution function. Thus, this solution might have been constructed by assuming the validity of the two-dimensional solutions in the present case and superimposing them. In this respect, the foregoing formulation serves only as a justification of reduction to the quasi-two-dimensional problem, as suggested in reference 1 on a physical basis.

A function $F(x, y, t)$ may be defined,

$$F(x, y, t) = \int_{LE}^{x} \gamma(\xi, y, t)\, d\xi \tag{4}$$

where LE is the streamwise location of the leading edge. The order of integration may be interchanged and Eq. (3) integrated by parts to give,

$$\phi(x, y, z, t) = \frac{1}{2\pi}\int_{-S(x)}^{S(x)} \frac{\partial F}{\partial \eta} \tan^{-1}\left(\frac{y - \eta}{z}\right) d\eta \tag{5}$$

Eq. (5) is then differentiated with respect to z,

$$\frac{\partial \phi}{\partial z}(x, y, z, t) = \frac{-1}{2\pi}\int_{-S(x)}^{S(x)} \frac{\partial F}{\partial \eta} \frac{(y - \eta)}{[(y - \eta)^2 + z^2]} d\eta \tag{6}$$

and the boundary condition is satisfied in the $z = 0$ plane in the usual manner of thin airfoil theory,

$$\frac{\partial \phi}{\partial z}(x, y, 0, t) = -w(x, y, t) = \frac{-1}{2\pi} \mathcal{J}\!\!\!\!\!\!-_{-S(x)}^{S(x)} \frac{\partial F}{\partial \eta} \frac{d\eta}{(y - \eta)} \tag{7}$$

In this, $w(x, y, t)$ is the vertical velocity on the airfoil, positive downward.

Eq. (7) is in a form suitable for the familiar Schwarz[11] inversion, becoming,

$$\frac{\partial F}{\partial y}(x, y, t) = \frac{-2}{\sqrt{S(x)^2 - y^2}} \mathcal{J}\!\!\!\!\!\!-_{-S(x)}^{S(x)} w(x, \eta, t) \frac{\sqrt{S(x)^2 - \eta^2}}{(y - \eta)} d\eta \tag{8}$$

The required form of the downwash is,

$$w(x, \eta, t) = f(x, t) \sum_n^N a_n \cos n\theta$$

$$\theta = \cos^{-1}[\eta/S(x)] \quad \psi = \cos^{-1}[y/S(x)] \tag{9}$$

The integrals are of the Glauert type and can be evaluated explicitly,

$$\frac{\partial F}{\partial y}(x, y, t) = \frac{-f(x, t)}{\sqrt{S(x)^2 - y^2}}\left\{2a_0 y + a_1 S(x)\cos 2\psi - 2S(x)\sin\psi \sum_{n=2}^{N} a_n \sin n\psi\right\} \tag{10}$$

A second integration gives,

$$F(x, y, t) = f(x, t)\sqrt{S(x)^2 - y^2}\left\{2a_0 + a_1\frac{y}{S(x)} + 2\sum_{n=2}^{N}\frac{a_n}{(n^2-1)}\left(n\sqrt{S(x)^2 - y^2}\cos n\psi - y\sin n\psi\right)\right\} \tag{11}$$

Differentiation with respect to x then yields γ and leads directly to the pressure distribution over the plan form as a function of x and y,

$$\Delta p(x, y, t) = \rho\left[U\gamma(x, y, t) + \frac{\partial F}{\partial t}(x, y, t)\right] \tag{12}$$

The applicability of Eq. (2) to steady or unsteady flow follows from the assumption of Eq. (1), leading to the conclusion that the influence of the wake in unsteady flow is negligible. Lawrence[7] has pointed out the fact that no low aspect ratio analog exists for the two-dimensional theory for high aspect ratio, and that, in fact, the zero aspect ratio theory of Jones corresponds to lifting-line theory for high aspect ratio. In that the large aspect ratio theory of Reissner reduces to lifting-line theory for steady flow, that the assumption of Eq. (1) is the opposite extreme of that made by Reissner, and that the result reduces to the Jones result for steady flow, the suggested zero aspect ratio theory for unsteady flow becomes the low aspect ratio analog to the Reissner theory for large aspect ratio.

In connection with the use of zero aspect ratio theory in unsteady flow, Miles has made the well-taken point that the Kutta condition remains unsatisfied at the trailing edge in steady flow, so that extension to unsteady subsonic flow is dubious. This point was discussed in reference 5, and Halfman and Ashley[8] have reported on such an application.

References

[1] Jones, R. T., *Properties of Low Aspect Ratio Pointed Wings at Speeds Below and Above the Speed of Sound*, N.A.C.A. Report No. 835, 1948.

[2] Spreiter, J. R., *Aerodynamic Properties of Slender Wing-Body Combinations at Subsonic, Transonic, and Supersonic Speeds*, N.A.C.A. T.N. No. 1662, 1948.

[3] Lomax, H., and Heaslet, M., *Linearized Lifting Surface Theory for Swept-Back Wings with Slender Planform*, N.A.C.A. T.N. No. 1992, 1949.

[4] Miles, J. W., *On Non-Steady Motion of Slender Bodies*, Aeronautical Quarterly, Vol. 2, pp. 183–194, November, 1950.

[5] Voss, H. M., *Flutter of Low Aspect Ratio Lifting Surfaces*, S.M. Thesis, M.I.T., 1951.

[6] Lomax, H., and Sluder, L., *Chordwise and Compressibility Corrections to Slender-Wing Theory*, N.A.C.A. T.N. No. 2295, 1951.

[7] Lawrence, H. R., *The Chordwise Lift Distribution of Low Aspect Ratio Wings and Wing-Body Combinations*, Cornell Aeronautical Laboratory Report No. AF-673-A-1, 1950.

[8] Halfman, R. L., and Ashley, H., *Aeroelastic Properties of Slender Wings*, Paper presented at First National Congress on Applied Mechanics, Chicago, June 11–16, 1951.

[9] Reissner, E., *On the General Theory of Thin Airfoils for Non-Uniform Motion*, N.A.C.A. T.N. No. 946, 1944.

[10] Reissner, E., *Effect of Finite Span on the Airload Distribution for Oscillating Wings, I—Aerodynamic Theory of Oscillating Wings of Finite Span*, N.A.C.A. T.N. No. 1194, 1947.

[11] Schwarz, L., *Berechnung der Druckverteilung einer harmonisch sich Verformenden Tragfläche in ebener Strömung*, Luftfahrtforschung Vol. 17, pp. 379–386, December, 1940.

Note About Secondary Flow in Cascades

Hans P. Eichenberger
Gas Turbine Laboratory, Massachusetts Institute of Technology

October 29, 1951

THE NOTE OF STEPHENSON[1] raises an interesting question about the trailing vorticity behind a cascade of airfoils in shear flow. Assuming that the number of blades is infinite, Stephenson adds the secondary vorticity to the trailing vorticity to obtain the resulting effect. The question arises whether this corresponds to physical reality.

The change of vorticity for inviscid flow is given by the Helmholz equation (reference 2, page 205) $(\bar{q}\cdot\nabla)\bar{\Omega} = (\bar{\Omega}\cdot\nabla)\bar{q}$, where $\bar{q}$ is the velocity vector and $\Omega = \nabla \cdot \bar{q}$. If u, v, and w are the components of $\bar{q}$ and ξ, η, and ζ are the components of $\bar{\Omega}$ in direction of r, φ, z, respectively, this equation can be written:

$$u\xi_r + \frac{v}{r}\xi_\varphi + w\xi_z = \xi u_r + \frac{\eta}{r}u_\varphi + \zeta u_z$$

$$u\eta_r + \frac{v}{r}\eta_\varphi + w\eta_z + \frac{v\xi}{r} = \xi v_r + \frac{\eta}{r}v_\varphi + \zeta v_z + \frac{\eta u}{r}$$

$$u\zeta_r + \frac{v}{r}\zeta_\varphi + w\zeta_z = \xi w_r + \frac{\eta}{r}w_\varphi + \zeta w_z$$

They show that we have to know the streamlines in order to compute the variation of $\bar{\Omega}$ *which does not stay constant, in general.* Assuming, as Squire and Winter[3] did, a basic free vortex flow and u, v, w small as compared to $v_0 = c/r$, we can linearize the above equations and obtain immediately:

(1) $\xi_\varphi = 0$, ξ stays constant
(2) $\eta = -2\xi_\varphi$ as obtained by Squire and Winter[3]
(3) $\zeta_\varphi = 0$, ζ stays constant

Eq. (2) is in disagreement with Eq. (1) of Stephenson's article because he assumed the vorticity constant. Fig. 1 illustrates qualitatively the variation of the vorticity; we assume that upstream of the cascade the axial velocity component only has a peaked profile. The line AB represents then a vortex tube; downstream of the cascade this line A′B′ is no longer parallel to AB, but A′ lags behind B′ since the flow (and with it the vorticity) goes more slowly on the pressure side than on the suction side of the blade.

Knowing the vorticity η in direction of the streamlines in the whole r-z plane at the outlet of the cascade, the problem of finding the secondary velocities has a unique solution, and the streamlines may look as sketched in Fig. 2. From this result we may, if we wish, calculate directly the so-called trailing vortices that behave like needle bearings between two rotating masses and form a vortex sheet. A vortex sheet is a name for the physical fact that we have a discontinuity in velocity over the plane of the sheet. This mathematical concept has proved to be useful in the

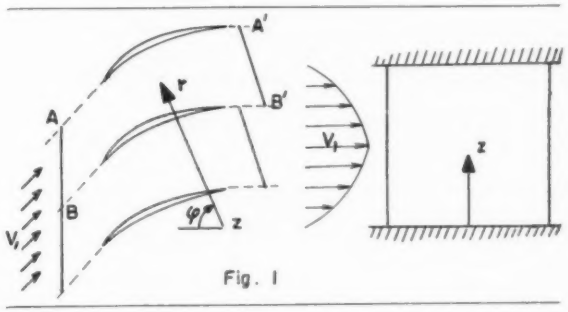

Fig. 1

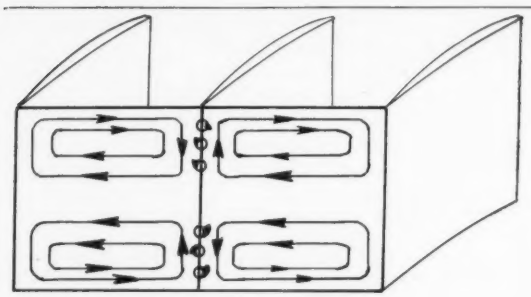

Fig. 2

theory of the finite wing in a potential flow, where on the pressure (suction) side the streamlines bend toward the wing tip (midspan) such that we have at the trailing edge a surface of discontinuity. From the magnitude of this discontinuity, we can calculate the induced velocities everywhere because the vorticity is zero everywhere except on the trailing vortex sheet. But in a cascade where the vorticity in the stream is different from zero, the knowledge of the trailing vortex sheet is useless for the calculation of the induced velocities. The knowledge of the distributed vorticity is necessary and sufficient to calculate the secondary velocity. The jump of velocity at the trailing vortex sheet then follows immediately. To add this trailing vorticity to the distributed vorticity seems not to have any physical meaning.

REFERENCES

[1] Stephenson, J. M., *Secondary Flow in Cascades*, Journal of the Aeronautical Sciences, Vol. 18, No. 10, p. 699, October, 1951.

[2] Lamb, H., *Hydrodynamics*; 1945.

[3] Squire, H. B., and Winter, K. G., *The Secondary Flow in a Cascade of Airfoils in a Nonuniform Stream*, Journal of the Aeronautical Sciences, Vol. 18, No. 4, p. 271, April, 1951.

On Chang's Function for Nonstationary Flow

John W. Miles*

Fulbright Lecturer, Auckland University College, Auckland, New Zealand

September 14, 1951

IN A RECENT REPORT on nonstationary airfoil theory,[1] Chang introduces (and recommends the calculation of) the function

$$C(\beta, M) = \frac{1}{\pi}\int_0^\pi \exp\,[-i\beta M(M - \cos\theta)^{-1}]\,d\theta \qquad (1)$$

where M is the Mach Number and β is twice the usual reduced frequency. It should be pointed out that this function may be expressed in terms of Schwarz's function,[2] $f_0(\lambda, M)$, according to

$$C(\beta, M) = 1 - i\beta M(M^2 - 1)^{-1/2} f_0[\beta M^2(M^2 - 1)^{-1}, M] \qquad (2)$$

Similarly, it is expected that his $C(\beta, M, \theta_1)$ can be related to his "incomplete Bessel function" $J_0(z, \theta_1)$.

To demonstrate Eq. (2), take the Laplace transform of Eq. (1) with respect to β, whence

$$F(s, M) = \int_0^\infty e^{-s\beta} C(\beta, M)\,d\beta \qquad (3a)$$

$$= \frac{1}{\pi}\int_0^\pi [s + iM(M - \cos\theta)^{-1}]^{-1}\,d\theta \qquad (3b)$$

$$= s^{-1} - is^{-1}M(M^2 - 1)^{-1/2}\{[s + iM^2 \times (M^2 - 1)^{-1}]^2 + M^2(M^2 - 1)^{-2}\}^{-1/2} \qquad (3c)$$

Taking the inverse transform of Eq. (3c), we find

$$C(\beta, M) = 1 - iM(M^2 - 1)^{-1/2} \times \int_0^\beta \exp\,[-iM^2(M^2 - 1)^{-1}\tau]\,J_0[M(M^2 - 1)^{-1}\tau]\,d\tau \qquad (4)$$

Introducing $u = \tau/\beta$ as the variable of integration and noting the definition

$$f_0(\lambda, M) = \int_0^1 e^{-i\lambda u}\,J_0(\lambda u/M)\,du \qquad (5)$$

Eq. (4) reduces to Eq. (2), *Q.E.D.*

REFERENCES

[1] Chang, C. C., *Transient Aerodynamic Behavior of an Airfoil Due to Different Arbitrary Modes of Nonstationary Motion in a Supersonic Flow*, N.A.C.A. T.N. No. 2333, April, 1951.

[2] Schwarz, L., *Untersuchung mit den Zylinderfunktionen Nullter Ordnung Verwandten Funktionen*, Luftfahrtforschung, Vol. 20, pp. 341–372, 1944.

On the Stability of the Boundary Layer with Respect to Disturbances of Large Wave Velocity

C. C. Lin

Associate Professor of Mathematics, Massachusetts Institute of Technology

October 26, 1951

RECENTLY, THERE HAS BEEN considerable interest in the stability of the boundary layer with a supersonic free stream.[1,2] In particular, the stabilizing effect of cooling at high Mach Numbers has been the center of discussion. Since "subsonic" disturbances only are considered proper to the stability problem, the wave speed c of the disturbance must satisfy the relation

$$c/U > 1 - (1/M)$$

where U is the free-stream velocity and M is the free-stream Mach Number. It is clear that for reasonably high Mach Numbers, the value of c/U is large.

It has been argued that the methods of evaluation of the integrals associated with the "inviscid" solutions are inadequate for large values of the wave speed. This is indeed the case, since they were developed analogous to those used for an incompressible fluid,[3] where the wave speed is usually small. This fact has been used explicitly in the original development of the method, and the procedure has been adopted in the compressible case[4] without essential modification. For wider applications, this restriction must be removed as has now been generally recognized.

There is, however, a much more basic restriction inherent in the theory developed by Lees and the present writer,[5] on which the calculations of Lees[4] were based. In Eq. (72) of reference 5, the velocity and density distributions are expressed as power series, and only the linear terms are retained by an examination of the order of magnitude. This step restricts the "viscous" solutions to the neighborhood of the critical layer and makes it unreliable, in the case of moderately large values of c/U, for the purpose of satisfying the boundary conditions at the wall. One might attempt to improve the accuracy by going to higher terms in Eq. (72), but the amount of labor required would be excessive if the density distribution across the boundary layer requires

* On leave from the University of California, Los Angeles.

several terms of the series for its accurate representation. Basically, the method associated with the use of Eq. (72) is also not satisfactory. It leads to the conditions [Eq. (95)] which, though adequate for the purpose at hand, have been recently shown by Cathleen S. Morawetz[6] to be inexact.

Since all the present calculations for large c/U are based on a procedure beyond the validity of the existing theory, attempts are now being made to revise the theory considerably to remove the restrictions mentioned above.

It should perhaps be pointed out in passing that all the developments in Section II of reference 5 are not influenced by the restrictions discussed above.

References

[1] Bloom, M., *The Effect of Surface Cooling on Laminar Boundary-Layer Stability*, Journal of the Aeronautical Sciences, Vol. 18, No. 9, pp. 635–636, September, 1951.

[2] Van Driest, E. R., *Cooling Required to Stabilize the Laminar Boundary Layer on a Flat Plate*, Journal of the Aeronautical Sciences, Vol. 18, No. 10, pp. 698–699, October, 1951.

[3] Lin, C. C., *On the Stability of Two-Dimensional Parallel Flows*, Quarterly of Applied Mathematics, Vol. 3, pp. 117–142, 218–234, 277–301, 1945, 1946.

[4] Lees, L., *The Stability of the Laminar Boundary Layer in a Compressible Fluid*, N.A.C.A. T.N. No. 1360, 1947; Reissued as Tech. Report No. 876.

[5] Lees, L., and Lin, C. C., *Investigation of the Stability of the Laminar Boundary Layer in a Compressible Fluid*, N.A.C.A. T.N. No. 1115, 1946.

[6] Morawetz, Cathleen S., *Asymptotic Solutions of the Stability Equations of a Compressible Fluid*, submitted to the N.A.C.A. under contract NAw 5981, July, 1951; to be published.

A Method of Solving the Linear Potential Equation for Axially Symmetric Flow

R. Probstein and J. V. Charyk
Department of Aeronautical Engineering, Princeton University

October 29, 1951

THE LINEARIZED POTENTIAL EQUATION for supersonic flow over a body of revolution whose axis is in the direction of the free stream velocity is,

$$(1 - M_1^2)\frac{\partial^2\phi}{\partial x^2} + \frac{\partial^2\phi}{\partial r^2} + \frac{1}{r}\frac{\partial\phi}{\partial r} = 0 \tag{1}$$

where ϕ is the disturbance potential that is a function only of x and r. The general, solution of Eq. (1) can be shown to be[1]

$$\phi = -\frac{1}{4\pi}\int_0^{x-\alpha r}\frac{f(\xi)\,d\xi}{\sqrt{(x-\xi)^2 - \alpha^2 r^2}} \tag{2}$$

where $\alpha = \sqrt{M_1^2 - 1}$ and $f(\xi)$ is the unknown source distribution function along the x-axis. Both the position and variation of the source strength, which is expressed by $f(\xi)$, are determined by the body shape.

At present, the general method used for solving this integral equation for the flow about an arbitrary pointed body of revolution is to break up the body into a series of conical flow sections and then superpose the readily soluble linearized solution for conical flow. For most body shapes, this procedure is extremely long, and, in many instances, the only practical method of solution would be to resort to computing machines. An alternate approach, which does not appear to have been used previously and which yields an apparently excellent approximation, is proposed.

If one recognizes that the source distribution function for linearized conical flow is given by $f(\xi) = K\xi$, then it would be reasonable to assume that the source distribution in the general case could be represented by a polynomial, such that,

$$f(\xi) = \sum_{n=1}^{p} A_n \xi^n \tag{3}$$

Here the coefficients A_n are determined by the boundary condition that the flow must everywhere be tangential to the body—that is, that

$$m = (dr/dx) = (\partial\phi/\partial r)/[U_1 + (\partial\phi/\partial x)] \tag{4}$$

To illustrate the simplicity of this method, let us calculate the pressure distribution over a body of revolution at zero angle of attack. Since Eq. (3) is rapidly convergent for reasonable body shapes, we shall chose $p = 3$. If we now make the transformation

$$\xi = x - \alpha r\cosh\beta \tag{5}$$

then the disturbance potential is given by,

$$\phi = -\frac{1}{4\pi}\int_0^{\cosh^{-1}(x/\alpha r)}\left[\sum_{n=1}^{3} A_n(x - \alpha r\cosh\beta)^n\right]d\beta \tag{6}$$

and it follows that,

$$\frac{\partial\phi}{\partial x} = -\frac{1}{4\pi}\int_0^{\cosh^{-1}(x/\alpha r)}\left[\sum_{n=1}^{3} nA_n(x - \alpha r\cosh\beta)^{n-1}\right]d\beta \tag{7}$$

and

$$\frac{\partial\phi}{\partial r} = \frac{\alpha}{4\pi}\int_0^{\cosh^{-1}(x/\alpha r)}\left[\sum_{n=1}^{3} nA_n(x - \alpha r\cosh\beta)^{n-1}\right]\cosh\beta\,d\beta \tag{8}$$

When the above equations are integrated, we obtain,

$$\frac{\partial\phi}{\partial x} = -\frac{1}{4\pi}\sum_{n=1}^{3} nA_n\left\{x^{n-1}\cosh^{-1}\frac{x}{\alpha r} - (n-1)x^{n-2}\sqrt{x^2 - (\alpha r)^2} + \frac{(n-1)(n-2)}{2}\frac{(\alpha r)^2}{2}\left[\frac{x}{\alpha r}\sqrt{\left(\frac{x}{\alpha r}\right)^2 - 1} + \cosh^{-1}\frac{x}{\alpha r}\right]\right\} \tag{9}$$

and

$$\frac{\partial\phi}{\partial r} = \frac{\alpha}{4\pi}\sum_{n=1}^{3} nA_n\left(x^{n-1}\sqrt{\left(\frac{x}{\alpha r}\right)^2 - 1} - \frac{(n-1)x^{n-2}\alpha r}{4-n}\left[\frac{x}{\alpha r}\sqrt{\left(\frac{x}{\alpha r}\right)^2 - 1} + \cosh^{-1}\frac{x}{\alpha r}\right] + \frac{(n-1)(n-2)}{2}\left\{\frac{(\alpha r)^2}{3}\sqrt{\left(\frac{x}{\alpha r}\right)^2 - 1}\left[\left(\frac{x}{\alpha r}\right)^2 + 2\right]\right\}\right) \tag{10}$$

The evaluation of the integrals in Eqs. (7) and (8) simply reduces through integration by parts to the evaluation of integrals of the hyperbolic cosine to various powers. The following recurrence relation permits the result to be readily written down.

$$\int\cosh^m\beta\,d\beta = \frac{1}{m}\sinh\beta\cosh^{m-1}\beta + \frac{m-1}{m}\int\cosh^{m-2}\beta\,d\beta$$

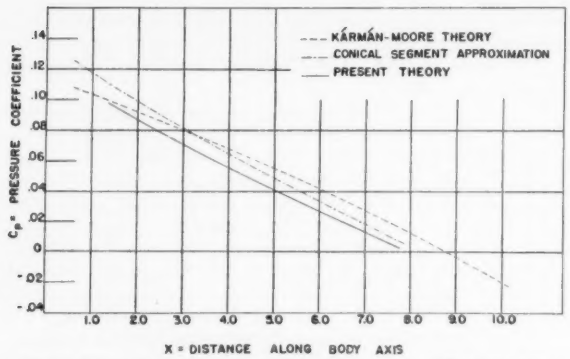

FIG. 1. Comparison of calculated pressure coefficients for a parabolic body of revolution described by $r = (x/100)(20 - x)$ at a free-stream Mach Number $M_1 = 2.6$.

Eqs. (9) and (10), since they are limited to $n = 3$, involve only the results of the integration of terms of the order $\cosh^2 \beta$ and $\cosh^4 \beta$, respectively. It will be noted later that the effect of angle of attack only demands the evaluation of integrals of $\cosh^3 \beta$ and $\cosh^4 \beta$ for the case $n = 3$—that is, the only complication is the raising of the degree of the cosh β in the integrals by one. The complexity of other methods when angle of attack is introduced is appreciably increased.

The boundary condition (4) applied at three points on the surface of the body can be expressed in the form:

$$m_n = \frac{\sum_{n=1}^{3} A_n a_n(x, \alpha r)}{U_1 + \sum_{n=1}^{3} A_n b_n(x, \alpha r)} \tag{11}$$

where, the a_n's and b_n's represent the functions of x and αr associated with the corresponding A_n's. The A_n's are now readily calculated from the following set of three equations.

$$U_1 \sum_{l=1}^{3} m_l = \sum_{l=1}^{3} \left[\sum_{n=1}^{3} A_n (a_{nl} - m_l b_{nl}) \right] \tag{12}$$

Here l represents the three points along the body at which the slope is taken. Since,

$$\frac{\partial \phi}{\partial x} = \sum_{n=1}^{3} A_n b_n(x, \alpha r) \tag{13}$$

we can calculate the pressure coefficient immediately from,

$$c_p = \frac{2}{U_1} \sum_{n=1}^{3} A_n b_n(x, \alpha r) \tag{14}$$

It should be pointed out that the problem is now solved *once and for all* for any body of revolution for which $p = 3$ yields a sufficiently convergent series in Eq. (3). It might be necessary to take a larger value of p for bodies in which the describing curve is of extremely high order; however, this does not modify the method of approach. If, for example, p were chosen to be 4, this would only necessitate integrating Eqs. (7) and (8) one more time, yielding a fourth-order determinant for Eq. (12) instead of a third-order one.

It should also be noted that the same method can be applied to bodies of revolution at an angle of yaw as well. One could then obtain simple series expressions for the stability derivatives. At present, this is done by resorting to the von Kármán-Moore approximation of extremely thin bodies[2] because of the cumbersomeness in the handling of the method of conical flows first described.

To show the accuracy of the method, calculations of the pressure coefficient were made for a parabolic body of revolution whose shape was given by $r = (x/100)(20 - x)$ at a free-stream Mach Number equal to 2.6. The results obtained are shown in Fig. 1 and are compared with the method of calculation by conical flows, as well as with the von Kármán-Moore approximation.

REFERENCES

[1] Ferri, A., *Elements of Aerodynamics of Supersonic Flows*, p. 213; The Macmillan Company, New York, 1949.
[2] *Ibid.*, p. 216.
[3] *Ibid.*, p. 220.

On Slender Wing-Body Theory

John W. Miles*
Fullbright Lecturer, Auckland University College, Auckland, New Zealand
November 14, 1951

THE FREQUENT REFERENCE to, and use of, Spreiter's analysis of the slender wing-body problem[1] (e. g., numerous N.A.C.A. reports) implies that Ward's more complete analysis of the same problem[2, 3] has not been fully appreciated in this country. In particular, Spreiter's results are incorrect for a winged body of varying cross section because of his failure to include properly the logarithmic term in the complex potential and the second-order terms in Bernoulli's equation. [A detailed criticism has been communicated privately to Spreiter (1950).]

The errors in Spreiter's analysis explain the disagreement between his results and those of Ward for a winged body of revolution, the latter obtaining a lift coefficient of similar form for all configurations for which the body cross section either remains constant or terminates aft of the maximum wing span.

REFERENCES

[1] Spreiter, J. R., *Aerodynamic Properties of Slender Wing-Body Combinations at Subsonic, Transonic, and Supersonic Speeds*, N.A.C.A. T.N. No. 1662, July, 1948.
[2] Ward, G. N., *Supersonic Flow Past Slender Pointed Bodies*, Quart. Journal Mech. & Appl. Math., Vol. 2, Part 1, pp. 75–97, 1949.
[3] Stocker, P. M., *Supersonic Flow Past Bodies of Revolution with Thin Wings of Small Aspect Ratio*, Aeronautical Quart., Vol. 3, pp. 61–79, May, 1951.

* On leave from University of California, Los Angeles.

A Note on the Design of Supersonic Wind-Tunnel Nozzles

R. E. Meyer
Institute for Fluid Dynamics and Applied Mathematics, University of Maryland, College Park, Md.
November 1, 1951

FOR THE DESIGN OF SYMMETRICAL NOZZLES for two-dimensional supersonic flow, it is customary to divide the field of flow into the subsonic and the supersonic part and to treat the latter by the numerical method of characteristics and the former by some other approximate method. It is then convenient not to extend the characteristics computation to the sonic line but to make the transition at some other isobar, where the velocity is slightly supersonic. One of the main purposes of the calculation for the subsonic part is then to find the position of, and the distribution of the stream direction on, this isobar.

Since test sections with a uniform distribution of velocity have been found desirable for some purposes, interest has been shown recently in obtaining a good approximation to the initial condi-

tions for the characteristics computation. It may be worth noting that the maximum value of the stream direction on such an isobar depends only on the velocity magnitude. This provides a useful check on the accuracy of the approximation used.

In a symmetrical nozzle, the two Mach lines through the sonic point on the axis are branch lines.[1] That is, the sense of variation on an isobar of the stream direction is reversed where the isobar crosses either of these Mach lines. Conversely, it can be shown[2] that such a reversal can occur on an isobar only across a branch line, if the wall curvature is continuous, upstream of the isobar.

The characteristic equations for the two-dimensional steady isentropic irrotational supersonic flow of a perfect gas are[3]

$$dy/dx = \tan(\theta - \mu); \quad \theta + t = \text{const.} = \alpha$$

and

$$dy/dx = \tan(\theta + \mu); \quad \theta - t = \text{const.} = \beta$$

where μ is the Mach angle, θ is the stream direction (measured counterclockwise from the downstream direction on the axis, which is the direction of x increasing), and

$$t = \mu + \lambda \cot^{-1}(\lambda \tan \mu) - (1/2)\pi$$

with

$$\lambda = \sqrt{[(\gamma + 1)/(\gamma - 1)]}$$

γ being the ratio of the specific heats. Bernoulli's equation relates μ to the velocity magnitude, q, so t is a function of q only. At the sonic point on the axis, $\theta = t = 0$, so the branch lines are the Mach lines $\alpha = 0$ and $\beta = 0$ and the maximum value of $|\theta|$ on the isobar $q = q_0$ is equal to $t(q_0)$.

References

[1] Lighthill, M. J., *The Hodograph Transformation in Trans-sonic Flow*, Part I, Symmetrical Channels, Proc. Roy. Soc. A, Vol. 191, pp. 323–341, 1947.

[2] Meyer, R. E., *Focusing Effects in Two-dimensional, Supersonic Flow*, Phil. Trans. Roy. Soc. A, Vol. 242, No. 844, pp. 153–171, December, 1949.

[3] Meyer, R. E., *The Method of Characteristics for Problems of Compressible Flow*, Part I, Quart. Journal of Mech. & Appl. Math., Vol. 1, No. 2, pp. 196–219, June, 1948.

Parameters Predicting Failure of Partial Diagonal Tension Beams

Bertram Klein

Structures Methods Group, Bell Aircraft Corp., Buffalo, N.Y.

October 4, 1951

PARTIAL DIAGONAL TENSION field beams can fail in various ways. Two distinct modes of failure of particular importance are those due to failure of the web and forced crippling of the vertical stiffeners (uprights). For these types of failure, rigorous theoretical analyses apparently do not exist. Much testing has been performed by which semiempirical analyses were evolved and criteria established for predicting the allowable loads and stresses connected with these failures.[1–7] Much scatter exists, however, when the test data are plotted according to those criteria for forced crippling. The author presents what he believes to be more rational parameters that reduce the scatter in this case. Also included are parameters that seem to give best results for predicting web failure.

(1) Web Failure

According to reference 1, the main parameters are: A_{u_e}/dt, $\tau_{cr.}/\tau_{ult.}$, and $\tau_{ult.}/\sigma_{tu}$. (For the meaning of these and following symbols, see Figs. 1 and 2.) The first two parameters also appear in the methods of reference 2. They are connected with

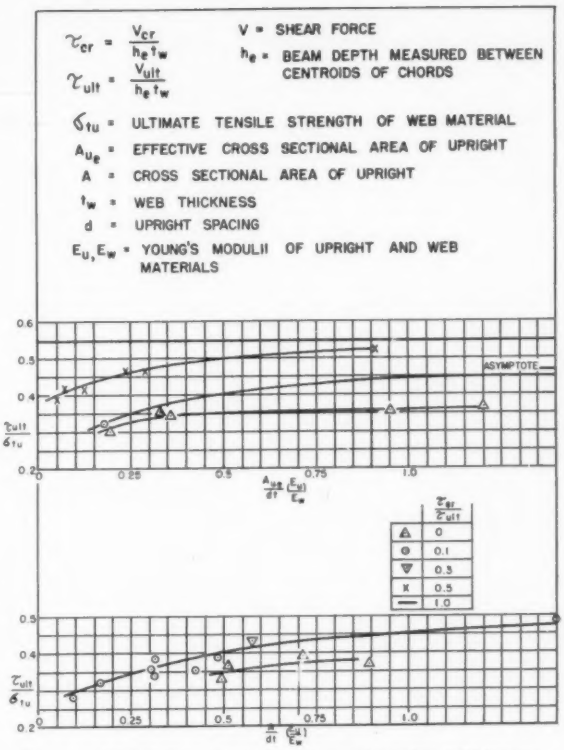

FIG. 1. Web failure in partial diagonal tension field beams.

the angle and degree of diagonal tension developed in the web. To account for differences in web and upright material, the factor E_u/E_w is incorporated in the first parameter. Experimental data taken from references 2 to 5 are plotted in Fig. 1. The reason the data of reference 5 have been plotted separately is due to the fact that it was not known whether single or double uprights were used in the tests. Although there is little scatter, it should be kept in mind that other factors that have to be considered be-

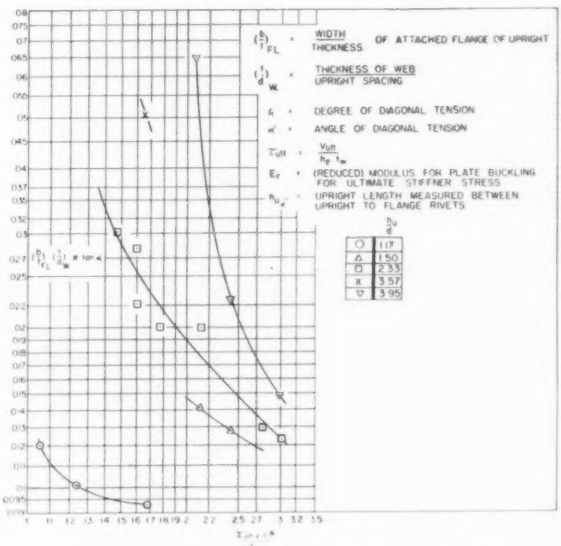
$(\frac{b}{t})_{FL}$ = WIDTH / THICKNESS OF ATTACHED FLANGE OF UPRIGHT
$(\frac{t}{d})_w$ = THICKNESS OF WEB / UPRIGHT SPACING
f_s = DEGREE OF DIAGONAL TENSION
α' = ANGLE OF DIAGONAL TENSION
$\tau_{ult} = \frac{V_{ult}}{h_e t_w}$
E_r = (REDUCED) MODULUS FOR PLATE BUCKLING FOR ULTIMATE STIFFNER STRESS
h_{u_e} = UPRIGHT LENGTH MEASURED BETWEEN UPRIGHT TO FLANGE RIVETS
$\frac{h_{u_e}}{d}$
1.17
1.50
2.33
3.57
3.95

FIG. 2. Forced crippling of single, bent-up uprights in partial diagonal tension field beams.

fore the picture is complete are: rivet spacing, flange flexibility, and type of web to flange attachment.

(2) Forced Crippling of Upright

Only single, bent-up uprights are considered here. From the work of reference 8, it appears that two factors to be considered are the distance between centerline of rivet and heel of upright and the stiffener to web rivet spacing. Since these quantities were not known for the test data used, the total length of the attached flange, b, was used. The effect of the rivet spacing was neglected. Based on the results of reference 8, one parameter is taken as $(b/t)_{FL}(t/d)_w k \tan \alpha$, the factor $k \tan \alpha$ accounting for the wrinkled state of the sheet. A second parameter is h_u/d, the aspect ratio of the panel, which controls the movability of the wrinkled sheet.

The experimental data of references 2 and 4 are plotted in Fig. 2. All specimens had bent-up uprights. It should be noted that an extruded section is more efficient than a bent-up section because the corner radius is eliminated. When the maximum stiffener compressive stress at failure, computed according to the methods of reference 2, was definitely in the plastic range, a reduced modulus was used.

The data appear to follow a reasonable trend. However, more test data should be incorporated before it is concluded that the chosen parameters are correct for this type of failure, as well as for web failure. Such unpublished data, no doubt, exist, and it would be of great interest to the author to learn how these data plot and compare, using the suggested parameters.

References

[1] Royal Aeronautical Society Data Sheets, *Stressed Skin Structures*, Fig. 02.03.13, 2nd Revision, September, 1943.

[2] Kuhn, P., and Peterson, J. P., *Strength Analysis of Stiffened Beam Webs*, N.A.C.A. T.N. No. 1364, July, 1947.

[3] Kuhn, P., *Ultimate Stresses Developed by 24S-T Sheet in Incomplete Diagonal Tension*, N.A.C.A. T.N. No. 833, December, 1941.

[4] Levin, L. R., and Sandlin, C. W., Jr., *Strength Analysis of Thick Beam Webs*, N.A.C.A. T.N. No. 1820, March, 1949.

[5] Langhaar, H. L., *Theoretical and Experimental Investigations of Thin-Walled Plate-Girder Beams*, Transactions of the A.S.M.E., Vol. 65, p. 790, October, 1943.

[6] Sechler, E. E., and Dunn, L. G., *Airplane Structural Analysis and Design*, p. 251; John Wiley and Sons, Inc., 1942.

[7] Hoose, E., *Engineering Development Work of the Consolidated Vultee Aircraft Co.*, Aeronautical Engineering Review, Vol. 2, No. 11, p. 31, November, 1943.

[8] Bijlaard, P. P., and Johnston, G. S., *Compressive Buckling of Plates Due to Forced Crippling of Stiffeners or Webs*, to be published.

Supersonic Flow Around Cones at Large Yaw

(*Continued from page 119*)

[2] Kopal, Z., *Tables of Supersonic Flow Around Yawing Cones*, M.I.T. Tech. Report No. 3, 1947.

[3] Kopal, Z., *Tables of Supersonic Flow Around Cones of Large Yaw*, M.I.T. Tech. Report No. 5, 1949.

[4] Taylor, G. I., and Maccoll, J. W., *The Air Pressure on a Cone Moving at High Speeds*, Proc. Roy. Soc., Vol. A139, p. 278, 1933.

[5] Stone, A. H., *On Supersonic Flow Past a Slightly Yawing Cone*, J. Math. Phys., Vol. 27, p. 67, April, 1948.

[6] Young, G. B. W., *An Elucidation of Stone's Solution for a Slightly Yawing Supersonic Cone*, Project RAND, The RAND Corporation, Research Memorandum RM-48, 1948.

[7] Cronvich, L. L., and Bird, K. D., O.A.L. Report No. 160 (forthcoming report).

[8] Van Dyke, M. D., Young, G. B. W., and Siska, C. P., *Proper Use of the M.I.T. Tables for Supersonic Flow Past Inclined Cones*, Readers' Forum, Journal of the Aeronautical Sciences, Vol. 18, p. 355, May, 1951.

[9] Ferri, A., *Supersonic Flow Around Circular Cones at Angles of Attack*, N.A.C.A. T.N. No. 2236, November, 1950.